UNIVERSIDADE FEDERAL DO RIO GRANDE DO SUL

INSTITUTO DE GEOCIÊNCIAS

PROGRAMA DE PÓS-GRADUAÇÃO EM GEOCIÊNCIAS

HETEROGENEIDADE MANTÉLICA NA REGIÃO SUL DO BRASIL EVIDENCIADA POR MINERALOQUÍMICA DE KIMBERLITOS

Larissa Colombo Carniel

ORIENTADORES:

Prof. Dr. Rommulo Vieira Conceição (Universidade Federal do Rio Grande do Sul, Brasil)

Prof. Dr. Stephan Klemme (Westfälische Wilhelms-Universität Münster, Alemanha)

Porto Alegre, 2017

UNIVERSIDADE FEDERAL DO RIO GRANDE DO SUL

INSTITUTO DE GEOCIÊNCIAS

PROGRAMA DE PÓS-GRADUAÇÃO EM GEOCIÊNCIAS

HETEROGENEIDADE MANTÉLICA NA REGIÃO SUL DO BRASIL EVIDENCIADA POR MINERALOQUÍMICA DE KIMBERLITOS

Larissa Colombo Carniel

ORIENTADORES:

Prof. Dr. Rommulo Vieira Conceição (Universidade Federal do Rio Grande do Sul, Brasil)

Prof. Dr. Stephan Klemme (Westfälische Wilhelms-Universität Münster, Alemanha)

BANCA EXAMINADORA:

Prof. Dr. Pedro Luiz Juchem (Universidade Federal do Rio Grande do Sul, Brasil)

Prof. Dr. Ricardo Kalikowski Weska (Universidade Federal do Mato Grosso, Brasil)

Prof. Dr. Silvio Roberto Farias Vlach (Universidade de São Paulo, Brasil)

Tese de doutorado apresentada como requisito parcial para a obtenção de Título de Doutor em Geociências.

Porto Alegre, 2017

Aos meus queridos pais, pelo amor e exemplo...

AGRADECIMENTOS

Agradeço especialmente ao Prof. Dr. Rommulo Vieira Conceição, por todo o apoio e incentivo durante os muitos anos de trabalho, que foi fundamental para o início e a continuidade das pesquisas desenvolvidas inicialmente na graduação, sendo para mim um exemplo como pesquisador e um bom amigo.

Ao Prof. Dr. Stephan Klemme, que me recebeu muito bem no Instituto de Mineralogia de Münster e foi muito importante para que eu desenvolvesse e aprimorasse a experiência em petrologia experimental, já adquirida na UFRGS.

Agradeço à Universidade Federal do Rio Grande do Sul e ao Programa de Pós-Graduação em Geociências pela oportunidade e infraestrutura oferecidas. Ao CNPq e ao Programa Ciência Sem Fronteiras pelas bolsas de doutorado no Brasil e na Alemanha, além do financiamento de custos laboratoriais que foram essenciais para o desenvolvimento da presente pesquisa.

Sou muito grata também ao Dr. Arno Rohrbach, ao Dr. Jasper Berndt, à Beate Schmitte e a Maik Trogisch, por toda a ajuda e por tudo o que eu aprendi durante o ano de pesquisas no laboratório de petrologia experimental da Universidade de Münster.

Agradeço com muito carinho à minha família, especialmente aos meus pais, que sempre me apoiaram e que são também responsáveis por essa tese. Sem eles, eu não teria chegado ao fim. Ao Felipe, que me apoiou sempre, inclusive no momento em que foi necessário largar a vida no Brasil e ir para a Alemanha, agradeço pelo incentivo, compreensão e ajuda.

À querida amiga Fernanda Gervasoni, agradeço pela amizade e pelo companheirismo durante o ano de trabalho na Alemanha. Agradeço também aos queridos amigos e colegas Daniel Cedeño, Márcio Souza, Roberto Quinteiro e Tiago Jalowitski, pelas discussões sobre petrologia experimental e geoquímica, e pela ajuda em laboratório. Finalmente, não poderia deixar de agradecer aos meus queridos amigos Lívia Brandrão, Leonardo Gruber, Tamara Manfredi, Susan Drago, Elisabete Pedrosa, Zairong Liu e Lena Böck pela ajuda nos experimentos e nas apresentações em congressos, por nossas conversas sobre ciência e principalmente pela amizade e incentivo.

RESUMO

Kimberlitos são rochas vulcânicas que, frequentemente, contêm diamante, grafite e/ou carbonato, sendo a presença destes componentes diretamente influenciada pela variabilidade da fugacidade de oxigênio (fO_2) do magma durante a sua ascenção. Segundo Chakhmouradian and Mitchell (2000), $CaTiO_3$-perovskitas podem ser usadas para revelar as condições de alguns dos múltiplos estágios de cristalização da história magmática destas rochas. No intuito de estabelecer a fugacidade de oxigênio de magmas kimberlíticos naturais, $CaTiO_3$-perovskitas foram cristalizadas experimentalmente em equilíbrio com um líquido kimberlítico sintético em altas temperaturas e diferentes condições de pressão e de fugacidade de oxigênio. Os experimentos mostraram que a perovskita incorporou maiores quantidades de Fe^{3+} com o aumento da fO_2. A equação do oxigênio barômetro desenvolvida neste estudo pode ser aplicada em rochas kimberlíticas de diferentes condições de fO_2, que contêm $CaTiO_3$-perovskita e olivina. Na presente pesquisa, nós aplicamos este oxigênio barômetro em amostras do kimberlito Rosário do Sul, que é um kimberlito transicional localizado no limite sudoeste da Bacia do Paraná. Os dados de minerais deste kimberlito sugerem que sua fonte é um produto da reação de um líquido silicático-carbonatítico com o manto. Idades U-Pb de ~ 128Ma em $CaTiO_3$-perovskitas (Conceição et al., *in prep.*) revelam que o kimberlito Rosário do Sul provavelmente entrou em erupção logo após o vulcanismo da Província Paraná-Etendeka. Temperaturas de cristalização, pressões e fO_2 dos kimberlitos Rosário do Sul e Alfeu-I, outro importante kimberlito situado no sul do Brasil, foram calculadas. As condições de suas fontes foram estimadas usando diferentes métodos a partir das composições de olivinas, espinélios, $CaTiO_3$-perovskitas, granadas, ortopiroxênios e clinopiroxênios. As temperaturas, pressões e condições de fO_2 dos kimberlitos Rosário do Sul e Alfeu-I sugerem que eles foram transportados para a superfície em condições nas quais fluidos ricos em CO_2 podem reagir com o manto silicático e produzir carbonatos. A composição mineral e as condições de formação do kimberlito Rosário do Sul indicam que a sua fonte pode ter sido metassomatizada por fluidos provenientes da reciclagem de uma placa oceânica subductada durante a quebra do Gondwana e abertura do Atlântico Sul, logo depois do vulcanismo da Província Paraná-Etendeka. As condições de formação dos kimberlitos Rosário do Sul e Alfeu-I são usadas também para estimar o potencial destes kimberlitos em preservar diamantes.

Palavras-chave: kimberlitos; fugacidade de oxigênio; $CaTiO_3$-perovskita; oxigênio barômetro; heterogeneidade mantélica

ABSTRACT

Kimberlites are volcanic rocks which often contain diamonds, graphite and/or carbonate, and the stability of these minerals is directly influenced by the variability of oxygen fugacity (fO_2) of the magma during its ascent. Second Chakhmouradian and Mitchell (2000), $CaTiO_3$-perovskites may be used to unravel the conditions of some of the multiple stages of crystallization in the magmatic history of these rocks. In order to establish oxygen fugacities of natural kimberlititic magmas, we experimentally equilibrated $CaTiO_3$-perovskites with synthetic kimberlitic melts at high temperatures, different oxygen fugacities and different pressures. The experiments show that perovskite incorporates increasing amounts of Fe^{3+} with increasing fO_2. The oxygen barometer equation developed in this study can be applied in kimberlite rocks that contain $CaTiO_3$-perovskite and olivine from different fO_2 conditions. In the present research, we applied this oxygen barometer in the Rosário do Sul kimberlite samples, which is a transitional kimberlite located in the southwestern edge of the Paraná Basin. The mineral data of this kimberlite suggest that its source is a product of the reaction of a silicate-carbonate liquid in the mantle. U-Pb ages of ~ 128 Ma on $CaTiO_3$-perovskites (Conceição et al., *in prep.*) reveal that the Rosário do Sul kimberlite probably erupted just after the volcanism of Paraná-Etendeka Province. We calculated crystallization temperatures, pressures and oxygen fugacities (fO_2) of Rosário do Sul and Alfeu-I kimberlites, another important kimberlite situated in the South of Brazil. Their source conditions are estimated using different methods from olivines, spinels, $CaTiO_3$-perovskites, garnets, orthopyroxenes and clinopyroxenes compositions. The calculated temperature, pressure and fO_2 values of Rosário do Sul and Alfeu-I kimberlites suggest that they were transported to the surface under fO_2 conditions in which CO_2-rich fluids may react with mantle silicates to produce carbonates. The mineral composition and fO_2 conditions of Rosário do Sul kimberlite indicate that its source may have been metasomatized by fluids generated from the recycling of a subducted oceanic plate during the Gondwana breakup and the South Atlantic opening, just after the Paraná-Etendeka Province volcanism. The source conditions of Rosário do Sul and Alfeu-I kimberlites are also used to estimate the potential of these kimberlites to preserve diamonds.

Keywords: kimberlites; oxygen fugacity; $CaTiO_3$-perovskite; oxygen barometer; mantle heterogeneity

SUMÁRIO

ESTRUTURA DA TESE

Esta tese de Doutorado está estruturada em torno de artigos publicados em periódicos ou publicações equivalentes. Consequentemente, sua organização compreende os seguintes capítulos:

- Introdução sobre o tema e descrição do objeto da pesquisa de Doutorado, onde estão sumarizados os objetivos da pesquisa desenvolvida, bem como o estado da arte sobre o tema de pesquisa;
- Metodologia de petrologia experimental utilizada para o desenvolvimento de parte da presente pesquisa;
- Análise integradora dos três manuscritos submetidos a periódicos internacionais, com corpo editorial permanente e revisores independentes, escritos pelo autor durante o desenvolvimento de seu Doutorado;
- Referências bibliográficas utilizadas na tese.

1. INTRODUÇÃO

1.1 Kimberlitos Rosário do Sul e Alfeu-I

Kimberlitos são rochas subsaturadas em sílica (de 30 a 40 peso% SiO_2), que contêm abundante quantidade de CO_2 e água, bem como altas concentrações de elementos incompatíveis (Mitchell, 1986). Segundo muitos pesquisadores (e.g., Wedephohl e Muramatsu, 1979), são rochas formadas a partir de baixo grau de fusão parcial de peridotitos do manto superior, em profundidades de cerca de 100km (equivalentes a aproximadamente 3GPa de pressão), e que geralmente ascendem para a superfície em alta velocidade (e.g. Bailey, 1993).

No Brasil, as principais ocorrências kimberlíticas são encontradas nas regiões central e noroeste como, por exemplo, os corpos kimberlíticos da área de Juína, no estado do Mato Grosso do Sul (Kaminsky, et al., 2009). No entanto, estudos recentes apontam para um magmatismo kimberlítico na região sul do país (Conceição et al., *in prep.*; Chaves et al., 2014; Adrião, 2015; Provenzano, 2016; Conceição et al., *in prep.*), com a presença de kimberlitos como o Rosário do Sul e o Alfeu-I, estudados na presente tese.

O kimberlito Rosário do Sul, que é um kimberlito transicional (Conceição et al., *in prep.*) pertencente à Província Kimberlítica de Rosário do Sul, ocorre encaixado em arenitos Fanerozóicos da Formação Pirambóia e está localizado na porção sudeste da bacia do Paraná, na região sul do Brasil (Adrião, 2015 e Edler et al., 1998) (Fig. 1). Idades U-Pb de aproximadamente 128Ma, feitas em $CaTiO_3$-perovskitas (Conceição et al., *in prep.*), indicam que este kimberlito entrou em erupção logo após o vulcanismo da Província Paraná-Etendeka, ocorrido a aproximadamente 132Ma, o que sugere que a fonte de calor responsável pela ascensão deste kimberlito poderia estar relacionada ao processo que desencadeou o magmatismo Paraná-Etendeka em um ambiente extensional. Esta hipótese indica a presença de uma heterogeneidade mantélica na fonte dos basaltos continentais da Bacia do Paraná devido à percolação de líquidos carbonatíticos.

Outros eventos alcalinos ocorrem na borda da Província Paraná-Etendeka, como o complexo de Lages, de idade próxima a 70-77Ma (Gibson et al., 1999), e o Complexo Araxá, com 89Ma (e.g. Hasui e Cordani, 1968), que incluem carbonatitos e lamprófiros do Cretáceo Superior (de 60 a 90Ma). Segundo Comin-Chiaramonti et al. (2002), o complexo

alcalino-carbonatítico de Anitápolis do Cretáceu Inferior (aprox. 132Ma), que está localizado a 100 km de distância dos basaltos do magmatismo Paraná-Etendeka, e seu análogo do Cretáceo Inferior, Arco da Ponta Grossa, são concomitantes às lavas toleíticas da Bacia do Paraná, sugerindo sua ocorrência durante os estágios iniciais de abertura do rift, antes da separação continental.

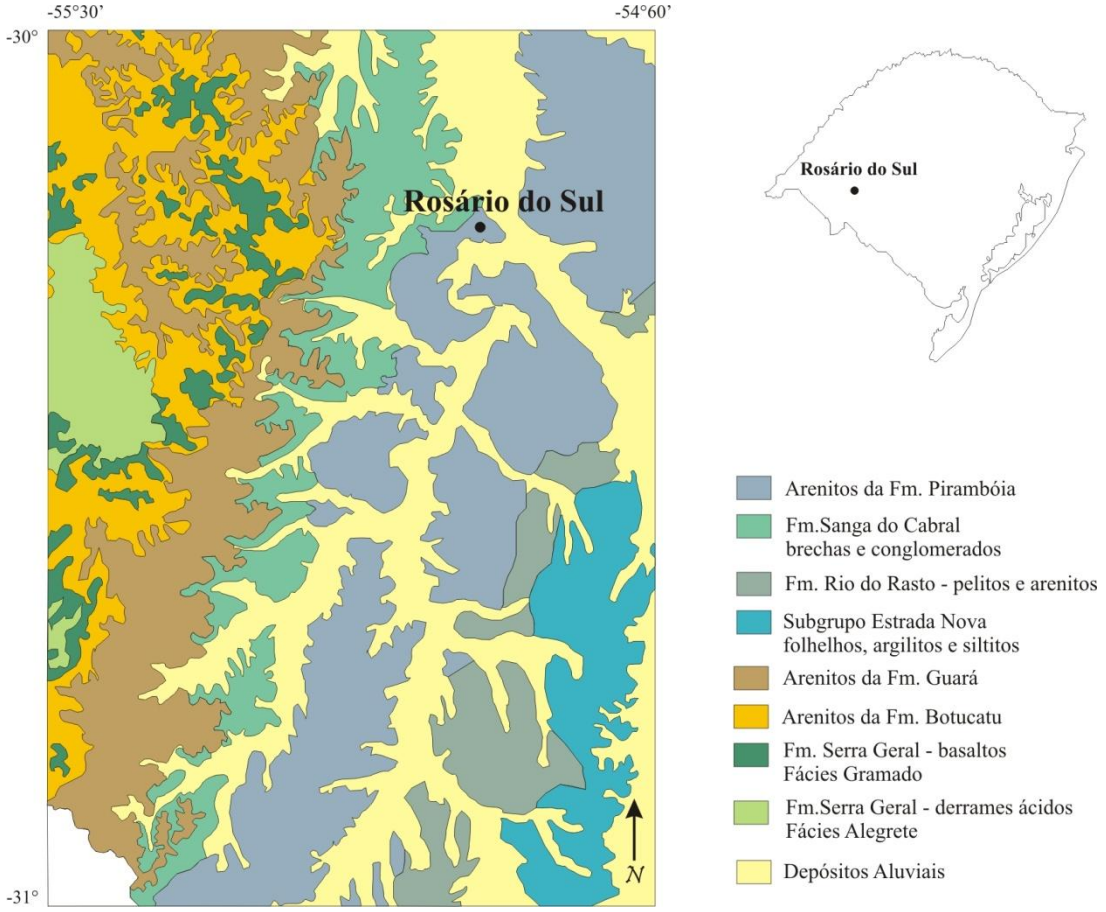

Fig. 1: Mapa geológico com a localização do kimberlito Rosário do Sul (fonte: Mapa geológico do Estado do Rio Grande do Sul, Escala 1:750.000- CPRM).

O kimberlito Alfeu-I é uma chaminé vulcânica intrusiva na Suíte Pinheiro Machado do domínio Pelotas, que ocorre na porção sul do escudo Sul-Riograndense (Fig. 2), a cerca de 200 km de distância do kimberlito Rosário do Sul. Segundo Provenzano (2016), ainda que dados de petrografia e mineralogia do kimberlito Alfeu-I sejam compatíveis aos kimberlitos do Grupo II, dados de química mineral indicam características transicionais entre

kimberlitos do Grupo I e II e lamproítos, indicando que a petrogênese do kimberlito Alfeu-I é similar a outros magmas potássicos sem uma forte afinidade com um grupo em particular.

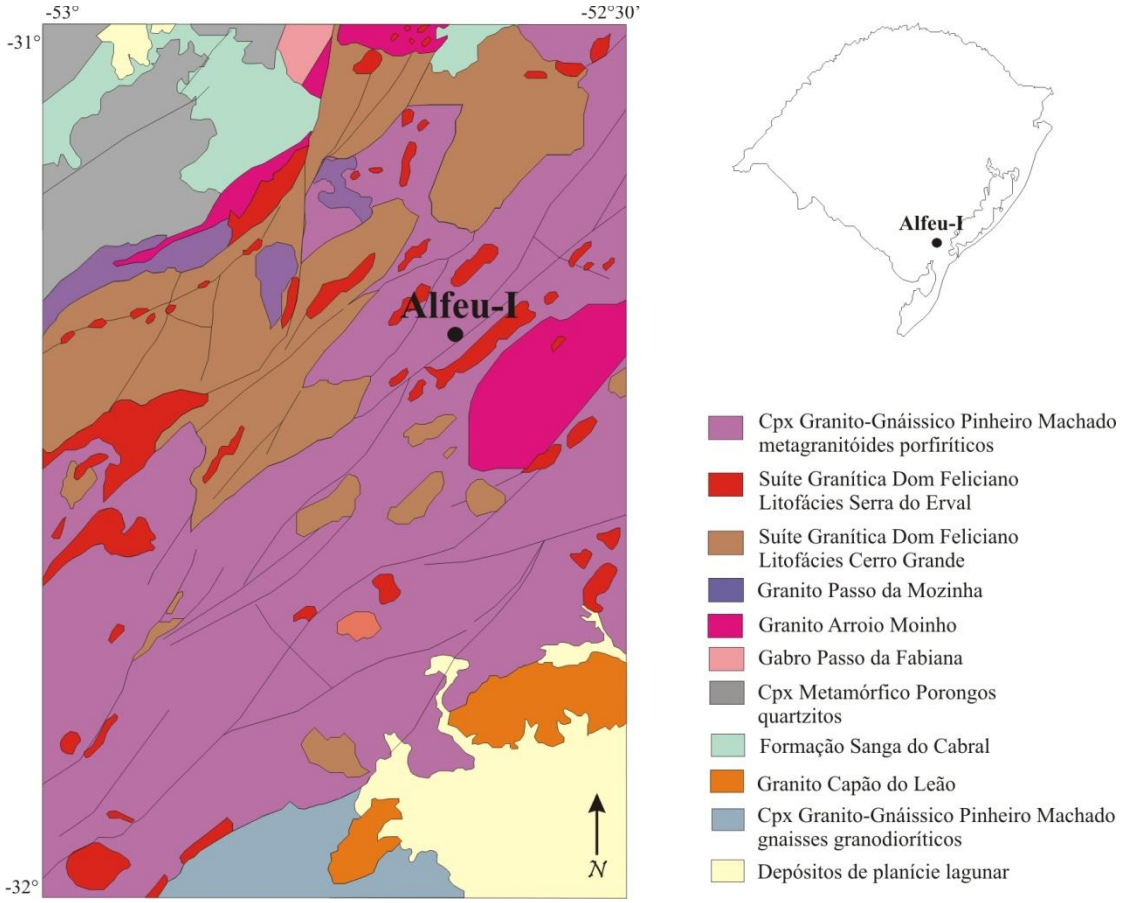

Fig. 2: Mapa geológico com a localização do kimberlito Alfeu-I (fonte: Mapa geológico do Estado do Rio Grande do Sul, Escala 1:750.000- CPRM).

1.2 Fugacidade de oxigênio, comportamento do ferro e estrutura da $CaTiO_3$-perovskita

Uma série de variáveis são responsáveis pelas características da assembléia mineral em uma rocha kimberlítica, como: composição do líquido, pressão, temperatura e fugacidade de oxigênio (fO_2). Desempenhando um importante papel na determinação da composição de qualquer fase fluida associada a rochas ígneas e metamórficas, a fugacidade de oxigênio é medida em unidade de pressão e definida como atividade química do oxigênio (Clark, 1999). A fO_2 diminui no manto com o aumento da pressão, variando de valores próximos do

tampão IW (ferro-wustita), em regiões mais profundas, abaixo de aproximadamente 250 km de profundidade (Rohrbach e Schmidt, 2011), até valores mais altos, como os do tampão HM (hematita-magnetita), em regiões mais próximas da superfície (Fig. 3). Estes tampões, ou *buffers*, são reações que controlam a relação entre fugacidade de oxigênio e temperatura.

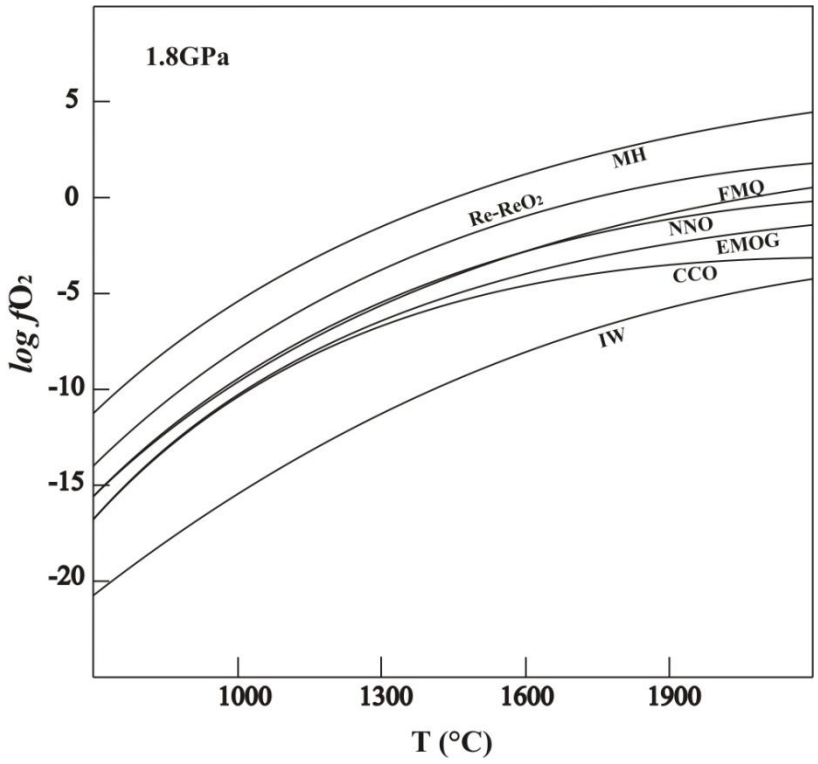

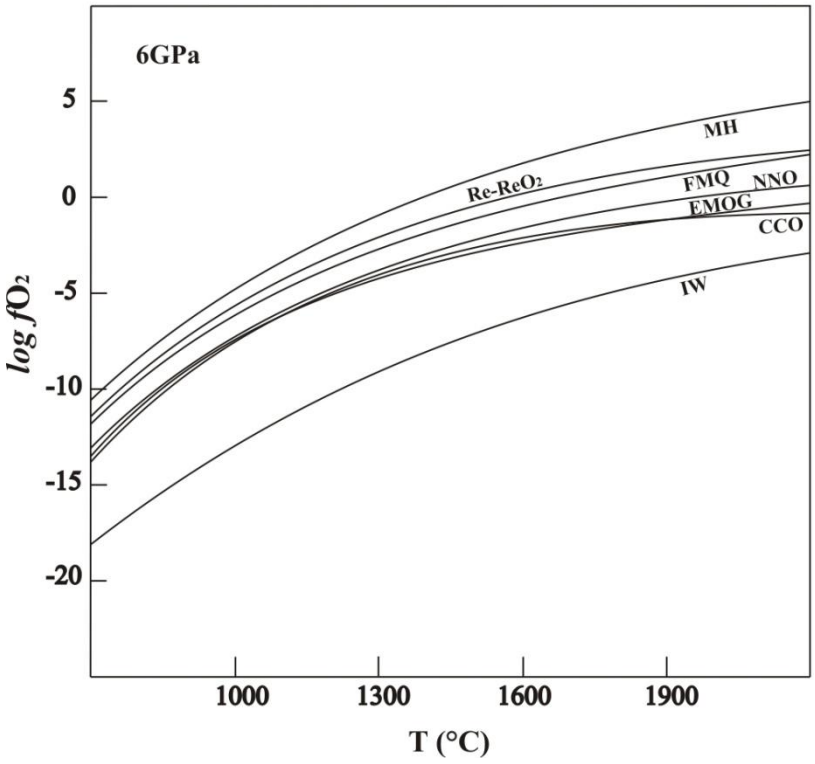

Fig. 3: Diagrama de comparação logfO_2 *versus* temperatura, a 1.8 e 6 GPa de pressão, dos seguintes tampões (*buffers*): MH (magnetita-hematita) (Ballhaus, 1991), Re-ReO_2 (rênio-óxido de rênio) (Campbell, 2009), FMQ (faialita-magnetita-quartzo) (Ballhaus, 1991), NNO (níquel-óxido de níquel) (Ballhaus, 1991), EMOG (enstatita-magnetita-olivina-grafite) (Zhao et al., 1999), CCO (carbono-monóxido de carbono) (Frost, 1997) e IW (ferro-wustita) (Ballhaus, 1991).

Líquidos como os kimberlíticos, derivados da fusão parcial do manto, poderiam ser redutores devido às condições de onde são formados, mas tornam-se mais oxidantes do que o manto cristalino ao seu redor, durante sua ascenção e erupção. Isto pode ser explicado devido a mudanças na fO_2. Estes líquidos comumente fracionam olivina e possivelmente piroxênio durante sua ascenção, diminuindo a concentração de Fe^{2+} no líquido, que entra na estrutura destes silicatos, e promovendo relativa oxidação durante a segregação do líquido e sua ascenção até a superfície (Ballhaus, 1993).

Segundo Kress e Carmichael (1988), a fO_2 governa a reação de oxidação do ferro em líquidos silicáticos. No entanto, o particionamento do ferro entre ferro férrico (Fe^{3+}) e ferro ferroso (Fe^{2+}) é influenciada também por outros fatores, como a concentração de álcalis (Carmichael e Nicholls, 1967). Rochas alcalinas como kimberlitos tendem a apresentar alto teor de Fe^{3+}, como confirmado por Fudali (1965).

A fO_2 aumenta com o aumento da temperatura devido à abundância de oxigênio livre no fluido, que ocorre através da dissociação de moléculas como H_2O, CO_2 ou SO_2, da reação de transformação do N_2 em NH_3 em fluidos aquosos, da precipitação do grafite ou da redução do ferro férrico (Frost, 1991). Além disso, em profundidades de cerca de 140 a 175 km, fluidos podem mudar de dominantemente reduzidos (H_2O–CH_4) para dominantemente oxidados (H_2O–CO_2) devido a mudanças nas condições de fO_2 do manto sob estas profundidades (Zhang e Duan, 2009). A preservação de diamantes em rochas kimberlíticas depende das condições de fugacidade de oxigênio do manto e do líquido kimberlítico. O estado de oxirredução do manto determina se o carbono está presente como forma oxidada (CO_2, carbonato ou líquido carbonatítico), ou como forma reduzida (grafite, diamante ou metano) (Rohrbach e Schmidt, 2011). Sendo assim, em condições de baixa fO_2, diamantes têm uma maior possibilidade de serem preservados em relação a condições de alta fO_2, quando os diamantes podem ser mais facilmente reabsorvidos ou mesmo desaparecer (Bellis e Canil, 2007).

$CaTiO_3$-perovskita é uma fase acessória muito comum em rochas ígneas com baixo teor de SiO_2 e altos teores de álcalis, CO_2 e H_2O. De acordo com Bellis e Canil (2007), $CaTiO_3$-perovskitas cristalizadas em líquidos kimberlíticos podem registrar se as condições de fugacidade de oxigênio da rocha são altas (de uma fonte mais oxidada ou produto de sua interação com um fluido rico em CO_2 e H_2O) ou baixas (de uma fonte mais redutora ou produto de um mecanismo envolvendo um fluido rico em carbono).

Na estrutura da $CaTiO_3$-perovskita (Fig. 4), o sítio dodecaédrico é ocupado por Ca^{2+} e o sítio octaédrico é ocupado por Ti^{4+} ou Fe^{3+}. O ferro incorporado no sítio octaédrico é normalmente ferro férrico (Fe^{3+}) (Muir et al., 1984; Mitchel et al., 1998) devido à cristalização da olivina ocorrer primeiro e incorporar a maior parte do Fe^{2+}, deixando para trás o Fe^{3+} no líquido para a posterior cristalização da perovskita. Desta forma, a razão Fe^{3+}/Fe^{2+} do sistema pode ser calculada medindo o conteúdo de Fe na perovskita (como Fe^{3+}) (McCammon et al., 2004) e na olivina (como Fe^{2+}). Bellis e Canil (2007) mostraram uma correlação positiva entre fO_2 e o conteúdo de Fe_2O_3 das perovskitas, implicando que, com o aumento da fO_2, mais Fe existe no líquido como Fe^{3+}, particionando mais facilmente na perovskita. Estes autores também encontraram uma menor variabilidade no conteúdo de Fe_2O_3 da perovskita em condições abaixo de $\Delta NNO = -3.5$ (fO_2 relativa ao tampão níquel-óxido de níquel), já que, nesta condição de fO_2, há provavelmente pouco Fe^{3+} disponível no líquido.

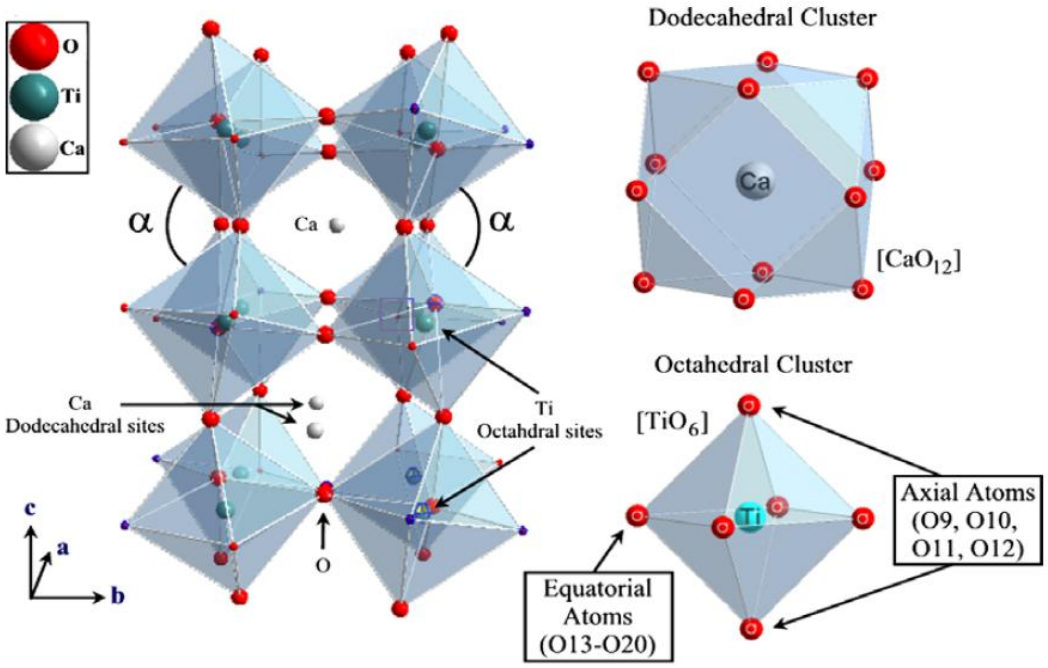

Fig. 4: Modelo esquemático da estrutura do mineral perovskita: sítios dodecaédricos e octaédricos com os átomos Ca e Ti, respectivamente (Moreira et al., 2009).

1.3 Objetivos da pesquisa

Com o objetivo de estabelecer as fugacidades de oxigênio de magmas kimberlíticos naturais, $CaTiO_3$-perovskitas forma equilibradas experimentalmente em líquidos kimberlíticos sintéticos em altas temperaturas, diferentes fO_2 e diferentes pressões. Uma vez que Bellis e Canil (2007) desenvolveram seus experimentos a 1atm de pressão, o objetivo deste estudo é o desenvolvimento de um oxigênio barômetro que seja usado como ferramenta para reconstruir as condições de oxirredução (fO_2) de um magma kimberlítico em altas pressões: 1.8 GPa (cerca de 65 km de profundidade) e 6 GPa (cerca de 210 km de profundidade), considerando as proporções modais de olivina e perovskita dos experimentos. Estas condições de pressão são consistentes com a profundidade das ocorrências kimberlíticas, uma vez que inclusões deste mineral já foram registradas em diamantes de kimberlitos originados em grandes profundidades (como no kimberlito de Juína; Kaminski et al., 2001). Considerando que olivinas somente incorporam Fe^{2+}, e perovskitas somente incorporam Fe^{3+}, é possível calcular a razão Fe^{3+}/Fe^{2+} e a fO_2 dos

líquidos kimberlíticos, a partir de medidas de microssonda eletrônica realizadas nestes minerais.

O presente estudo também teve como objetivo a determinação da mineraloquímica do kimberlito Rosário do Sul, a partir de análises de microssonda eletrônica de elementos traços e maiores, em sua assembleia mineral, tendo como meta fazer considerações a respeito da fonte deste kimberlito e sua relação com o Magmatismo do Paraná.

Para examinar as temperaturas de cristalização e fugacidades de oxigênio do líquido kimberlítico Rosário do Sul, o oxigênio-geotermobarômetro de olivina-espinélio de Ballhaus et al., (1991) foi aplicado juntamente com o oxigênio barômetro de Carniel et al., (*submitted*). Para determinar a razão Fe^{3+}/Fe^{2+} do líquido, foi utilizada a equação de Carniel et al., (*submitted*), com o objetivo de obter um melhor entendimento do estado de oxirredução da fonte do magma e da consequente preservação de diamantes. Considerando que não há perovskitas na assembleia mineral do kimberlito Alfeu-I, foi utilizado o oxigênio-geotermobarômetro de olivina-espinélio de Ballhaus et al., (1991) com a finalidade de estimar a temperatura de cristalização e a fO_2 deste corpo kimberlítico. A temperatura foi também estimada com o geotermômetro de ortopiroxênio-clinopiroxênio de Wells (1977), e a pressão foi estimada a partir do geotermobarômetro de granada-ortopiroxênio de Nickel and Green (1985).

2. PETROLOGIA EXPERIMENTAL

Os experimentos em condições oxidantes foram realizados usando cápsulas de platina (Pt) com uma folha de rênio (Re), de aproximadamente 3mm, em seu interior (Fig. 5). A folha de Re serve para limitar que a fugacidade de oxigênio do experimento fique próxima do tampão Re-ReO_2 (Campbell et al., 2009), bem como para evitar a perda de Fe da amostra para a cápsula. Nos experimentos em condições redutoras de fugacidade de oxigênio, foram utilizadas cápsulas de platina com cápsulas de grafite em seu interior, restringindo sua fO_2 para próximo do tampão C-CO (Frost, 1997).

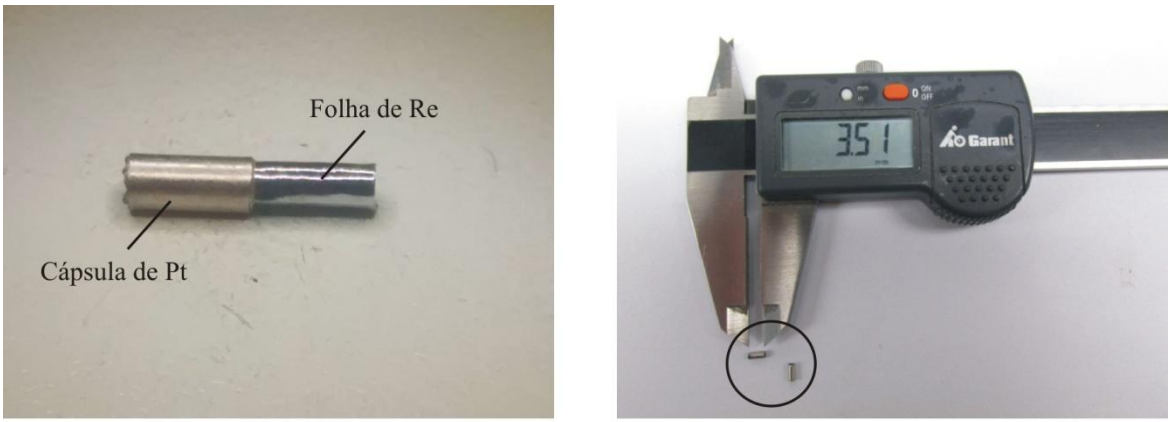

A B

Fig. 5: (A) cápsula de Pt forrada internamente com folha de Re, utilizada para experimentos em condições oxidantes; (B) cápsulas de Pt já soldadas, prontas para serem utilizadas nos experimentos, com tamanho de 3.51mm.

Os experimentos a 1.8 GPa foram realizados em uma prensa pistão-cilindro do Instituto de Mineralogia da Universidade de Münster (Prowatke and Klemme, 2006) (Fig. 6A). A configuração consiste de um cilindro de grafite, que serve como forno, colocado dentro de um cilindro de vidro-*pyrex*, que por sua vez é posicionado dentro de um cilindro de pirofilita. O vidro-*pyrex* e a pirofilita são materiais macios que garantem a distribuição da pressão de forma uniforme em todas as direções dentro da amostra, que está localizada aproximadamente no centro da configuração, de forma que se possa chegar o mais próximo possível de uma pressão hidrostática. A cápsula soldada com a amostra é inserida dentro de um cilindro de Al_2O_3 que é colocado, juntamente com outro cilindro de Al_2O_3 maciço, dentro do forno de grafite (Fig. 6B). Esta configuração é posicionada dentro de um cilindro de aço, com uma tampa de grafite na base, para conduzir a corrente, e um termopar no topo (Fig. 6C). Posteriormente, este cilindro de aço vai encaixado dentro da prensa pistão-cilindro.

A configuração utilizada foi calibrada usando as reações: faialita = quartzo + ferrosilita (Bohlen et al., 1980), e pirocromita + quartzo = enstatita + eskolaita (Klemme and O'Neill, 1997; Klemme and O'Neill, 2000). Os experimentos foram realizados usando a rotina de processamento de Klemme (2010): inicialmente, uma pressão de cerca de 0.5 GPa é aplicada; em seguida, a amostra é aquecida até cerca de 400ºC para amaciar o vidro; por último, pressão e temperatura são aumentadas, gradualmente e simultaneamente, até alcançar os parâmetros desejados para cada experimento. A pressão é manualmente mantida em nível constante (±0.05 GPa) durante os experimentos, usando um sistema hidráulico.

Temperaturas são medidas com termopares $W_{95}Re_5$-$W_{74}Re_{26}$ inseridos axialmente na configuração em tubos de Al_2O_3 de quatro furos. A amostra é colocada no ponto mais quente da configuração para evitar um maior efeito da variação do gradiente térmico, que é menor do que 20°C ao longo do comprimento da cápsula. A duração dos experimentos foi de 24 horas para assegurar o equilíbrio entre as fases cristalinas e os líquidos coexistentes.

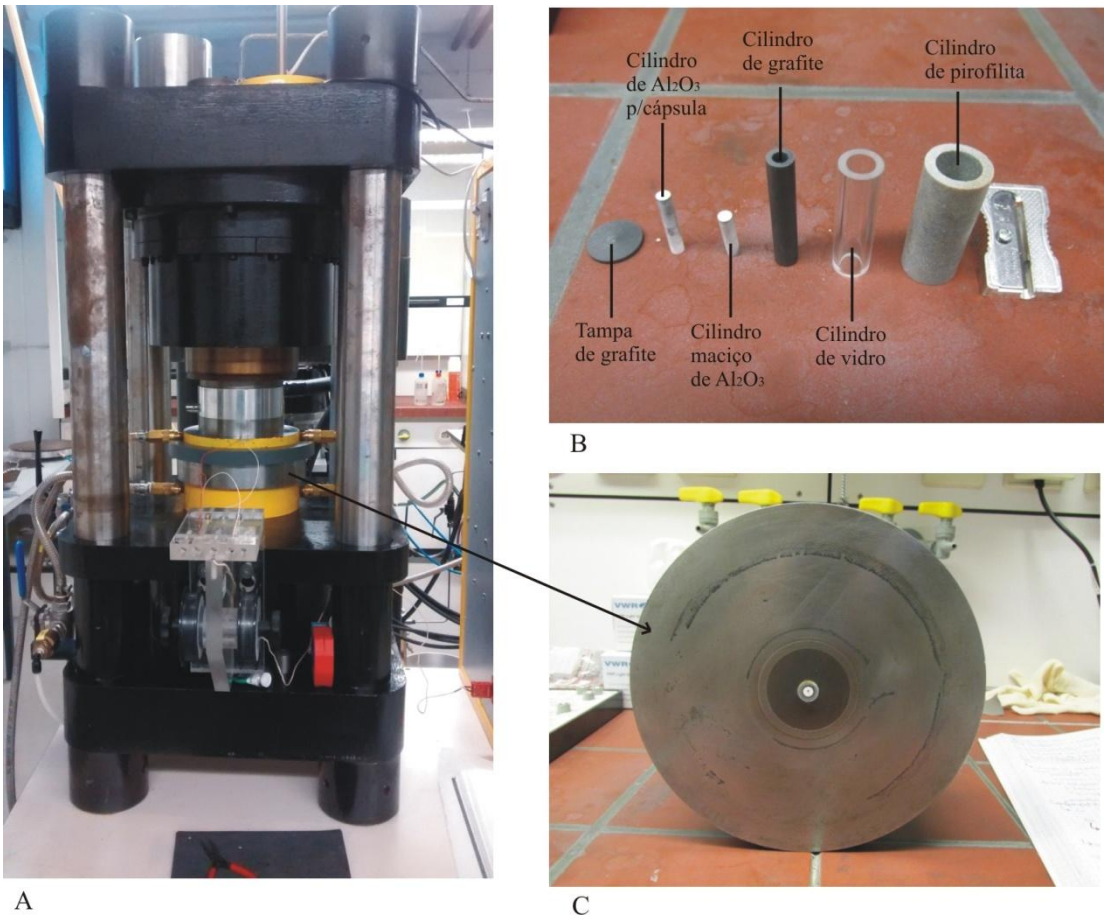

Fig. 6: (A) prensa pistão-cilindro, utilizada em experimentos a 1.8 GPa; (B) configuração utilizada nos experimentos a 1.8 GPa; (C) cilindro com a configuração em seu interior, pronto para ser colocado na prensa.

Os experimentos a 6 GPa foram realizados em uma prensa multi-anvil, do tipo Walker, de 1000 ton, do Instituto de Mineralogia da Universidade de Münster (Fig. 7A), usando cubos de carbeto de tungstênio (WC) de 25.4 mm, e configurações 18/12 (octaedros Aremco Ceramacast^{TM} com arestas de 18 mm de comprimento e truncamentos de 12 mm de comprimento) (Fig. 7C). A configuração consiste em um forno de grafite, cilindros de Al_2O_3 e duas tampas de molibdênio, na base e no topo, para garantir o contato elétrico entre a

amostra e os cubos de WC (Fig. 7B). A configuração 18/12 foi calibrada usando as transições de fases do metal bismuto (Bi) em temperatura ambiente, bem como as transições de fase do quartzo para coesita, e $CaGeO_3$-granada para $CaGeO_3$-perovskita, a 1100°C. A temperatura é medida com o termopar $W_{95}Re_5$-$W_{75}Re_{25}$. Pressão e temperatura são mantidas constantes durante o experimento, usando controladores *Eurotherm*. As incertezas nas medidas de temperatura são resultantes de pequenas flutuações durante o experimento, e o gradiente térmico, na configuração, é estimado como sendo ±15°C.

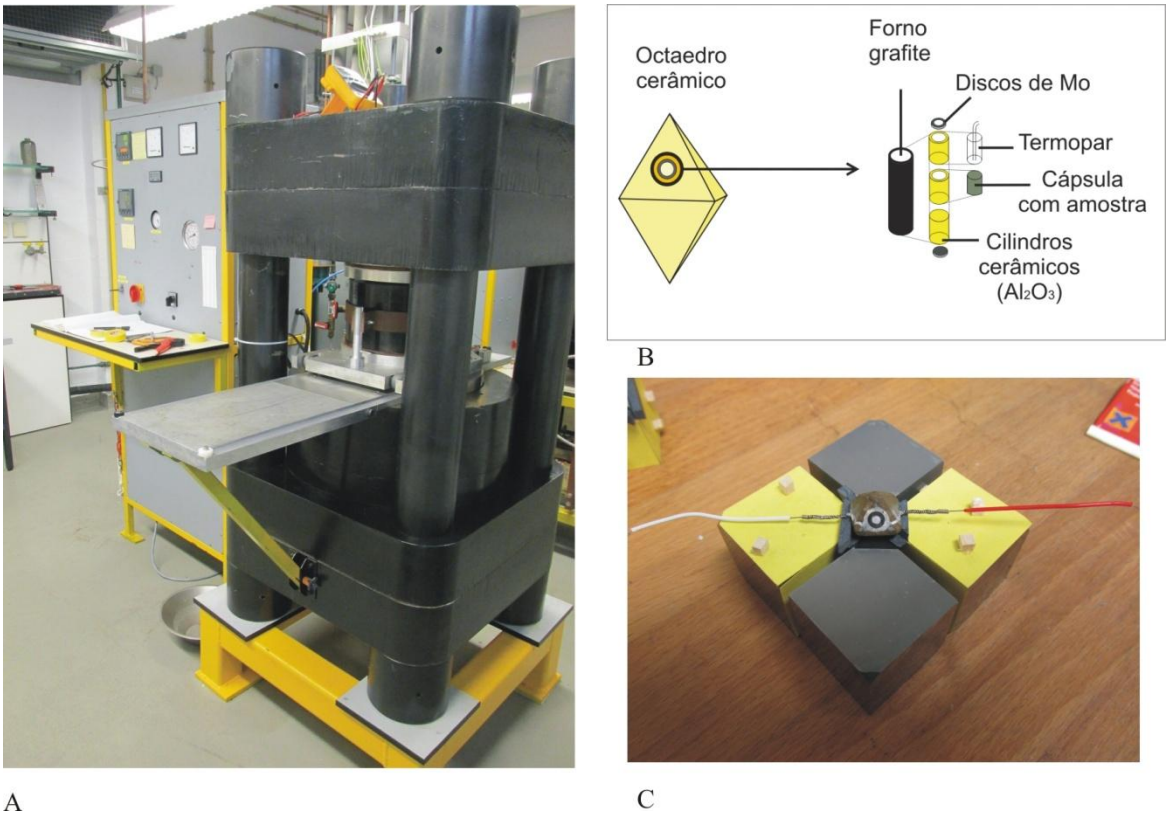

Fig. 7: (A) prensa multi-anvil, utilizada em experimentos a 6 GPa; (B) octaedro utilizado nos experimentos a 6 GPa; (C) octaedro montado com o termopar e colocado entre os cubos.

3. ANÁLISE INTEGRADORA DOS MANUSCRITOS SUBMETIDOS

3.1 Manuscrito: "The effects of redox conditions on ferric iron in $CaTiO_3$-perovskite from kimberlitic magmas"

Submetido à revista científica *Chemical Geology*

Assunto: CHEMGE10705: Notice of manuscript number

Remetente: Chemical Geology eesserver@eesmail.elsevier.com

Para: larissa.colombo@ufrgs.br; larissageo@gmail.com

Responder para: Chemical Geology eesserver@eesmail.elsevier.com

Data: 2017-08-01 23:29

Dear Miss Carniel,

Your submission entitled "The effects of redox conditions on ferric iron in CaTiO3-perovskite from kimberlitic magmas" has been assigned the following manuscript number: CHEMGE10705.

You will be able to check on the progress of your paper by logging on https://ees.elsevier.com/chemge/ as Author.

Thank you for submitting your work to this journal.

Kind regards,

Chemical Geology

The effects of redox conditions on ferric iron in $CaTiO_3$-perovskite from kimberlitic magmas

L.C.Carniel[1*], S. Klemme[2], R. V. Conceição[1], A. Rohrbach[2], J.Berndt[2]

[1] Instituto de Geociências, Universidade Federal do Rio Grande do Sul, Brazil

[2] Institut für Mineralogie, Westfälische Wilhelms-Universität Münster, Germany

*Corresponding author: larissa.colombo@ufrgs.br

Abstract

Kimberlites are volcanic rocks which often contain diamonds, graphite and/or carbonate, and the stability of these minerals is directly influenced by the variability of oxygen fugacity (fO_2) of the magma during its ascent. It is well known that kimberlites experience multiple stages of crystallization under changing conditions during ascent, and it has been suggested that natural perovskites may be used to unravel parts of the magmatic history of these rocks (Chakhmouradian and Mitchell 2000). In order to establish oxygen fugacities of natural kimberlititic magmas, we experimentally equilibrated perovskites with synthetic kimberlitic melts at high temperatures, different oxygen fugacities and different pressures. The experiments show that perovskite incorporates increasing amounts of Fe^{3+} with increasing fO_2. Given that olivine only incorporates Fe^{2+}, and perovskite only incorporates Fe^{3+}, it is possible to calculate an Fe^{3+}/Fe^{2+} ratio of the kimberlitic melt from Fe in perovskite and Fe in olivine electron microprobe measurements. The results indicate that the Fe-concentration in perovskite and in the melt of a kimberlite critically depends on fO_2. The oxygen barometer equation developed in this study can be applied in kimberlite rocks that contain perovskite and olivine from different fO_2 conditions.

Keywords: kimberlite; oxygen fugacity; perovskite; olivine; ferric iron

Highlights:

- Since kimberlites experience multiple stages of crystallization under changing conditions during ascent, the Fe content and modes of perovskites and olivines are used as an important tool to estimate the redox conditions of these rocks.
- Given that olivine only incorporates Fe^{2+}, and perovskite only incorporates Fe^{3+}, it is possible to calculate an Fe^{3+}/Fe^{2+} ratio of the kimberlitic melt.
- The results indicate that the Fe-concentration in perovskite and in the melt of a kimberlite critically depends on fO_2.
- The oxygen barometer equation developed in this study can be applied in kimberlite rocks that contain perovskite and olivine from different fO_2 conditions.

1. Introduction

Oxygen fugacity (fO_2) is one of the variables, together with melt composition, pressure and temperature that governs the mineral assemblages in the rock, and plays an important role in determining the composition of any fluid phase associated with igneous and metamorphic rocks. Although the upper mantle is affected by metasomatism, partial melting, and recycling of oxidized material by subduction (Frost and McCammon, 2008), it is still the most intriguing part of the Earth to measure the oxygen fugacity. With increasing pressure, fO_2 decreases in the mantle, and in deeper regions, below ~ 250km depth, fO_2 can only vary from values around the IW (iron-wüstite) buffer (Rohrbach and Schmidt, 2011).

The oxygen fugacity also indicates whether iron is present in its native state or as a divalent or trivalent ion, if it is included in a silicate or in an oxide (Frost, 1991). According to Kress and Carmichael (1988), the iron oxidation reaction in silicate melts is commonly expressed in terms of the reaction:

$2FeO\ (melt) + 1/2O_2\ (gas) = Fe_2O_3\ (melt)$

The buffering capacity of mantle material depends on the total iron content and the oxidation state of iron (Arculus, 1985; Ballhaus, 1993). In natural liquids, the partitioning of iron between ferric iron (Fe^{3+}) and ferrous iron (Fe^{2+}) is influenced by different factors. One of them is alkali concentration (Carmichael and Nicholls, 1967). Alkaline rocks as kimberlites tend to present high ferric iron content, as studied by Fudali (1965), who confirmed that alkalis tend to increase the ferric iron content of the melt.

The oxygen fugacity of all buffers increases with increasing temperature due to the increasing devolatilization of oxygen. The sources of oxygen are the result of H_2O, CO_2, or SO_2 dissociation, the reaction of N_2 into NH_3 in aqueous fluids, the precipitation of graphite or the reduction of ferric iron (Frost, 1991), beyond the free oxygen in the fluid. Furthermore, around 140 to 175 km depth, fluids can change from dominantly reduced (H_2O–CH_4) to dominantly oxidized (H_2O–CO_2) due to the changes in the fO_2 conditions of the mantle under these depths (Zhang and Duan, 2009).

Melts like kimberlites, derived from partial melting of the mantle, could be reducing in the deep mantle but become more oxidized than crystalline mantle counterpart during ascent or before the eruption. This can be explained due to a change in fO_2 buffering mechanism. Melts are likely to fractionate some olivine and possibly pyroxene during ascent (i.e. loose components with a bulk $Fe^{3+}/\Sigma Fe$ ratio lower than that of the melt), and this process will promote relative oxidation when the melt segregates and rises to the surface (Ballhaus, 1993). The diamond preservation in kimberlite rocks depends on the oxygen fugacity conditions of the mantle and the kimberlitic melts. The redox state of the mantle determines if carbon is present as CO_2, carbonate or carbonatite melt (oxidized form), or as graphite, diamond or methane (reduced form) (Rohrbach and Schmidt, 2011). Therefore, in

conditions with low fO_2, diamonds can be preserved. However, in conditions with high fO_2, diamonds can be reabsorbed or even disappear.

$CaTiO_3$-perovskite is an accessory phase very common in low SiO_2 igneous rocks. As kimberlites are low SiO_2 and high alkalis, CO_2 and H_2O rocks, $CaTiO_3$-perovskite is easily found in their groundmass. According to Canil and Bellis (2007), perovskites from kimberlites can record if the oxygen fugacity conditions of this rock are extremely high (i.e. an oxidized mantle source) or very low (i.e. a mechanism involving buffering by carbon-fluid equilibria or a very reduced mantle source).

In the $CaTiO_3$-perovskite structure, the dodecahedral site is occupied by Ca^{2+} and the octahedral site is occupied by Ti^{4+} or Fe^{3+}. The iron incorporated in the octahedral site is mainly ferric iron (Fe^{3+}) (Muir et al., 1984; Mitchel et al., 1998) because olivine crystallizes first and incorporates most of the Fe^{2+}, leaving behind Fe^{3+} in the liquid for the perovskites. Therefore, the Fe^{3+}/Fe^{2+} ratio in the system can be calculated measuring Fe in perovskite (as Fe^{3+}) (McCammon et al., 2004) and in olivine (as Fe^{2+}). Bellis and Canil (2007) found a positive correlation between fO_2 and the Fe_2O_3 content of perovskites, implying that with increasing fO_2, more Fe exists in the liquid as Fe^{3+}, partitioning easily into perovskite. They also found less variability in the Fe_2O_3 content of perovskite at conditions below of $\Delta NNO = -3.5$, because at this fO_2 there is probably very little Fe^{3+} available in the liquid. Since Bellis and Canil (2007) developed their experiments at 1 atm pressure, the aim of this study is the development of a tool to reconstruct the redox conditions (fO_2) of a kimberlitic magma at high pressures: 1.8 GPa (around 65 km depth) and 6 GPa (around 210 km depth); considering the modal proportions of olivine and perovskite in the runs. This conditions are consistent with depth of kimberlites occurrences, since $Ca(Ti,Si)O_3$ inclusions have been recorded in very deep diamonds from kimberlites (i.e. Juina kimberlite) (Kaminski, et.al, 2001).

2. Experimental methods

2.1. **Starting material and experiments**

Three different synthetic kimberlitic compositions (Table 1) were produced from reagent grade oxides (SiO_2, TiO_2, Al_2O_3), hydroxides ($Mg(OH)_2$) and carbonates ($CaCO_3$, K_2CO_3), which were homogenized under acetone in an agate mortar. Compositions were subsequently dehydrated and decarbonated in a Pt crucible by stepwise heating to 1000°C. FeO was added to the mixtures after the decarbonation to avoid iron oxidation. In the LCM-10 synthetic kimberlitic composition, H_2O (from $Mg(OH)_2$) and CO_2 (from $CaCO_3$) were also added to the mixture after decarbonation. The starting compositions are similar to the compositions used by Bellis and Canil (2007) to facilitate comparison. To promote the crystallization of $CaTiO_3$ perovskite, TiO_2 and CaO were added to the synthetic kimberlitic composition LCM-5. LCM-7 is a composition more similar to a natural kimberlite, and LCM-10 is similar to LCM-5 but with additional TiO_2, CaO and also 3wt.% of H_2O and 4 wt.% of CO_2 to investigate whether volatiles have a significant influence on perovskite stability and composition. All starting material compositions are given in Table 1.

Start. material	**SiO_2**	**TiO_2**	**Al_2O_3**	**FeO***	**CaO**	**MgO**	**K_2O**	**H_2O**	**CO_2**
LCM-5	29.6	23.7	2.95	11.83	17.7	11.83	2.37	-	-
LCM-7	34.2	7.8	0.3	13.4	22.2	21.3	-	-	-
LCM-10	25	25	2	5	24	10	2	3	4

Table 1: Starting compositions (wt.%) used in the experiments. *all Fe added as FeO.

We carried out experiments at different pressures (1 atm, 1.8 GPa, 6 GPa), temperatures (1250-1350°C), and different oxygen fugacities using a gas mixing in the 1 atm experiments, and solid buffer such as Re-ReO_2 and C-CO in high pressure experiments.

The experiments were performed at the Institut für Mineralogie, Universität Münster. Table 2 summarizes the run conditions and the resulting phases. The experiments at atmospheric pressure were performed in a conventional vertical gas-mixing furnace. The samples were mounted on Pt loops, which were suspended in the hot zone of the vertical furnace (Gero GmbH, Germany). For oxidizing conditions, the experiment was run in air (ΔNNO = +6.3, fO_2 relative to the nickel-nickel oxide (NNO) buffer; Frost, 1991), and more reducing conditions, (ΔNNO = -2.09; Frost, 1991), were achieved by mixing CO and CO_2 in appropriate ratios (Deines, 1974). All experiments were run for 24 hours.

run#	**T(°C)**	**Pressure**	**d(h)**	**Buffer**	**Start mat.**	**ΔNNO**	**Phases present**
F-2	1250	1 atm	24	Re-ReO_2	LCM-7	6.33	ol, pv, cpx, sp, melt
F-3	1250	1 atm	24	C-CO	LCM-7	-2.09	ol, pv, cpx, melt
PC-22	1300	1.8 GPa	24	Re-ReO_2	LCM-5	1.38	ol, pv, cpx, melt
PC-24	1300	1.8 GPa	24	C-CO	LCM-5	-1.75	ol, pv, cpx, melt
PC-27	1250	1.8 GPa	24	Re-ReO_2	LCM-10	1.44	pv, cpx, rut, tit, melt
PC-30	1250	1.8 GPa	24	C-CO	LCM-10	-1.64	pv, cpx, sp, tit, melt
MA-9	1350	6 GPa	24	Re-ReO_2	LCM-5	1.53	pv, cpx, sp, melt
MA-8	1350	6 GPa	24	C-CO	LCM-5	-0.99	pv, cpx, sp, melt

Table 2: Experimental run conditions and experimental results. (T) temperature in °C, (d) duration in hours, ΔNNO is the oxygen fugacity relative to the NNO buffer. Phases: olivine (ol), perovskite (pv), clinopyroxene (cpx), spinel (sp), rutile (rut), titanite (tit).

The experiments at 1.8 and 6 GPa, under oxidizing conditions were carried out using Pt capsules lined with a Re foil (3 mm long). The Re foil has the purpose to avoid Fe loss in the runs and to constrain fO_2 at the Re-ReO_2 buffer (Campbell et al., 2009). The experiments at 1.8 and 6 GPa under reducing conditions at the C-CO buffer (Ulmer and Luth, 1991) were performed using Pt capsules lined with an inner graphite capsule. The experiments at 1.8 GPa were conducted in an end-loaded piston cylinder apparatus (Prowatke and Klemme, 2006). The 1/2 inch piston cylinder assemblies consisted of a graphite heater surrounded by

pyrexglass and talc sleeves. This assembly has been pressure calibrated using the fayalite = quartz + ferrosilite (Bohlen et al., 1980), and picrochromite + quartz = enstatite + eskolaite reactions (Klemme and O'Neill, 1997; Klemme and O'Neill, 2000). Experiments were conducted using the "piston-in" routine (Klemme, 2010): first, a pressure of about 0.5 GPa was applied; then the sample was heated up to about 400°C to soften the glass; at last, pressure and temperature were raised stepwise and simultaneously. Pressure was kept constant (±0.05 GPa) manually during the experiments using a hydraulic system. Temperatures were measured with $W_{95}Re_5$-$W_{74}Re_{26}$ thermocouples inserted axially into the assembly using four-bore high-purity Al_2O_3 tubing. The sample was placed in the hotspot of the assembly; temperature uncertainties throughout the capsule length were calibrated to be less than 20°C. The experiments were run for durations of 24 hours to ensure equilibrium of crystalline phases and coexisting melts.

Experiments at 6 GPa were carried out in a 1000-ton Walker-type multi-anvil apparatus, using 25.4 mm tungsten carbide (WC) cubes, a 18/12 assembly (18 mm edge length cast Aremco Ceramacast^{TM} octahedra with a truncation edge length of 12 mm). The 18/12 assembly was calibrated using the phase transitions of Bi-metal (room temperature) as well as the quartz-coesite and $CaGeO_3$ garnet to perovskite phase transitions at 1100°C. The assembly consisted of a straight graphite furnace, a ZrO_2 thermal insulation sleeve, MgO spacers, and molybdenum metal plugs to ensure electrical contact between assembly and WC cubes. Temperature was measured with $W_{95}Re_5$-$W_{75}Re_{25}$ thermocouples. Pressure and temperature were kept constant during the run using Eurotherm controllers. The total temperature uncertainty resulting from minor temperature fluctuations during the run and temperature gradients in the assembly is estimated to be ±15°C.

3. Analytical methods

Experimental run products were mounted in epoxy resin, polished with non-hydrous diamond-based polishing pastes, and checked using optical microscopy and scanning electron microscopy (SEM - JEOL JSM 6610LV).

The experimental run products were subsequently analyzed for major and minor elements using a JEOL JXA 8900 and JEOL JXA 8530F electron microprobes at the Institut für Mineralogie, Münster. Analyses were performed using an accelerating voltage of 15 kV and a beam current of 10 nA. Counting times were 20s on the peak and 5s on each background. The standards used were: jadeite (Na), olivine San Carlos (Mg), disthene (Al), hypersthenes (Si), sanidine (K), diopside (Ca), Re metal (Re), Cr_2O_3 (Cr), fayalite (Fe), rutile (Ti) and rhodonite (Mn).

4. Results

4.1. Experimental textures and phase associations

In this work we report results of melting experiments performed on kimberlitic compositions at 1 atm, 1.8 GPa and 6 GPa. The run products are well crystallized, showing equilibrium among all phases and the presence of glass in all samples, which is in some experiments quenched. Back-scattered electron images from figure 1 show homogeneous phases with no significant zoning in terms of major element composition.

Different phase assemblages were obtained among the experiments due to changes in composition, pressure and oxygen fugacity. The 1 atm run at oxidizing conditions (1250°C – 24h) (F-2) crystallized olivine, clinopyroxene, perovskite and spinel (Fig. 1a) and the run product at 1 atm (1250°C – 24h) under reducing conditions (F-3) crystallized olivine,

clinopyroxene and perovskite (Fig. 1b). Crystals are euhedral to slightly subhedral, and range in size from about 5 to 20 µm.

In experiments performed at 1.8 GPa and 1300°C (24h) (PC-22 and PC-24), perovskite crystallized in a kimberlitic composition equilibrated at oxygen fugacity equivalent to those of the Re-ReO_2 buffer (oxidizing conditions) and C-CO buffer (reducing conditions) (Fig. 1d and f). In both experiments, olivine and clinopyroxene are crystallized in equilibrium with perovskites crystals. In experiment PC-22 (oxidizing conditions), crystals are euhedral to subhedral and range in size from 3 to 15 µm. Localized parts of the melt show quench features, but in general the glass is enough for good-quality analyses. The reducing conditions run (PC-24) present some large crystals of olivine, clinopyroxene and perovskite (10 to 100µm) in a large amount of silicate melt quenched to glass. Figure 1 (c and e) show examples of the two kinds of capsules: double capsule Pt-Re for oxidizing conditions experiments; and double capsule Pt-graphite for reducing conditions experiments.

As shown in figure 1 (g and h), the experiments at 1.8 GPa and 1250°C (24h) with H_2O and CO_2 in the starting composition (PC-27 and PC-30) show different paragenesis due to changes in oxygen fugacity conditions. The oxidizing conditions run present euhedral to subhedral smaller crystals of clinopyroxene, perovskite, titanite and rutile, ranging in size from 2-10 µm, while larger spinel crystals (up to 30 µm) are present in the reducing conditions run, together with smaller clinopyroxene and perovskite grains, all of them surrounded by melt. There is no olivine crystallized in both experiments with H_2O and CO_2.

The 6 GPa runs at 1350°C (24h), on oxidizing and reducing conditions (MA-9 and MA-8), crystallized euhedral to subhedral clinopyroxene (up to 20 µm), perovskite and spinel (1 to 5 µm), but olivine was not found (Fig. 1 i and j). The most abundant phase is clinopyroxene. Melt is present but not preserved as glass.

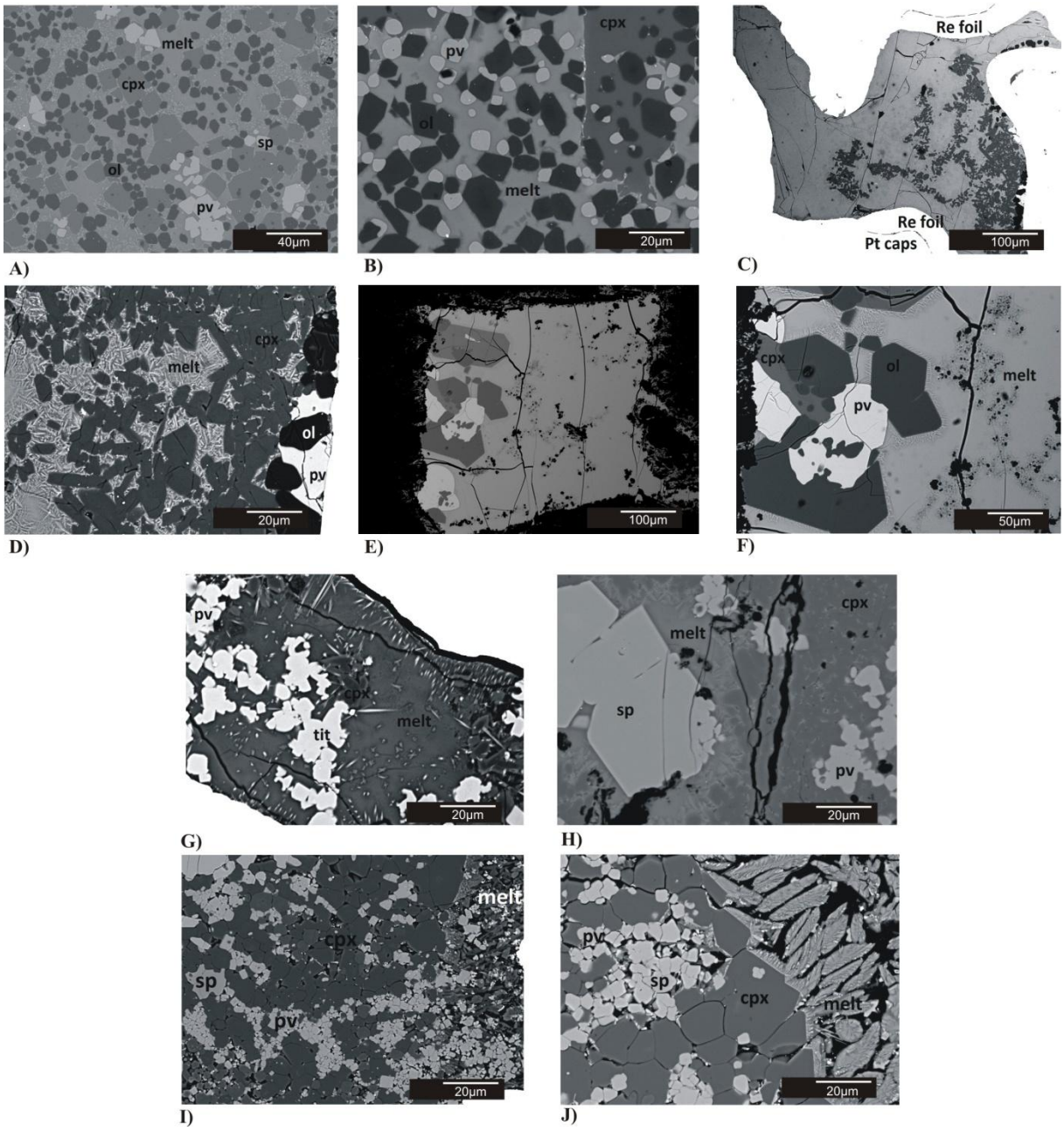

Fig. 1: Back-scattered electron images of representative experimental run products: (A) F-2: 1 atm/1250°C (24h) – oxidizing conditions; (B) F-3: 1 atm/1250°C (24h) – reducing conditions; (C) PC-22: Pt capsule lined on the inside with a Re foil for oxidizing conditions; (D) PC-22: 1.8 GPa/1300°C (24h) – oxidizing conditions; (E) PC-24: graphite capsule for reducing conditions; (F) PC-24: 1.8 GPa/1300°C (24h) – reducing conditions; (G) PC-27: 1.8GPa/1250°C (24h) – oxidizing conditions; (H) PC-30: 1.8GPa/1250°C (24h) – reducing conditions; (I) MA-9: 6 GPa/1350°C (24h) – oxidizing conditions; (J) MA-8: 6 GPa/1350°C

(24h) – reducing conditions. The phases present in images are: perovskite (pv), olivine (ol), clinopyroxene (cpx) and spinel (sp), titanite (tit), in addition to quenched melt.

In agreement with Bellis and Canil (2007), the crystallization of perovskite is virtually independent of fO_2 and controlled primarily by pressure, temperature and liquid composition, i.e. mainly driven by TiO_2 and SiO_2 activities in melts. We could only find olivine in experiments at 1 atm and 1.8 GPa without H_2O and CO_2. Experiments at 1.8 GPa with H_2O and CO_2 and at 6 GPa do not contain olivine. Alternatively, these experiments contain large amounts of clinopyroxene and spinel, or clinopyroxene, titanite and rutile in one of them (LC-27).

4.2. Phase compositions

According to the microprobe data (Table 3 and 4), olivines from all experiments are Mg-rich (Mg# from 0.76 to 0.98) with FeO concentrations of about 1-13wt.%. Clinopyroxenes show Mg# from 0.77 to 0.91 and are SiO_2 (from 43.17wt.% to 52.92wt%) and CaO (from 22.07 to 40.12) rich. Perovskites are SiO_2-poor (0.03 to 2.19wt.%), and CaO and TiO_2 enriched, near to 39 wt.% and 57wt.%, respectively.

The Fe contents in olivine and clinopyroxene from 1 atm experiments (F-2 and F-3) are lower in the experiment under oxidizing conditions (1.1wt.% in olivine and 1.6wt.% in clinopyroxene), than in reducing conditions (13.5wt.% in olivine and 3.6wt.% in cpx). In contrast, the Fe content in perovskite is higher (1.2wt.%) in oxidizing conditions relative to reducing conditions (1.1wt.%), which is explained by the higher concentration of Fe^{2+} in reducing conditions parts of the mantle, while the Fe^{2+} is oxidized to Fe^{3+} in more oxidized regions. Spinel is only present in oxidizing conditions runs, and has 68.9 wt.% of Fe, which could decrease the concentration of Fe in olivine and clinopyroxene. Despite the presence of

spinel, the Fe^{3+} in perovskite is still higher than in the experiment without spinel, from reducing conditions.

As shown in table 3, olivine and clinopyroxene from oxidizing conditions experiment at 1.8 GPa (PC-22) have lower contents of Fe (8.0 and 3.4 wt.%) compared to olivine and clinopyroxene from reducing conditions experiment (11.2 and 3.3 wt.%, respectively) at the same pressure and temperature (PC-24). Perovskite contains slightly higher contents of Fe (0.72 wt.%) in oxidizing conditions than in runs at reducing conditions (0.66 wt.%). This behavior is supported by McCammon et al. (2004), who show that Fe^{3+} in perovskite is controlled mainly by oxygen fugacity, occupying sites in octahedral coordination through the stabilization of cation vacancies in the structure of the perovskite.

Experiments at the same pressure but with the addition of H_2O and CO_2 indicate a different paragenesis. In the experiment at oxidizing conditions (PC-27) rutile and titanite crystallized, in addition to clinopyroxene and perovskite, with low contents of FeO (0.23 to 0.24 wt.%). Thereafter, the experiment at reducing conditions (PC-30) contains spinel grains, instead of rutile and titanite. Spinels are very rich in TiO_2 (58.7 wt.%) and also have high content of FeO (20.1 wt.%). The Fe content of clinopyroxene is higher in reducing conditions (2.6 wt.%) and Fe of perovskite is higher in runs under oxidizing conditions (1.5 wt.%).

The 6 GPa run products show the same paragenesis for oxidizing and reducing conditions, i.e. clinopyroxene, perovskite, spinel and quenched melt. Spinels are rich in TiO_2 and FeO, while clinopyroxene and perovskite are similar in composition at both oxygen fugacities. Clinopyroxene contain slightly higher FeO in reducing conditions, and perovskite have slightly higher FeO content at oxidizing conditions (Table 3).

run#	Phase	SiO_2	Al_2O_3	FeO	MgO	CaO	TiO_2	K_2O	Na_2O	Total
F-2	**Ol (20)**	42.2(0.4)	n.d.	1.1(0.1)	55.7(0.4)	1.7(0.2)	0.2(0.2)	0.01(0.02)	0.02(0.02)	100.9
	Cpx (10)	44(0.3)	0.5(0.2)	1.6(0.3)	13.5(0.4)	39.9(0.6)	0.2(0.09)	0.01(0.03)	0.6(0.1)	100.2
	Pv (4)	2.2(1.4)	0.06(0.04)	1.2(0.4)	0.6(0.3)	39.2(1.1)	55.9(3.5)	n.d.	0.6(0.2)	99.9
	Sp (10)	0.2(0.8)	0.9(0.04)	69(1)	22.6(0.4)	0.5(0.8)	5.7(0.3)	0.01(0.04)	0.02(0.03)	98.8
	Melt (9)	35.2(1.4)	0.9(0.1)	15.1(1.9)	8.8(1.2)	26.1(1.6)	12.9(2.6)	0.04(0.06)	1(0.2)	100
F-3	**Ol (5)**	39.2(0.7)	n.d.	13.5(0.6)	42.8(0.9)	3.3(0.2)	0.3(0.1)	n.d.	n.d.	99.2
	Cpx (7)	43.2(0.4)	0.3(0.06)	3.6(0.9)	11.7(0.6)	40.1(0.3)	0.2(0.06)	n.d.	0.1(0.04)	99.2
	Pv (5)	0.1(0.04)	0.08(0.03)	1.1(0.4)	0.09(0.03)	40.7(0.4)	57.3(0.7)	n.d.	0.04(0.02)	99.4
	Melt (12	35.9(2.4)	1.7(0.4)	17.2(1.8)	6.7(3.4)	26.2(1.6)	12.1(2.9)	0.02(0.03)	0.07(0.07)	100
PC-22	**Ol (5)**	40.3(0.6)	0.03(0.02)	8(0.5)	50.6(0.5)	0.5(0.05)	0.2(0.1)	0.02(0.05)	n.d.	99.7
	Cpx (5)	50.4(1.1)	1.8(0.5)	3.0(0.4)	17.5(0.4)	22.6(0.5)	3.2(0.7)	0.06(0.05)	0.06(0.03)	98.7
	Pv (5)	0.03(0.05)	0.1(0.02)	0.7(0.2)	0.2(0.06)	39.2(0.5)	57.8(1.1)	0.2(0.08)	0.05(0.07)	98.3
	Melt (6)	28.4(0.7)	3.3(0.2)	10(0.6)	11.6(0.3)	16.3(0.5)	27.5(1.8)	2.8(0.2)	0.2(0.2)	100
PC-24	**Ol (5)**	40.0(0.4)	0.03(0.04)	11.2(0.3)	48.3(0.4)	0.6(0.1)	0.2(0.06)	0.01(0.01)	0.02(0.04)	100.4
	Cpx (5)	49.8(0.6)	2.4(0.4)	3.3(0.2)	17.2(0.2)	22.7(0.5)	4.1(0.4)	0.03(0.06)	0.06(0.04)	99.5
	Pv (5)	0.03(0.02)	0.1(0.02)	0.7(0.2)	0.2(0.02)	39.5(0.7)	58.9(0.8)	0.09(0.06)	0.06(0.06)	99.5
	Melt (5)	28.9(0.7)	3.30(0.07)	12.1(0.8)	10.3(0.4)	16.2(1.0)	24.5(0.3)	2.4(0.4)	2.4(0.08)	100
PC-27	**Cpx (6)**	48.2(2.7)	4.1(1.0)	1.6(0.2)	17.3(1.1)	22.5(0.7)	4.1(2.1)	0.2(0.1)	0.15(0.05)	98.3
	Pv (6)	0.07(0.04)	0.2(0.04)	0.37(0.06)	0.18(0.04)	39.0(0.5)	57.8(0.6)	0.2(0.08)	0.05(0.04)	98.9
	Rut (3)	0.05(0.05)	0.3(0.06)	0.2(0.07)	0.09(0.02)	0.4(0.4)	97.2(0.3)	0.1(0.07)	n.d.	98.5
	Tit (5)	28.7(0.3)	0.5(0.08)	0.2(0.1)	0.5(0.2)	27(0.3)	41.1(1.0)	0.2(0.1)	0.03(0.03)	98.3
	Melt (5)	30.4(1.7)	5.7(0.6)	3.8(0.7)	13.3(0.9)	22.8(1.9)	17.4(1.8)	6(0.7)	0.6(0.3)	100
PC-30	**Cpx (4)**	51.2(1.2)	2.7(0.3)	2.6(0.1)	17(0.5)	23.3(0.1)	3.4(0.5)	0.1(0.07)	0.2(0.09)	100.6
	Pv (13)	0.3(0.7)	0.2(0.1)	0.6(0.3)	0.2(0.2)	40.4(0.9)	57.1(1.0)	0.2(0.2)	0.03(0.04)	99.0
	Sp (7)	0.1(0.4)	0.7(0.2)	20(5)	17(4)	2.5(9)	58.7(0.8)	0.03(0.04)	0.01(0.03)	99.1
	Melt (3)	35(2.2)	6.2(0.4)	8.3(1.3)	8(2)	14.7(1.6)	19.5(2.2)	7.5(1.6)	0.7(0.2)	100
MA-9	**Cpx (4)**	52.9(1.6)	1.5(0.3)	3.6(0.3)	16.8(0.9)	22.1(0.3)	0.7(0.07)	0.7(1)	0.3(0.06)	98.5
	Pv (5)	0.3(0.4)	0.2(0.09)	1.1(0.2)	0.2(0.1)	37.5(1.2)	57(0.8)	1(0.4)	0.08(0.08)	97.4
	Sp (5)	0.3(0.1)	1.0 (0.02)	29.9(0.4)	12.7(0.2)	0.8(0.5)	53.5(0.3)	0.4(0.1)	0.02(0.06)	98.9
	Melt (6)	32.5(11.9)	3.6(0.8)	12.6(5.7)	12.6(5.5)	16.6(11.6)	15(8.9)	6.8(5.5)	0.3(0.2)	100
MA-8	**Cpx (4)**	52.3(0.4)	2.2(0.6)	3.6(0.3)	17(0.3)	22.3(0.4)	1.1(0.3)	0.2 (0.04)	0.2 (0.03)	99.0
	Pv (7)	0.2(0.1)	0.2(0.06)	1.1(0.2)	0.2(0.07)	38.5(0.7)	58.3(1.1)	0.3(0.09)	0.05(0.05)	98.7
	Sp (3)	0.09(0.04)	1.16(0.005)	28(0.5)	13.1(0.06)	0.3(0.1)	57.9(0.9)	0.07(0.06)	0.05(0.03)	100.6

Melt (5)	26.4(5.6)	4(0.6)	17.1(1.8)	11.8(0.8)	9.4(3.8)	27.2(3.3)	3.9(6.4)	0.1(0.2)	100

Table 3: Major element compositions (wt.%) of experimental run products. Melt compositions were recalculated to 100 wt.%. Notes: n.o.a., number of analysis (x); all errors are 2 σ, given as last significant digits in brackets; n.d., not detected.

run#	Phase	Si	Al	Fe	Mg	Ca	Ti	K	Na	Total
F-2	Ol	0.989	0	0.022	1.948	0.044	0.003	0	0.001	3.008
	Cpx	1.714	0.024	0.052	0.782	1.665	0.005	0	0.049	4.293
	Pv	0.197	0.007	0.093	0.080	3.786	3.790	0	0.108	8.063
	Sp	0.069	0.324	17.99	10.51	0.181	1.342	0.004	0.012	30.43
F-3	Ol	0.996	0.000	0.286	1.620	0.090	0.006	0	0	2.999
	Cpx	1.718	0.016	0.119	0.696	1.710	0.006	0	0.008	4.272
	Pv	0.009	0.009	0.088	0.012	3.987	3.939	0	0.006	8.051
PC-22	Ol	0.985	0	0.163	1.843	0.013	0.004	0	0	3.011
	Cpx	1.686	0.078	0.094	0.969	0.897	0.090	0.003	0.004	4.006
	Pv	0.003	0.014	0.056	0.024	3.870	4.005	0.019	0.008	7.999
PC-24	Ol	0.985	0.001	0.230	1.772	0.017	0.004	0	0.001	3.011
	Cpx	1.836	0.104	0.103	0.943	0.897	0.113	0.002	0.005	4.002
	Pv	0.003	0.016	0.050	0.024	3.840	4.023	0.010	0.011	7.977
PC-27	Cpx	1.791	0.179	0.051	0.959	0.897	0.115	0.010	0.011	4.014
	Pv	0.006	0.017	0.029	0.024	3.858	4.017	0.023	0.009	7.985
	Rut	0	0.005	0.003	0.002	0.006	0.990	0.002	0	1.008
	Tit	3.826	0.077	0.026	0.104	3.852	4.114	0.036	0.008	12.04
PC-30	Cpx	1.861	0.117	0.078	0.921	0.909	0.092	0.007	0.011	3.998
	Pv	0.026	0.018	0.046	0.030	3.965	3.933	0.021	0.006	8.045
	Sp	0.028	0.202	3.988	6.003	0.637	10.50	0.009	0.005	21.37
MA-9	Cpx	1.961	0.064	0.112	0.928	0.876	0.019	0.034	0.019	4.014
	Pv	0.026	0.018	0.089	0.029	3.741	3.997	0.119	0.014	8.034
	Sp	0.085	0.303	6.243	4.744	0.219	10.05	0.130	0.010	21.78
MA-8	Cpx	1.928	0.096	0.112	0.932	0.882	0.031	0.011	0.015	4.006
	Pv	0.014	0.022	0.084	0.022	3.778	4.017	0.033	0.009	7.979
	Sp	0.022	0.330	5.656	4.703	0.067	10.51	0.021	0.023	21.33

Table 4: Cations per formula unit (cpfu) of experimental run products.

4.3. The relationship between fO^2 and Fe^{3+}/Fe^{2+} in minerals and melts

Figure 2 illustrates a comparison between the iron content of perovskite from experiments, that is only ferric iron (McCammon et al., 2004), at different pressures and fO_2. As perovskite only incorporates ferric iron (Fe^{3+}), the Fe_{total} of perovskites, as measured with electron microprobe, equates to ferric iron. Our data show that the ferric iron in perovskite is a strong function of fO_2 in our experiments. With increasing fO_2 at 1 atm or at high pressures (1.8 and 6 GPa), the amount of ferric iron in perovskite will also increase. However, there is quite a spread of the data, e.g. at 1.8 GPa, our data shows quite variable Fe content of perovskite. This data spread is caused by different modal proportions of olivine, and most importantly, perovskite in our runs. For comparison, we also plotted Fe^{3+} content of perovskites from the Bellis and Canil (2007) experiments, and different fO_2. Both our data and the Bellis and Canil (2007) data show considerable spread of the Fe content of perovskite. Therefore, the simple oxybarometer which links Fe content with fO_2 Bellis and Canil (2007) can certainly be improved by a more refined treatment of the data.

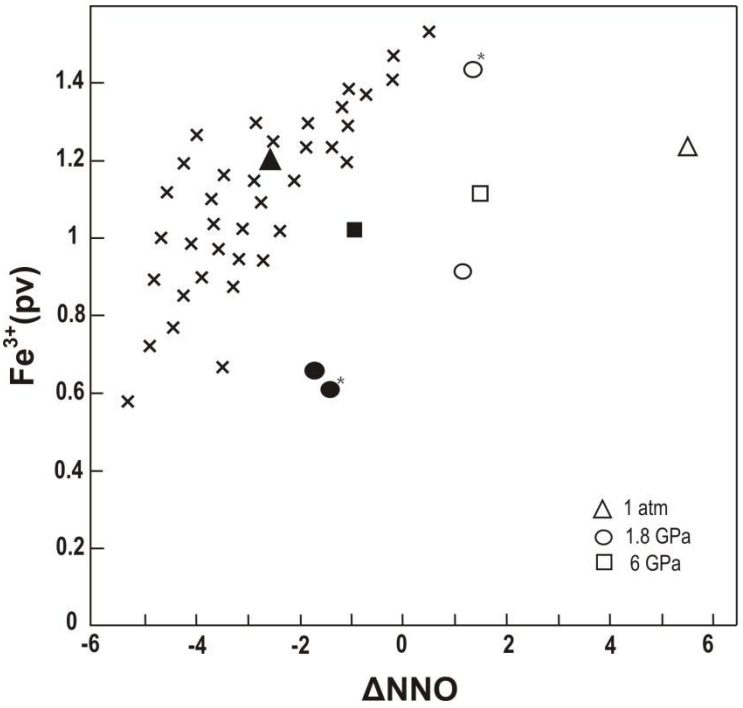

Fig. 2: The diagram presents the amount of Fe^{3+} in perovskite *versus* fO_2 plotted in terms of ΔNNO (Frost, 1991). Filled symbols represent experiments using the C-CO buffer (Ulmer and Luth, 1991); empty symbols represent experiments using the Re-ReO_2 buffer (Campbell et al., 2009); crosses represent Bellis and Canil (2007) data. The *experiments denote runs that contain H_2O and CO_2.

Our overall aim is to calculate fO_2 of kimberlite melts using the Fe content of minerals. It is fortuitous that our experiments and in fact, many natural kimberlites contain two minerals that only incorporate one sort of Fe: perovskite mainly incorporates Fe^{3+}, and olivine is known to incorporates mainly Fe^{2+}. We use these simple facts to constrain the Fe^{3+}/Fe^{2+} ratio of the melt by measuring Fe in olivine and perovskite using electron microprobe analyses of coexisting phases. Using this simple ruse, we developed an equation for kimberlitic melts saturated in these phases, which enable us to calculate whether a kimberlite is more oxidized or not, and whether diamonds are likely to have been absorbed during the ascent of the melt to the surface or not.

In order to use this equation, however, the D (distribution coefficient) of iron between olivine and melt, and perovskite and melt, is needed. The distribution coefficient represents

the Fe exchange between olivine and melt, and perovskite and melt. This parameter depends mainly on temperature, but also on composition:

$$\frac{Fe^{3+}}{Fe^{2+}}(melt) = \frac{Fe^{3+}(pv) * D(\frac{ol}{melt})}{Fe^{2+}(ol) * D(\frac{pv}{melt})} \qquad (1)$$

where ol is olivine, pv is perovskite, D(ol/melt) is the distribution coefficient of Fe^{2+} between olivine and melt, and D(pv/melt) is the distribution coefficient of Fe^{3+} between perovskite and melt. D(ol/melt) has been measured many times in experimental studies (i.e. Roeder and Emslie, 1970; Toplis, 2005) and the average value for D(ol/melt) is 0.3, valid over wide ranges of temperature and composition. D(pv/melt) was calculated from our experiments (Table 5) and from Bellis and Canil (2007) data. In the experiments without olivine (e.g. the runs at 1.8 GPa with H_2O and CO_2 and at 6 GPa) the Fe^{2+} content was calculated from the Fe^{2+} contents in olivine from other experiments with the same oxygen fugacity condition.

run#	**P(GPa)**	**T°C**	**ΔNNO**	**D_{Fe}(pv/melt)**	**D_{Fe}(ol/melt)**	**Fe^{3+}/Fe^{2+}(melt)**
LF-2	1 atm	1250	6.3	0.09	0.3	3.5(0.18)
LF-3	1 atm	1250	-2.1	0.07	0.3	0.3(0.02)
PC-22	1.8GPa	1300	1.4	0.08	0.3	0.4(0.02)
PC-24	1.8GPa	1300	-1.7	0.06	0.3	0.3(0.01)
PC-27	1.8GPa	1250	1.4	0.12	0.3	0.4(0.02)
PC-30	1.8GPa	1250	-1.6	0.08	0.3	0.2(0.01)
MA-9	6GPa	1350	1.5	0.10	0.3	0.7(0.03)
MA-8	6GPa	1350	-1.0	0.07	0.3	0.6(0.03)

Table 5: Results of D_{Fe}(pv/melt) calculated from our experiments, D_{Fe}(ol/melt) is from literature data (i.e. Roeder and Emslie, 1970; Toplis, 2005). Fe^{3+}/Fe^{2+}(melt) is the result of equation (1), calculated from our experiments. We assumed analytical uncertainties of 5%, given as last significant digits in brackets.

Figure 3 shows the result of the Fe^{3+}/Fe^{2+} ratio calculated from equation 1, applied to our experiments data. In this diagram, we compare these results with the respective fO_2

(ΔNNO) of the experiments. We found that there is a positive correlation between fO_2 increasing and Fe^{3+} in the melt of the experiments.

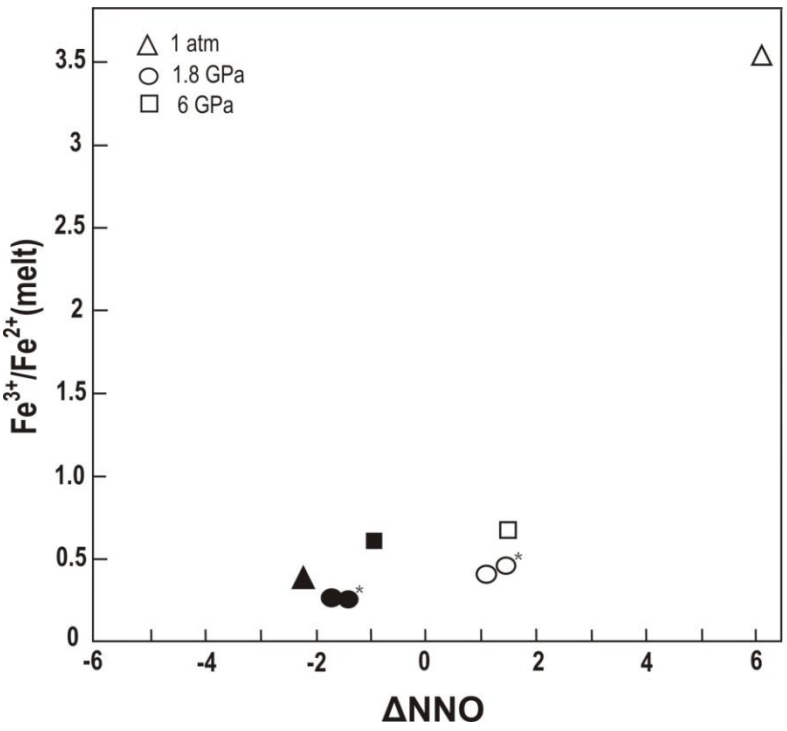

Fig. 3: Comparison of the ratio Fe^{3+}/Fe^{2+} in the melt and fO_2 (ΔNNO) (Frost, 1991) of experiments. Filled symbols represent experiments using the C-CO buffer; empty symbols represent experiments using the Re-ReO_2 buffer. The *experiments denote runs that contain H_2O and CO_2.

4.4.Oxygen barometer equation:

To link measured Fe concentrations of perovskite, olivine, with minerals modes, temperature, pressure and fO_2 (ΔNNO) (Table 6), we used multiple linear regression to define a new oxygen barometer:

$$\Delta NNO = - 0.648 \times Fe(ol) + 0.591 \times Fe(pv) - 0.036 \times n(ol) - 0.023 \times n(pv) + 0.006 \times T - 0.767 \times P \quad (2)$$

where Fe(ol) is the total Fe in olivine (Fe^{2+}), Fe(pv) is the total iron in perovskite (Fe^{3+}), n(ol) is the modal quantity of olivine, n(pv) is the modal quantity of perovskite, T is temperature (°C) and P is pressure (GPa). The best-fit (Fig.4) reproduces data from all experiments (Table 6) and has a standard error of the estimate (α_{est}) of 0.09, which is a measure of the accuracy of the fit.

	Fe(ol) wt.%	**Fe(pv) wt.%**	**n(ol) vol.%**	**n(pv) vol.%**	**T °C**	**P GPa**	**ΔNNO***	**ΔNNO eq. (2)**
LCF-2	1.13	1.24	30	10	1250	0.0001	6.3	6.2(0.01)
LCF-3	13.6	1.20	35	15	1250	0.0001	-2.1	-2.2(0.01)
LCE-22	8	0.90	10	5	1300	1.8	1.4	1.3(0.01)
LCE-24	11.2	0.66	13	11	1300	1.8	-1.7	-1.2(0.3)
LCE-27	8	1.45	1	20	1250	1.8	1.4	1.3(0.01)
LCE-30	11.5	0.60	1	30	1250	1.8	-1.6	-1.7(0.01)
LCMA-9	4.7	1.15	1	10	1350	6.0	1.5	0.9(0.4)
LCMA-8	7.5	1.10	1	15	1350	6.0	-1	-1.1(0.01)

Table 6: Fe(ol) is the total Fe in olivine, Fe(pv) is the total iron in perovskite, n(ol) is the modal quantity of olivine, n(pv) is the modal quantity of perovskite, temperature in °C and pressure in GPa. In the experiments without olivine, we assumed n(ol) = 1vol.%. ΔNNO* is the oxygen fugacity from literature (Frost, 1991; Campbell et al., 2009; Ulmer and Luth, 1991). ΔNNO eq. (2) is the oxygen fugacity calculated with oxygen barometer equation (2). The squared errors are given in brackets.

The 1:1 line (Fig.4) consists of the correlation of ΔNNO of calculations based on oxybarometer equation (2) and ΔNNO of our experiments (Table 6) and Bellis and Canil (2007) experiments. ΔNNO of Bellis and Canil (2007) experiments were calculated using the FeO content and modes of perovskites, temperature and pressure from Bellis and Canil (2007) supplementary data. Olivines FeO content and modes, were inferred from general kimberlite rock data (Fe(ol) = 12 and n(ol) = 50 vol.%). Both our data and the Bellis and Canil (2007) data show a good correlation between the fO_2 of the experiments and the fO_2 calculated from the oxygen barometer equation (2). A larger divergence between oxygen

barometer calculated data and experiments data can be observed in some experiments from Bellis and Canil (2007) at lower fO_2 (ΔNNO -3.5 to -3.8), which was also noted by the authors using their oxygen barometer equation. This divergence is attributed by the authors as resulting to the presence of Fe^{2+} in perovskites at very low fO_2. Regarding this, further experiments on a larger range of oxygen fugacity are required.

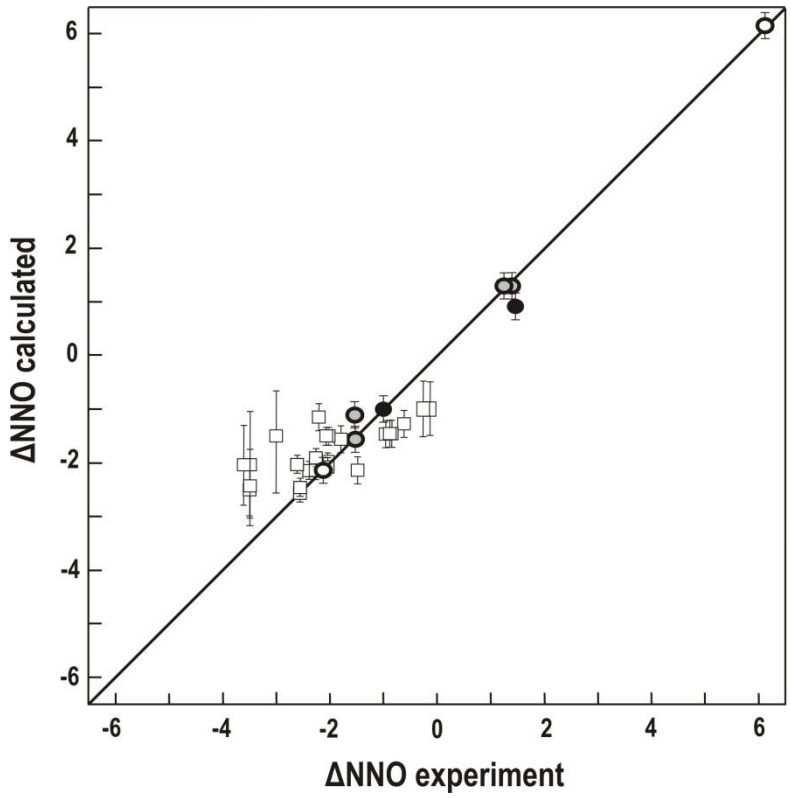

Figure 4: A scatter plot of multiple linear regression of experimental data (Equation 2 and Table 6) shows a comparison of fO_2 (relative to NNO buffer) of calculations, based on the oxybarometer equation (2) (y axis), and experiments (x axis). Symbols: white circles represent experiments at 1 atm; grey circles, 1.8 GPa; black circles, 6.0 GPa; white squares are Bellis and Canil (2007) experiments. Error bars of 2 σ from all experiments.

Equation (2) is applicable to kimberlite rocks that contain perovskite and olivine in a range of fO_2 of ΔNNO -2 to +6. In order to use this equation, however, the FeO content (Fe_{total}) in perovskites and olivines is needed, as well as calculated temperature and pressure of formation. Contrasting from Bellis and Canil (2007) oxygen barometer, the modal proportions of olivine and perovskite in the rock are also required, considering that the

contents of Fe^{2+} in olivines and Fe^{3+} in perovskites may vary depending on the total amount of crystallized minerals in the kimberlitic rock. Using the Fe content in olivine and perovskite we can better understand the redox state of the melt and consequent potential of this rock to preserve diamonds. Since the diamond preservation grade has a negative correlation with the increasing of fO_2, the more reduced kimberlite rock has a greater chance that the diamonds carried by this rock from the deep mantle will be preserved than in rocks that have a higher oxygen fugacity. When diamonds are exposed to oxidized melts, they can easily react and form CO_2 or carbonates. According Fedortchouk et al. (2007), a fluid rich in H_2O and CO_2 that percolate a kimberlite rock during its ascent, will oxidize the melt and produce different dissolution surface features in the diamonds, with similar oxidation rates.

The range of observed fO_2 values represents variations in the oxidation/reduction processes in the kimberlite magmas. Thus, perovskite and olivine compositions can be used to investigate the relationship between the fO_2 of the melt, calculated from FeO content and modal proportion of the minerals, and the diamond preservation in a kimberlitic rock. However, the fO_2 of a kimberlite melt changes depending on a number of factors that need to be considered with respect to diamond preservation, e.g. the velocity of eruption, the volatile content of the melt and the mixing with other magmas and fluids (Fedortchouk et al., 2005 and Ogilvie-Harris et al., 2009).

5. Conclusions

We have demonstrated that ferric iron concentration in perovskites from kimberlitic melts increases with increasing fO_2, under 1 atm, 1.8 and 6 GPa. These parameters are correlated under high pressure and in the experiments with H_2O and CO_2. Temperature and liquid composition, instead oxygen fugacity, are strong variables in controlling phase

appearance. The bulk Fe content of the starting materials has no influence on the saturation temperature of perovskite. The Fe^{3+}/Fe^{2+} ratio (equation 1) connects Fe content in olivine (Fe^{2+}) and ferric iron in perovskite (Fe^{3+}) with Fe^{3+}/Fe^{2+} ratio in melts, which also contribute to better understand the redox state of the rock and the possibility of having diamonds or not.

The oxygen barometer developed in this study (equation 2) reproduces all experimental data, at more reducing and more oxidizing conditions, and is applicable to kimberlite rocks that contain perovskite and olivine. For calculations, FeO content and modal proportion of olivines and perovskites are needed, as well as temperature and pressure estimates of the melt formation.

Since kimberlites experience multiple stages of crystallization under changing conditions during ascent, the Fe content and modes of perovskites and olivines is an important tool to estimate the redox conditions of the rock in some part of this complex event. This information is of great importance to predict diamond quality and, therefore, the value of a kimberlite pipe.

Aknowledgments

We would like to thank funding from CNPq (National Counsel of Technological and Scientific Development) and the Science without Borders Program from Brazil. We would also to thank members of the workshops at Münster University (Institut für Mineralogie) for their efforts with the experimental laboratories: Beate Schmitte, Jonas Kemmann, Maik Trogisch and Michael Feldhaus.

References

Arculus, R. (1985) “Oxidation status of the mantle:past and present” Ann. Rev. Earth Planet. Sci.13 : 75-95.

Ballhaus, C. (1993) “Redox States of Lithospheric and Asthenospheric Upper Mantle.” Contributions to Mineralogy and Petrology 114(3): 331–48.

Bellis, A. and Canil, D. (2007) “Ferric Iron in $CaTiO_3$ Perovskite as an Oxygen Barometer for Kimberlitic Magmas I: Experimental Calibration.” Journal of Petrology 48(2): 219–30.

Bohlen, S.R., Essene, E.J. and Boettcher, A.L. (1980) “Reinvestigation and application of olivine-quartz-orthopyroxene barometry.” Earth and Planetary Science Letters, 47, 1-10.

Campbell, A. J., Danielson, L., Righter, K., Seagle, C.T., Wang, Y, Prakapenka, V.B . (2009) “High Pressure Effects on the Iron-Iron Oxide and Nickel-Nickel Oxide Oxygen Fugacity Buffers.” Earth and Planetary Science Letters 286(3-4): 556–64.

Canil, D. and Bellis A.J. (2007) “Ferric Iron in $CaTiO_3$ Perovskite as an Oxygen Barometer for Kimberlite Magmas II: Applications.” Journal of Petrology 48(2): 231–52.

Carmichael, I.S.E, and Nicholls, J. (1967) “Iron-titanium oxides and oxygen fugacities in volcanic rocks.” Journal of Geophysical Research, 72, 18, 4665-4686.

Chakhmouradian, A. R., and Mitchell, R. H. (2000) “Occurrence, Alteration Patterns and Compositional Variation of Perovskite in Kimberlites.” Canadian Mineralogist 38(4): 975–94.

Deines, P., Nafziger R.H., Ulmer, G.C., Woermann E. (1974) “T-fO_2 tables for selected gas mixtures in the C-H-O system at one atmosphere total pressure.” Bull. Earth Mineral Sci. Exp. Stn, 88, 1-29.

Fedortchouk, Y., Canil, D. and Carlson, J.A. (2005) "Dissolution forms in Lac de Gras diamonds and their relationship to the temperature and redox state of kimberlite magma." Contributions to Mineralogy and Petrology, 150, 54-69.

Fedortchouk, Y., Canil, D., Semenets. E. (2007) "Mechanisms of diamond oxidation and

their bearing on the fluid composition in kimberlite magmas." American Mineralogist, 92, 1200-1212.

Frost, B. R. (1991) “Introduction to Oxygen Fugacity and Its Petrologic Importance.” Reviews in Mineralogy and Geochemistry 25(1): 1–9.

Frost, D. J., and McCammon, C. A. (2008) “The Redox State of Earth’s Mantle.” Annual Review of Earth and Planetary Sciences 36(1): 389–420.

Fudali, R. F. (1965) “Oxygen fugacities of basaltic and andesitic magmas.”Geochimica et Cosmochimica Acta, 29,1063-1075.

Kaminsky, F.V., Zakharchenko, O.D., Davies, R., Griffin, W.L., Khachatryan-Blinova, G.K., Shiryaev, A.A. (2001) “Superdeep diamonds from the Juina area, Mato Grosso State, Brazil.”Contributions to Mineralogy and Petrology, 140 (6), 734-753.

Klemme, S. and O’Neill, H.S. (1997) “The reaction $MgCr_2O_4+SiO_2=Cr_2O_3+MgSiO_3$ and the free energy of formation of magnesiochromite ($MgCr_2O_4$).” Contributions to Mineralogy and Petrology, 130, 59-65.

Klemme, S. and O’Neill H.S. (2000) “The effect of Cr on the solubility of Al in orthopyroxene: experiments and thermodynamic modeling.” Contributions to Mineralogy and Petrology, 140, 84-98.

Klemme, S. (2010) “Experimental constraints on the evolution of iron and phosphorous-rich melts: experiments in the system $CaO-MgO-Fe_2O_3-P_2O_5-SiO_2-H_2O-CO_2$.”Journal of Mineralogical and Petrological Sciences, 105, 1-8.

Kress, V. C., and Carmichael, I.S.E. (1988) “Stoichiometry of the Iron Oxidation Reaction in Silicate Melts.” American Mineralogist 73(11-12): 1267–74.

McCammon, C.A., Frost, D.J., Smyth, J.R., Laustsen, H.M.S., Kawamoto, T., Ross, N.L., van Aken, P.A. (2004) "Oxidation state of iron in hydrous mantle phases: implications for subduction and mantle oxygen fugacity". Physics of the Earth and Planetary Interiors 143-144, 157-169.

Mitchell, R. H., Choi, J. B., Hawthorne, F. C., McCammon, C. A. and Burns, P. C. (1998) “Latrappite: a re-investigation.” Canadian Mineralogist 36, 107-116.

Muir, I. J., Metson, J. B. and Bancroft, G. M. (1984) "^{57}Fe Mössbauer spectra of perovskite and titanite." Canadian Mineralogist 22, 689-694.

Ogilvie-Harris, R.C., Field, M., Sparks R.S.J., Walter, M.J. (2009) "Perovskite from the Dutoitspan kimberlite, Kimberley, South Africa: implications for magmatic processes." Mineralogical Magazine, 73(6) 915-928.

Prowatke, S., and Klemme, S. (2006) "Trace Element Partitioning between apatite and silicate melts." Geochimica et Cosmochimica Acta, 70: 4513–27.

Roeder, P.L., Emslie, R.F. (1970) "Olivine–liquid equilibrium." Contributions to Mineralogy and Petrology. 29:275–289

Rohrbach, A., and Schmidt, M.W. (2011) "Redox Freezing and Melting in the Earth's Deep Mantle Resulting from Carbon-Iron Redox Coupling." Nature 472(7342): 209–12.

Toplis, M. J. (2005) "The Thermodynamics of Iron and Magnesium Partitioning between Olivine and Liquid: Criteria for Assessing and Predicting Equilibrium in Natural and Experimental Systems." Contributions to Mineralogy and Petrology 149(1): 22–39.

Ulmer, P., and Luth, W. (1991) "The Graphite-COH Fluid Equilibrium in P , T , fO_2 Space." Contributions to Mineralogy and Petrology 106: 265–72.

Zhang, C. and Duan, Z. (2009) "A Model for C-O-H Fluid in the Earth's Mantle." *Geochimica et Cosmochimica Acta* 73(7): 2089–2102.

3.2 Manuscrito: "Heterogeneity in the South Brazilian Mantle evidenced by the major and trace element compositions of Rosário do Sul kimberlite minerals"

Submetido à revista científica *Contributions to Mineralogy and Petrology*

Assunto: CTMP-D-17-00210 : Submission Confirmation

Remetente: Contributions to Mineralogy and Petrology (CTMP)

Para: Larissa Colombo Carniel

Responder para: Contributions to Mineralogy and Petrology (CTMP)

Data: Qui 17:30

Dear Mrs. Carniel,

Thank you for submitting your manuscript, Heterogeneity in the South Brazilian Mantle evidenced by the major and trace element compositions of Rosário do Sul kimberlite minerals, to Contributions to Mineralogy and Petrology.

During the review process, you can keep track of the status of your manuscript by accessing the journal's Editorial Manager site.

The submission id is: CTMP-D-17-00210

Please refer to this number in any future correspondence.

Please contact the Handling Editor if you have questions regarding the peer review process. When you do please make sure to copy the Editors-in-Chief:

tlgrove@mit.edu

othmar.muntener@unil.ch

Should you require any further assistance please feel free to contact the Editorial Office by clicking on the "contact us" in the menu bar to send an email to us.

Thank you very much.

With kind regards,

Springer Journals Editorial Office

Contributions to Mineralogy and Petrology

Heterogeneity in the South Brazilian Mantle evidenced by the major and trace element compositions of Rosário do Sul kimberlite minerals

L.C.Carniel[1*], R.V. Conceição[1], S. Klemme[2], F.Gervasoni[3], D.G.Cedeño[1], J. Berndt[2]

[1] Programa de Pós-Graduação em Geociências (PPGGEO), Universidade Federal do Rio Grande do Sul

Bento Gonçalves 9500, Porto Alegre, Brazil

[2] Institut für Mineralogie, Westfälische Wilhelms-Universität Münster

Corrensstraße 24, Münster, Germany

[3] Faculdade de Ciências e Tecnologia, Universidade Federal de Goiás

Mucuri – Setor Conde dos Arcos, Aparecida de Goiânia, Brazil

*Corresponding author: larissa.colombo@ufrgs.br; Tel: +1551996990296

Abstract

Rosário do Sul kimberlite is a hypabyssal kimberlite that belongs to the Rosário do Sul Kimberlitic Province, located in the southeastern edge of the Paraná Basin, in the southern part of Brazil. Its geochemical signature is similar to those of transitional kimberlites of Kaapvaal Craton, Southern Africa, and U-Pb ages of ~ 128 Ma on $CaTiO_3$-perovskites (Conceição et al., *in prep.*) reveal that Rosário do Sul kimberlite probably erupted just after the volcanism of Paraná-Etendeka Province. Based on petrographic evidences as the presence of phlogopites, serpentinized olivines and carbonates, and the major and trace element compositions of the minerals, we suggest that the Rosário do Sul kimberlite mantle source is product of the reaction of a silicate-carbonate liquid in the mantle. The high Ti content of some minerals as Mg-chromite, Mg-ulvöspinel, phlogopite and melilite, and the presence of $CaTiO_3$-perovskite, suggest a Ti-rich source, whereas the calculated melt composition based on Rosário do Sul phlogopites, $CaTiO_3$-perovskites and apatites trace

element contents, indicates a source very rich in Rb, Nb, Cs and Ba. Based on our data, we suggest that the Rosário do Sul mantle source is a depleted mantle metasomatized by CO_2-rich fluids from the recycling of a subducted oceanic plate during the South Atlantic opening, and just after the Paraná-Etendeka Province volcanism.

Keywords: mantle heterogeneity; kimberlite source; mineral chemistry; CO_2-rich fluids; recycling of a subducted slab

1. Introduction

Kimberlites are undersaturated rocks (from 30 to 40 wt.% SiO_2), which contain abundant amount of volatiles (CO_2 + H_2O) and high concentrations of incompatible elements (Mitchell, 1986). Most of the authors agree that kimberlites are formed by small degrees of partial melting of upper mantle peridotite at more than 100 km depth (around 3 GPa) (e.g., Wedephohl and Muramatsu, 1979), and generally have a rapid ascent related to small crust extension movements (e.g. Bailey, 1993).

In Brazil, the most researched kimberlite occurrences are found in the central and in the northwest part of the country; e.g. the kimberlitic pipes in the Juína area, in the State of Mato Grosso do Sul (Kaminsky, et.al, 2009). However, some recent studies (Chaves et al., 2014; Adrião, 2015; Provenzano, 2016; Conceição et al., *in prep.*) has provided information about kimberlitic magmatism also in the southernmost part of Brazil, at the State of Rio Grande do Sul.

Rosário do Sul kimberlite is a transitional kimberlite that belongs to the Rosário do Sul Kimberlitic Province (Edler et al., 1998), located in the southeastern edge of the Paraná Basin, in the southernmost part of Brazil. The Rosário do Sul geochemical signature is

similar to the Group I kimberlites and to the transitional kimberlites from the Kaapvaal Craton, Southern Africa (Conceição et al., *in prep.*). The geochemical and isotopic data (Conceição et al., *in prep.*) suggests that the Rosário do Sul kimberlite source is a depleted mantle metasomatized by carbonatitic liquids. U-Pb ages of ~ 128 Ma on $CaTiO_3$-perovskites (Conceição et al., *in prep.*) reveal that Rosário do Sul probably erupted just after the volcanism of Paraná-Etendeka Province at ~ 132 Ma (Renne et al., 1992, 1996; Turner et al., 1994; Ernesto et al., 2002), which suggests that the processes related to mantle metasomatism and the heat source responsible for kimberlite generation and ascension could be related to the process that triggered the Paraná-Etendeka magmatism in an extensional environment. This hypothesis indicates the presence of mantle heterogeneity on the source of Paraná continental flood basalts due to percolation of carbonatitic melts. Other alkaline events occur in the border of Paraná-Etendeka Province as the Lages complex (70-77 Ma; Gibson et al., 1999) and Araxá complex (89 Ma; e.g. Hasui and Cordani, 1968), that include carbonatite and lamprophyres from the Late Cretaceous (from 60 Ma to 90 Ma). Comin-Chiaramonti et al. (2002) found that the Early Cretaceous Anitápolis alkaline-carbonatitic complex (~132 Ma; Sonoki and Garda, 1988), which is located 100km far from the basalts of Paraná-Etendeka magmatism (Santa Catarina state in the South of Brazil), and in general the Early Cretaceous analogues, e.g. Ponta Grossa Arch (Brazil), Paraguay and Uruguay, are concomitant with the main flood tholeiites of the Paraná Basin and, therefore, occurred during the early stages of rifting, before the continental separation. They also suggest that the alkaline-carbonatitic magmatism in Southern Brazil is concentrated in regions affected by regional thermal anomalies in the deep mantle (Ernesto et al., 2002) which offer an alternative non-plume-related heat source for the generation of intracontinental magmatic provinces. Furthermore, a number of authors (Turner et al., 1994; Turner and Hawkesworth, 1995; Peate and Hawkesworth, 1996; Comin-Chiaramonti et al., 1997; Peat et al., 1999 and

Marques et al., 1999) emphasize that the Tristan da Cunha mantle plume could have only acted as a thermal perturbation that may triggered the Paraná flood basalt generation, without any influence in its source. Bellieni et al. (1984), Peate et al. (1999) and Marques et al. (1999), based on the chemical and isotopic data, proposed a heterogeneous lithospheric mantle melting as the source of the Paraná flood basalts, whereas, Rocha-Júnior et al. (2012, 2013) shown Re-Os and Sr-Nd-Pb isotopic results indicating that the asthenospheric source of the basalts was enriched by fluids or magmas related to the Neoproterozoic subduction processes.

This research shows major and trace element compositions of the Rosário do Sul kimberlite minerals, and our aim is to drive considerations regarding the kimberlite source and its relation to the Paraná flood basalts event and the South Atlantic opening. The focus of this study is based on the relation between composition of incompatible trace elements and the mantle origin of the kimberlite magma.

2. Geological setting and samples

The Rosário do Sul Kimberlitic Province, which contains four clusters of kimberlitic/lamproitic rocks (São Gabriel, Capivaras, São Xavier and Rosário do Sul), is located in the southeastern edge of the Paraná Basin, in the southernmost part of Brazil. This kimberlitic province is embedded in Phanerozoic sandstones of the Piramboia formation of the Paraná Basin and occurs distributed throughout NW-SE oriented structures, generally in the intersections of the Ibaré lineament and younger faults (Adrião, 2015 and Edler et al., 1998). We will focus our study in the Rosário do Sul cluster, since is the only cluster of the Rosário do Sul Kimberlitic Province with cohesive rocks able to generate good quality samples for geochemical analysis.

The Rosário do Sul kimberlitic rocks investigated in this study are from a hypabyssal body associated to a root zone or a feeder magma dyke (Conceição et al., *in prep.*). The Rosário do Sul outcrop occurs in the Ibicuí River and is exposed for ~7 m^2. Only fresher samples were selected for the present study, providing thin sections in which the inequigranular texture is observed, with several crystal sizes ranging from megacrysts (> 10 mm), to macrocrysts (2 – 10 mm) and microphenocrysts (< 2 mm) in a very fine groundmass. The samples have a fine-grained microporphyritic texture with olivine megacrysts from peridotite mantle xenoliths and pelletal lapilli immersed in a heterogeneous and segregated matrix. The Rosário do Sul mineral assemblage consists of macrocrysts and microphenocrysts of olivine, and microphenocrysts of phlogopite and apatite, all immersed in a groundmass of serpentinized olivines, monticellites, melilites, phlogopites, $CaTiO_3$-perovskites, Mg-chromites, Mg-ulvöspinels and apatites. Furthermore, a mesostasis of phlogopite, soda melilite, akermanite and carbonate is concomitant to the groundmass. The petrography is better described in Conceição et al. (*in prep.*).

3. Analytical methods

Rosário do Sul thin sections were first described using an optical microscopy and a scanning electron microscopy SEM - JEOL JSM 6610LV. Mineral compositions from Rosário do Sul thin sections were determined using a JEOL JXA 8530F electron microprobe at the Institut für Mineralogie, Münster. Microprobe analyses were performed using an accelerating voltage of 15 kV, a beam current of 10 nA and counting times of 20s on the peak and 5s on each background. The standards used were: jadeite (Na), San Carlos olivine (Mg), disthene (Al), hypersthenes (Si), sanidine (K), diopside (Ca), Cr_2O_3 (Cr), fayalite (Fe), rutile (Ti) and rhodonite (Mn).

Trace element concentrations of Rosário do Sul thin sections were determined by spot analyses with a laser ablation inductively coupled mass spectrometre LA-ICP-MS at the Institut für Mineralogie, Münster. Sample ablation was performed with a pulsed 193 nm ArF excimer laser (Analyte G2, Photon Machines). A repetition rate of 5 or 10 Hz and energy of ~ 3-4 J/cm^2 were used throughout the entire session. The beam spot diameter varied between 15 and 30 µm. Elemental analysis has been carried out with an Element 2 mass spectrometer (ThermoFisher). Forward power was 1300 W and reflected power < 2 W, gas flow rates were about 1 l/m for He (carrier gas of ablated material), 0.7 l/m and 0.9 l/m for the Ar-auxiliary and sample gas, respectively. Cooling gas flow rate was set to 16 l/min. Before starting analysis, the system (torch position, lenses, gas flows) has been tuned on a NIST 612 reference glass measuring ^{139}La, ^{232}Th and ^{232}Th^{16}O to get stable signals and high sensitivity, as well as low oxide rates (^{232}Th^{16}O/^{232}Th < 0.1%) during ablation. A total of 32 elements was quantitatively analyzed using the NIST 612 glass as an external reference material and ^{29}Si, ^{43}Ca (silicates), ^{47}Ti (Fe-Ti-oxides) and ^{26}Mg (spinels) as internal standards, which have been previously determined by electron microprobe. Overall time of a single analysis was 75s (20s for background, 40s for peak after switching laser on, 15s washout time). Concentrations of measured elements were calculated using the Glitter software (Griffin et al., 2008 and Van Achterbergh et al., 2001). Standard reference glasses BCR2-G and BIR1-G were analyzed as monitor for precision and accuracy for silicate phases of the course of this study. Obtained results match the published range of concentrations given in the GeoReM database (version 18) (Jochum et al. 2005).

4. Results

4.1. Mineral compositions

Olivine

Olivine is the most abundant mineral in the Rosário do Sul kimberlite. Olivine megacrysts (> 10 mm) are resultants of disaggregated mantle xenoliths, as described by Conceição et al. (*in prep.*). These olivine megacrystals are widespread and represent around 20 vol.% of the total volume of the rock, however, they cannot be considered to understand the crystallization process of the kimberlite. Olivine macrocrysts (2 – 10 mm) and microphenocrysts (< 2 mm) are dispersive in a segregated groundmass (Fig. 1a - d). The olivine macrocrysts are rounded, with euhedral to subhedral shape and present relict cores and serpentinized rims. These serpentinized rims and the microphenocrysts commonly have inclusions of Mg-chromite and melt pockets, which contain a mixture of melt, phlogopite, apatite, melilite and $CaTiO_3$-perovskite (Fig. 1a, b and f). Some olivine macrocrysts and microphenocrysts are partially enclosed by a necklace texture of $CaTiO_3$-perovskite and monticellite. The chemical composition of olivine macrocrystals ranges from Fo_{80-92} in the fresh cores and Fo_{89-97} in the serpentinized rims, while olivine microphenocrysts are always completely serpentinized and have chemical composition equal to the megacrysts serpentinized rims. The iron content (from 5 to 6 wt.%) and MgO content (from 31 to 36 wt.%) of the serpentinized olivines (macrocrystal rims and microphenocrysts) are lower than those of olivine macrocrystal cores (from 10 to 13 wt.% FeO and from 47 to 49 wt.% MgO) (Table 1). The groundmass olivines (5 – 15 μm) are completely serpentinized, enriched in Al_2O_3 (~ 8 - 14 wt.%) and show composition from Fo_{78-84}, where Fo = 100*[Mg/(Mg+Fe)]

in mol%. They commonly occur surrounding olivine macrocrysts and microphenocrysts together with $CaTiO_3$-perovskite and monticellite.

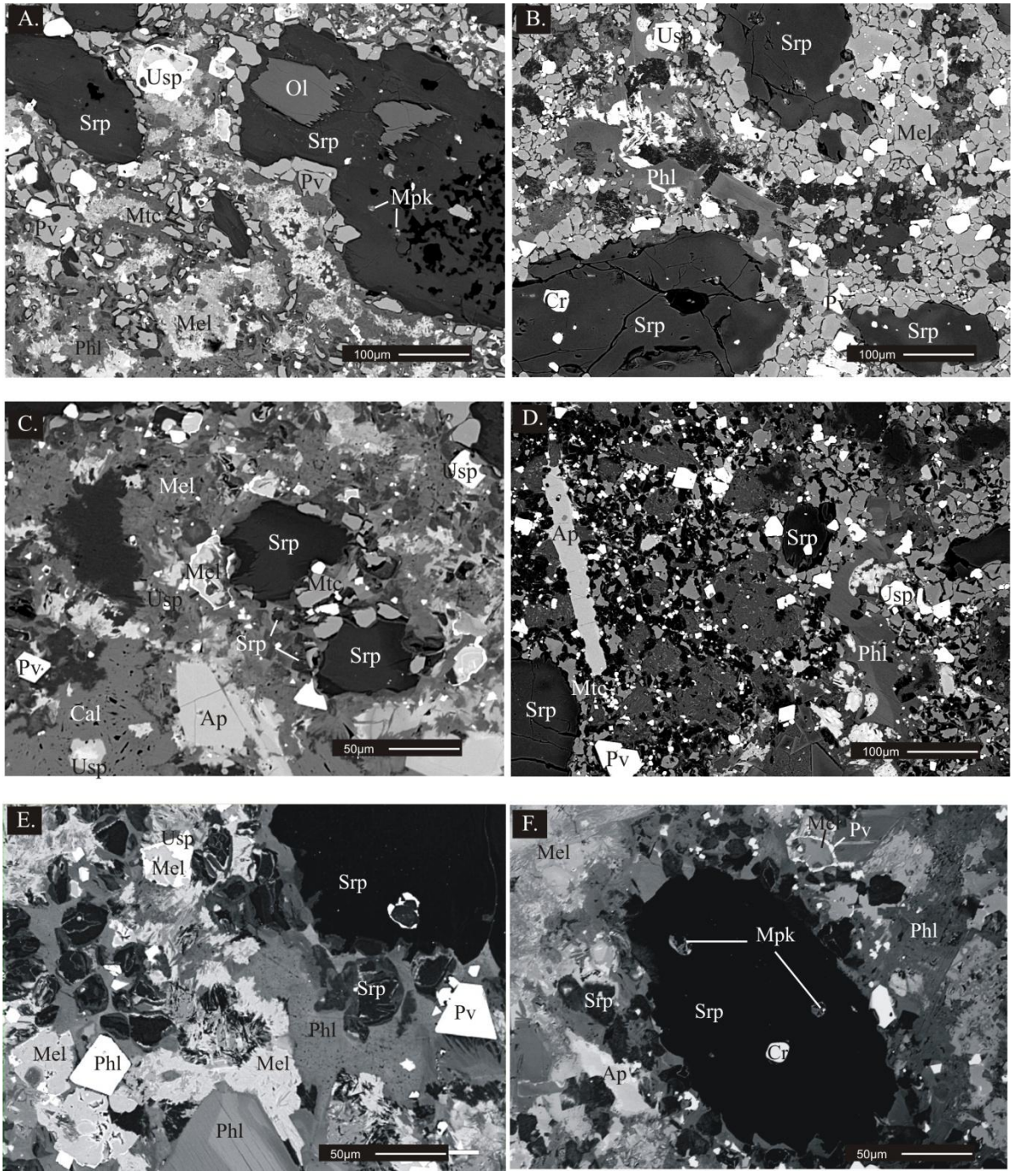

Fig. 1: Backscattered electron images of the thin sections from Rosário do Sul kimberlite showing representative textures and minerals of Rosário do Sul kimberlite. Main phases are: olivine (Ol), serpentinized olivine microphenocryst (Srp), monticellite (Mtc), melilite (Mel), phlogopite (Phl), $CaTiO_3$-perovskite (Pv), Mg-chromite (Cr), Mg-ulvöspinel (Usp),

apatite (Ap), calcium carbonate (Cal) and melt pockets (Mpk). A. Olivine macrocryst with preserved core and serpentinized border; melt pockets inclusions in olivine; skeletal Mg-ulvöspinel; monticellite with serpentinized borders; subhedral $CaTiO_3$-perovskite; melilite in the mesostasis. B. Phlogopite microphenocryst; Mg-chromite inclusion in a fracturated and serpentinized olivine microphenocryst; $CaTiO_3$-perovskite; Mg-ulvöspinel and melilite in the groundmass. C. serpentinized olivine microphenocrysts and groundmass; monticellite with serpentinized borders; Mg-ulvöspinel with Fe-rich zonation; melilite-rich mesostasis; calcium carbonate segregates. D. euhedric apatite microphenocryst with corroded borders; serpentinized olivines microphenocrysts and groundmass; monticellite, phlogopite, Mg-ulvöspinel and $CaTiO_3$-perovskite in the groundmass. E. Phlogopite microphenocryst and groundmass; reaction between olivine and phogopite; olivine microphenocrysts and Al-rich groundmass olivine; skeletal ulvöspinel filled with melilite; euhedral perovskite. F. Olivine microphenocryst with Mg-chromite inclusion and melt pockets; Al-rich groundmass olivine; melilite with necklace texture of perovskites; phlogopite groundmass; apatite microphenocryst; melilite mesostasis.

Sample	*Olivine*			*Serpentine*			*Al-rich serpentine*	
(n.o.a.)	CAR3A(6)	CA03D(5)	CAR301(4)	CAR3A(2)	CA03D(4)	CAR301(9)	CAR3A(10)	CA-03D(4)
SiO_2	41(1)	40.1(0.4)	40.7(0.7)	46.3(0.7)	44(2)	40(1)	33(1)	35(1)
TiO_2	0.04(0.03)	0.04(0.03)	0.02(0.02)	0.06(0.04)	0.02(0.01)	0.1(0.2)	0.12(0.06)	0.07(0.05)
Al_2O_3	n.d.	0.03(0.03)	0.03(0.01)	0.06(0.05)	0.4(0.5)	1.5(0.4)	13(1)	12(3)
FeO*	13(5)	10.3(0.6)	10.6(0.6)	6.0(0.3)	5(2)	6(1)	10(1)	8(2)
MnO	0.22(0.06)	0.16(0.06)	0.14(0.02)	0.40(0.06)	0.3(0.2)	0.21(0.02)	0.31(0.08)	0.3(0.1)
MgO	47(4)	49.1(0.9)	48.3(1.3)	31(1)	33(6)	36(1)	25(2)	25(5)
CaO	0.4(0.5)	0.25(0.25)	0.1(0.1)	1.20(0.06)	1.2(0.8)	0.4(0.3)	1.1(0.8)	3 (3)
Na_2O	0.02(0.02)	0.02(0.02)	0.02(0.02)	0.03(0.03)	0.02(0.02)	0.02(0.02)	0.22(0.07)	0.4(0.5)
K_2O	n.d.	n.d.	n.d.	0.04(0.03)	0.02(0.01)	0.02(0.02)	1.7(0.9)	2(2)
Cr_2O_3	0.03(0.03)	0.04(0.04)	0.04(0.04)	0.02(0.02)	0.04(0.04)	0.1(0.2)	0.02(0.02)	0.02(0.01)
Total	100.9	100.4	100.4	85.7	83.6	84.4	84.6	86.7
Fo	87	89	89	90	92	92	82	82
Cations per formula unit based on 4 oxygens.								
Si	1.0	0.988	1.002	1.269	1.234	1.126	0.951	1.0
Ti	0	0.001	0	0.001	0.001	0.003	0.003	0.002
Al	0	0.001	0.001	0.002	0.012	0.049	0.459	0.390
Fe	0.260	0.213	0.218	0.137	0.106	0.131	0.240	0.186
Mn	0	0.003	0.003	0.009	0.008	0.005	0.008	0.006
Mg	1.726	1.802	1.772	1.283	1.368	1.524	1.091	1.073
Ca	0.010	0.007	0.004	0.035	0.037	0.014	0.034	0.098
Na	0.001	0.001	0.001	0.002	0.001	0.001	0.012	0.024
K	0	0	0	0.001	0.001	0.001	0.065	0.083
Cr	0.116	0.137	0.140	0.064	0.077	0.156	0.085	0.064
Total	3.12	3.15	3.14	2.80	2.85	2.92	2.95	2.93

Table 1: Representative mineral compositions (wt.%) of olivine (macrocrysts preserved cores), serpentine (macrocrysts serpentinized rims and microphenocryts) and Al-rich serpentine (groundmass) of the Rosário do Sul kimberlite. *Total Fe reported as FeO. Notes: n.d., not detected; n.o.a., (x) number of analysis; all standard deviations are given in 1σ, as last significant digits in brackets.

The trace element analysis of olivine microphenocrysts (Table 2), show that they have generally low contents for all elements compared to other minerals as spinels, phlogopites and perovskites, except for Ni, which reaches compositions from 901 to 4518 ppm. The V, Co and Ba contents range from 4.8 to 24 ppm, 11 to 149 ppm and 1.0 to 455 ppm, respectively. Compared to olivines from Alto Paranaíba kimberlites (Melluso et al., 2008), V and Ni contents are very similar, while Ba contents are significantly higher in Rosário do Sul olivines.

	Olivine		**Monticellite**		**Mg-chromite**		**Mg-ulvöspinel**		**Phlogopite**		**$CaTiO_3$-pv**		**Apatite**	
	Min...	Max	Min...	Max	Min...	Max	Min...	Max	Min...	Max	Min...	Max	Min...	Max
Li	-	-	30	31	21	173	17	82	8.4	186	11	49	-	-
Sc	2.3	37	13	13	26	61	66	134	8.1	112	4.6	28	-	-
V	4.8	24	28	55	1042	1593	735	1725	41	564	193	393	619	4773
Co	11	149	82	64	248	593	116	388	4.7	75	1.3	98	-	-
Ni	901	4518	552	555	694	7538	709	2221	69	586	160	914	58	255
Rb	0.4	65	45	30	2.1	32	2.2	713	4.6	1380	2.5	899	-	-
Sr	21	48	175	589	5.8	148	12	1697	4.1	1831	1883	5349	8913	22168
Y	-	-	21	41	-	-	0.9	26	0.6	43	133	255	37	96
Zr	-	-	30	64	33	176	135	723	37	5661	432	992	17	151
Nb	-	-	0.7	137	2.0	34	4.22	316	4.9	140	2547	4283	-	-
Ba	1.0	455	162	191	15	1502	6.7	10263	342	21276	26	8502	622	7684
La	-	-	3.2	167	-	-	0.3	263	0.1	92	1760	3364	16	393
Ce	-	-	7.3	349	-	-	0.3	452	0.04	209	3027	7745	22	537
Pr	-	-	0.9	37	-	-	0.1	52	-	-	322	911	2.8	52
Nd	-	-	4.7	142	-	-	0.5	205	-	-	1273	3349	12	196
Sm	-	-	1.4	28	-	-	-	-	-	-	211	454	5	37
Eu	-	-	1.4	7.8	-	-	-	-	-	-	75	117	-	-
Gd	-	-	4	17	-	-	-	-	-	-	161	247	6.7	36
Ho	-	-	-	-	-	-	-	-	-	-	8.6	12	1.4	3.4
Yb	-	-	-	-	-	-	-	-	-	-	3.3	7.5	1.3	3.4
Ta	-	-	0.2	11	-	-	-	-	-	-	101	339	-	-
Th	-	-	0	22	-	-	-	-	-	-	112	930	-	-

Table 2: The trace element minimum and maximum contents (ppm) of the Rosário do Sul kimberlite of olivine microphenocrysts, monticellites, Mg-chromites, Mg-ulvöspinels, phlogopites, $CaTiO_3$-perovskites and apatites. Detailed data of major and trace elements can be found in *Supplementary data*.

Monticellite

Monticellite is a very common mineral in Group I kimberlites, usually absent in Group II kimberlites and lamproites (Mitchell, 1995) and its occurrence suggests that the pressure

of crystallization of this rock is not higher than ~ 3 GPa (Edgar et al., 1988). The structure of monticellite is essentially the same as that of the (Mg,Fe)-olivines with an expanded unit cell due to the replacement of half of the (Mg,Fe) by Ca (Deer et al., 1992). Rosário do Sul monticellites (5 – 20 μm) occur in the groundmass, surrounding olivine macrocrysts and microphenocrysts. They are commonly subhedral to anhedral with borders partially or completely corroded and replaced to serpentine (Fig. 1A). They have Mg-chromite and $CaTiO_3$-perovskite inclusions which suggest that they crystallize after these minerals, and prior to late-stage primary groundmass minerals. The chemical composition of Rosário do Sul monticellites is very homogeneous, with solid solutions of monticellite ($CaMgSiO_4$ - 92 mol%), and kirschsteinite ($CaFeSiO_4$ - 8 mol%). The iron, magnesium and silica contents of monticellite in Rosário do Sul (~ 7 wt.% FeO, ~ 22 wt.% MgO, and 36.9 - 37.8 wt.% SiO_2) is lower than that of olivine (10 – 13 wt.% FeO, 47 - 49 MgO, and ~ 40wt.% SiO_2), while the CaO content (~ 32 wt.%) is higher (Table 3). Compared to monticellites from the Leslie kimberlite (Canada), Rosário do Sul monticellites have a very similar composition, excepting the Fe content which is significantly higher in Rosário do Sul monticellites (Abersteiner et al., *in press*). Rosário do Sul monticellites present low abundance of trace elements (Table 2), with low to moderate contents of Ni (552 – 555 ppm), Sr (175 – 589 ppm), Nb (0.1 – 137 ppm), Ba (162 – 191 ppm), La (3.2 – 167 ppm), Ce (7.3 – 349 ppm) and Nd (4.7 – 142 ppm), compared to other Rosário do Sul minerals, as spinels and phlogopites.

Sample	*Monticellite*				*Melilite*	
(n.o.a.)	CAR3A(4)	CA03D(14)	CAR301(5)	CAR3I(2)	CA03D(1)	CAR301(6)
SiO_2	37.8(0.4)	37.0(0.5)	37.6(0.2)	36.9(0.1)	40.5	24.6(0.4)
TiO_2	0.11(0.03)	0.13(0.07)	0.11(0.04)	0.101(0.004)	0.08	2.9(0.1)
Al_2O_3	n.d.	0.04(0.08)	0.01(0.01)	n.d.	7.34	12.6(0.3)
FeO*	7.4(0.3)	7.6(0.7)	7.1(0.2)	7.1(0.5)	1.43	9.2(0.3)
MnO	0.29(0.04)	0.30(0.03)	0.28(0.04)	0.312(0.007)	0.08	0.14(0.01)
MgO	22.2(0.5)	22.2(0.4)	22.8(0.4)	22.03(0.05)	3.49	2.5(0.7)
CaO	32.2(0.2)	31.7(0.2)	32.0(0.2)	32.8(0.1)	31.4	33(1)
Na_2O	0.10(0.04)	0.08(0.04)	0.07(0.05)	0.12(0.04)	0.03	0.07(0.01)
K_2O	0.03(0.04)	0.04(0.03)	0.03(0.03)	0.04(0.04)	0.50	0.3(0.1)
Cr_2O_3	n.d.	0.03(0.03)	0.02(0.03)	n.d.	0.001	0.33(0.05)
Total	100.5	99.3	100.3	99.4	86	86
Mo	92	91	92	92	-	-
Ki	8.4	8.7	8.0	8.0	-	-
Cations per formula unit based on 4 (monticellite) and 14 (melilite) oxygens.						
Si	1.01	1.002	1.005	0.997	4.183	2.784
Ti	0.002	0.003	0.002	0.002	0.006	0.246
Al	0	0.001	0	0	0.893	1.673
Fe	0.165	0.172	0.159	0.160	0.123	0.867
Mn	0.007	0.007	0.006	0.007	0.007	0.013
Mg	0.884	0.895	0.907	0.888	0.537	0.419
Ca	0.922	0.920	0.916	0.950	3.474	4.014
Na	0.005	0.004	0.004	0.006	0.215	0.016
K	0.001	0.001	0.001	0.001	0.066	0.048
Cr	0.027	0.119	0.072	0	0.001	0.029
Total	3.02	3.12	3.07	3.01	9.50	10.13

Table 3: Representative mineral compositions (wt.%) of monticellite and melilite minerals of the Rosário do Sul kimberlite. *Total Fe reported as FeO. Notes: n.d., not detected; n.o.a., (x) number of analysis; all standard deviations are given in 1σ, as last significant digits in brackets.

Melilite

Melilite are present in the segregated groundmass of the Rosário do Sul kimberlite and frequently show reaction with the mesostasis. Melilite crystals range in size from 10 to 70 µm and are subhedral to anhedral. The subhedral crystals commonly present inclusions of phlogopite, olivine and $CaTiO_3$-perovskite. Other textures as necklaces of $CaTiO_3$-perovskite, and Mg-ulvöspinel borders producing skeletal texture, are common (Fig. 1C, E and F). Subhedral melilite is also found together with monticellite as inclusions in the olivine macrocrysts and microphenocrysts borders, indicating a substitution of monticellite to melilite (Fig. 2). Anhedral melilite occurs in the groundmass and in the mesostasis, as acicular microlites. In the Rosário do Sul mesostasis (Fig. 1A), melilite and soda melilite are concomitant to akermanite, phlogopite and carbonate. The subhedral and anhedral melilites have compositions that vary from high SiO_2 (40 wt.%) and low TiO_2 (0.08 wt.%), Al_2O_3 (7.34 wt.%) and FeO (1.4 wt.%) contents, to low SiO_2 (24.6 wt.%) and high TiO_2 (2.9 wt.%), Al_2O_3 (12.6 wt.%) and FeO (9.2 wt.%) contents (Table 3). The MgO (from 2.5 to 3.5wt.%) and CaO (from 31 to 33 wt.%) contents are homogeneous in all crystals. Eventually, melilite crystals present Ti-zonation, with Ti-enriched cores and Fe-enriched rims.

According to Conceição et al. (*in prep.*), Rosário do Sul monticellites and melilites are the product of a reaction between olivine and a liquid enriched in calcium and carbonate. CaO + Al_2O_3 and MgO + FeO diagram (Fig. 2) shows a comparison among olivine megacryst cores and serpentinized rims, serpentinized olivine microphenocrysts, serpentinized groundmass olivines, monticellites and melilites. According to the trend 1 (Fig. 2), the serpentinization of the groundmass olivine is a product of fresh olivine alteration, in which part of the Mg and Fe cations are replaced by Al. Following the trend 2,

there is an enrichment in the Al content, and Al-rich serpentinized olivines are product of an alteration process that resulted in the crystallization of monticellite and melilite. Monticellite crystallizes as a product of olivine alteration with the replacement of Mg and Fe by Ca, and melilite crystallizes from a Ca and Al contents increasing followed by a decreasing in Fe and Mg contents in the crystalline structure.

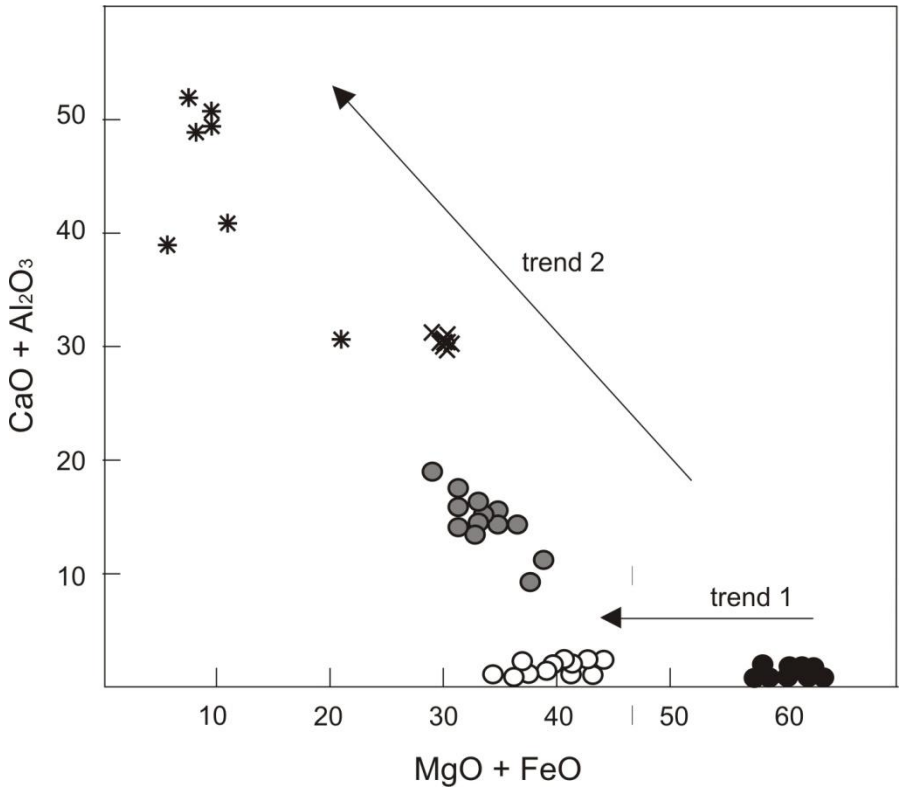

Fig. 2: Diagram CaO + Al_2O_3 *versus* MgO + FeO, where: open circles are olivine macrocrystals fresh cores; filled circles are olivine macrocrystals serpentinized rims and serpentinized microphenocrysts; partially filled circles are serpentinized groundmass olivines; crosses are monticellites; and stars are melilites. Trend 1 represents the olivine serpentinization, whereas trend 2 shows the alteration of serpentinized olivine to Al-rich serpentinized olivine, monticellite and melilite.

Spinel

The Rosário do Sul spinels have two different compositions: Mg-chromite, which has MgO and Cr_2O_3 contents from 13.7 to 15 wt.% and 41 to 43 wt.%, respectively; and Mg-ulvöspinel, product of a solid solution between magnetite and ulvöspinel, with FeO contents of 65.7 to 74 wt.% , TiO_2 contents of 9 to 11 wt.%, and MgO contents of 6.5 to 9.5 wt.% (Table 4). Mg-chromites are euhedric to subhedric, from 5 to 10 µm and are usually found as inclusions in olivine macrocrysts and microphenocrysts (Fig.1B and D), being less often in the groundmass. Eventually, present zonations of Cr- and Al-enriched cores to Fe- and Ti-enriched rims. Mg-ulvöspinels are euhedral to anhedral, from 10 to 40µm and are commonly found in the groundmass, but sometimes included in microphenocrysts of phlogopite, monticellite, $CaTiO_3$-perovskite and apatite. Skeletal texture is observed, where Mg-ulvöspinel border surrounds melilite, apatite, monticellite and olivine crystals (Fig.1A and E). There is a very common Fe-Ti zonation in the Mg-ulvöspinel crystals, with Ti-enriched cores and Fe-enriched rims (Fig. 1C). Ti content probably was consumed during and after the crystallization of $CaTiO_3$-perovskite, being replaced by Fe in the Mg-ulvöspinel crystalline structure. This zonation indicates that crystallization of Mg-ulvöspinel occurs after the $CaTiO_3$-perovskite that probably consumed the major amount of Ti.

Sample	*Mg-chromite*			*Mg-ulvöspinel*		
(n.o.a.)	CA03D(2)	CAR301(1)	CAR3I(5)	CAR3A(3)	CA03D(10)	CAR301(3)
SiO_2	0.15(0.03)	0.16	0.14(0.01)	0.07(0.01)	0.07(0.02)	0.06(0.02)
TiO_2	1.6(0.1)	1.47	1.3(0.2)	10.4(0.4)	9(1)	11.0(0.3)
Al_2O_3	19.2(0.3)	19.3	19(1)	2.2(2.3)	1.0(0.4)	4.5(0.5)
FeO*	19.6(0.6)	19.14	21(2)	72(5)	74(4)	65.7(0.8)
MnO	0.47(0.03)	0.44	0.42(0.02)	0.57(0.03)	0.55(0.04)	0.55(0.04)
MgO	15.0(0.4)	15.0	13.7(0.2)	7(2)	6.5(0.4)	9.5(0.4)
CaO	0.07(0.01)	0.14	0.03(0.01)	0.19(0.08)	0.25(0.09)	0.3(0.1)
Na_2O	n.d.	n.d.	0.02(0.01)	0.01(0.01)	0.02(0.02)	0.05(0.02)
K_2O	n.d.	0.02	n.d.	0.03(0.03)	0.02(0.02)	0.03(0.03)
Cr_2O_3	43(1)	43.41	41(1)	1.5(0.9)	3.4(4.4)	2.5(0.3)
Total	99.5	99.2	96.7	94.5	95.3	94.6
Cations per formula unit based on 32 oxygens.						
Si	0.037	0.040	0.038	0.023	0.021	0.022
Ti	0.298	0.278	0.265	2.688	2.442	2.722
Al	5.687	5.730	5.713	0.889	0.425	1.723
Fe	4.121	4.034	4.639	20.61	21.42	18.0
Mn	0.101	0.094	0.093	0.168	0.163	0.152
Mg	5.641	5.628	5.347	3.772	3.349	4.664
Ca	0.020	0.039	0.008	0.068	0.092	0.108
Na	0.002	0.002	0.009	0.008	0.017	0.030
K	0	0.006	0.002	0.012	0.008	0.014
Cr	8.610	8.648	8.489	0.409	0.933	0.656
Total	24.52	24.50	24.60	28.65	28.87	28.08

Table 4: Representative mineral compositions (wt.%) of spinel group minerals of the Rosário do Sul kimberlite. *Total Fe reported as FeO. Notes: n.d., not detected; n.o.a., (x) number of analysis; all standard deviations are given in 1σ, as last significant digits in brackets.

Mg-chromite and Mg-ulvöspinel of the Rosário do Sul kimberlite are plotted in the Cr – Al – (Fe^{2+} + 2Ti) diagram (Fig. 3) with spinels from: Alto Paranaíba kimberlites and

kamafugites (Melluso et al., 2008), which have chemical affinities with the Group II kimberlites; Lac de Gras kimberlite (Canada) (Fedortchouk & Canil, 2004), that present chemical affinities with Group I kimberlites; and kimberlites and a carbonatite from Arkhangelsk kimberlite province (Russia) (Beard et al., 2000). The Rosário do Sul Mg-chromites plot close to the Lac de Gras and Arkhangelsk spinels but have lower Cr content. Mg-ulvöspinels plot very close to the Magnetite + Ulvöspinel vertex, together with spinels from Arkhangelsk kimberlites and carbonatite.

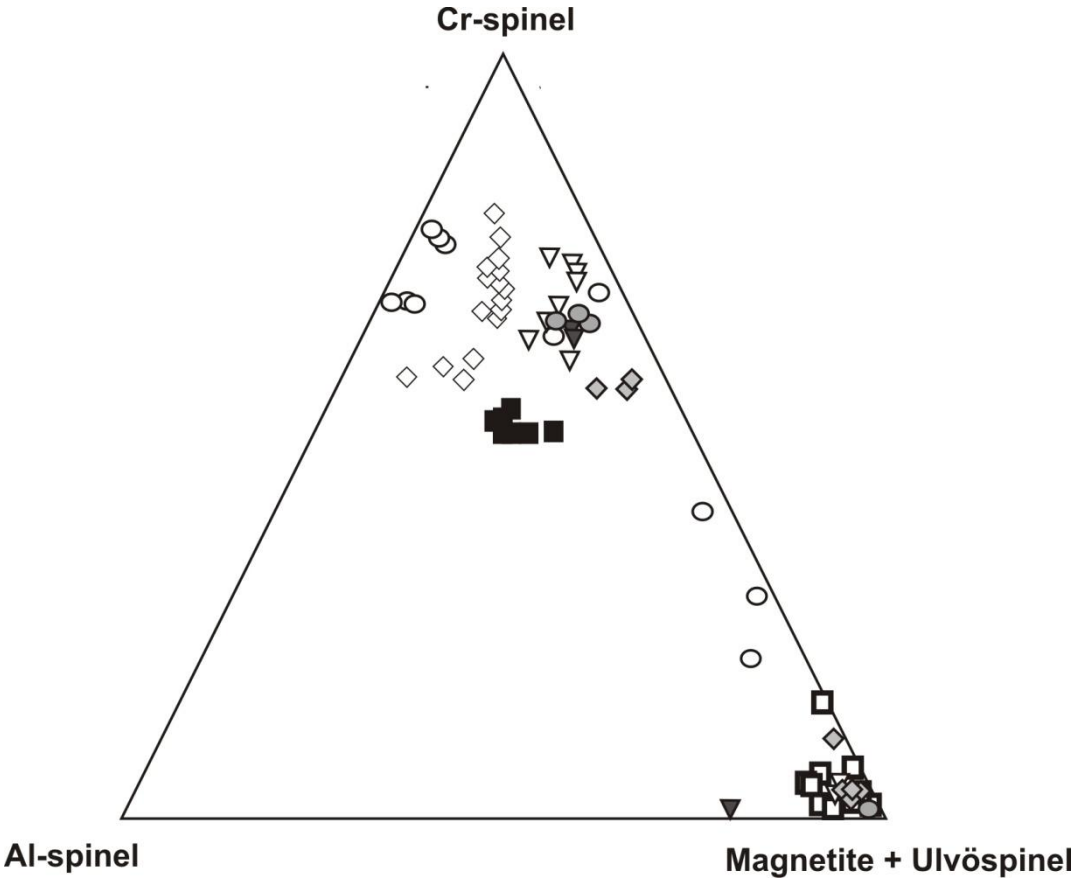

Fig. 3: Cr – Al – (Fe^{2+} + 2Ti) diagram for spinel-group minerals. Spinels from the Rosário do Sul kimberlite are plotted as filled (Mg-chromite) and open squares (Mg-ulvöspinel); Alto Paranaíba kimberlites and kamafugites spinels are shown by open circles (Melluso et al., 2008) and represent spinels from Group II kimberlites; spinels from Lac de Gras kimberlite (Canada) are open diamonds (Fedortchouk & Canil, 2004) and represent spinels

of the Group I kimberlites; spinels from Arkhangelsk kimberlite province are shown by: open down-triangles (Group II diamondiferous kimberlites of Zolotitsa Field), gray down-triangles (kimberlite of Mela Field), gray diamonds (Group I diamond-poor Ti-Fe-rich kimberlites from other Arkhangelsk fields), and gray circles (calciocarbonatite of Mela Field) (Beard et al., 2000).

In figure 4A, a comparison between MgO and Al_2O_3 (wt.%) of groundmass spinels shows that Mg-chromites have higher Al_2O_3 and MgO contents, while Mg-ulvöspinels have lower Al_2O_3 and MgO contents. Figure 4B shows Ti/(Ti+Cr+Al) *versus* $Fe^{2+}/(Fe^{2+} + Mg)$ in molar fractions, and spinel trend 1 and trend 2 proposed by Mitchell (1986). Trend 1 represents spinels from Group I kimberlites with typically Mg-chromite zoned to Mg-ulvöspinel. Trend 2 represents spinels from Group II kimberlites (orangeites) and also lamproites that contain Mg-chromite rarely zoned to Ti-magnetite, and do not present Mg-ulvöspinels. Trend 2 is rare in kimberlites of Group I, but can be observed in varieties with macrocrystal mica Mitchell (1995). The Rosário do Sul spinels plot in the spinel trend 2. Mg-chromites have lower Ti/(Ti+Cr+Al) ratios, while Mg-ulvöspinels have higher Ti/(Ti+Cr+Al) ratios. For comparison: spinels from Alto Paranaíba kimberlites and kamafugites (Melluso et al., 2008); and from kimberlites and a carbonatite from Arkhangelsk kimberlite province (Russia) (Beard et al., 2000).

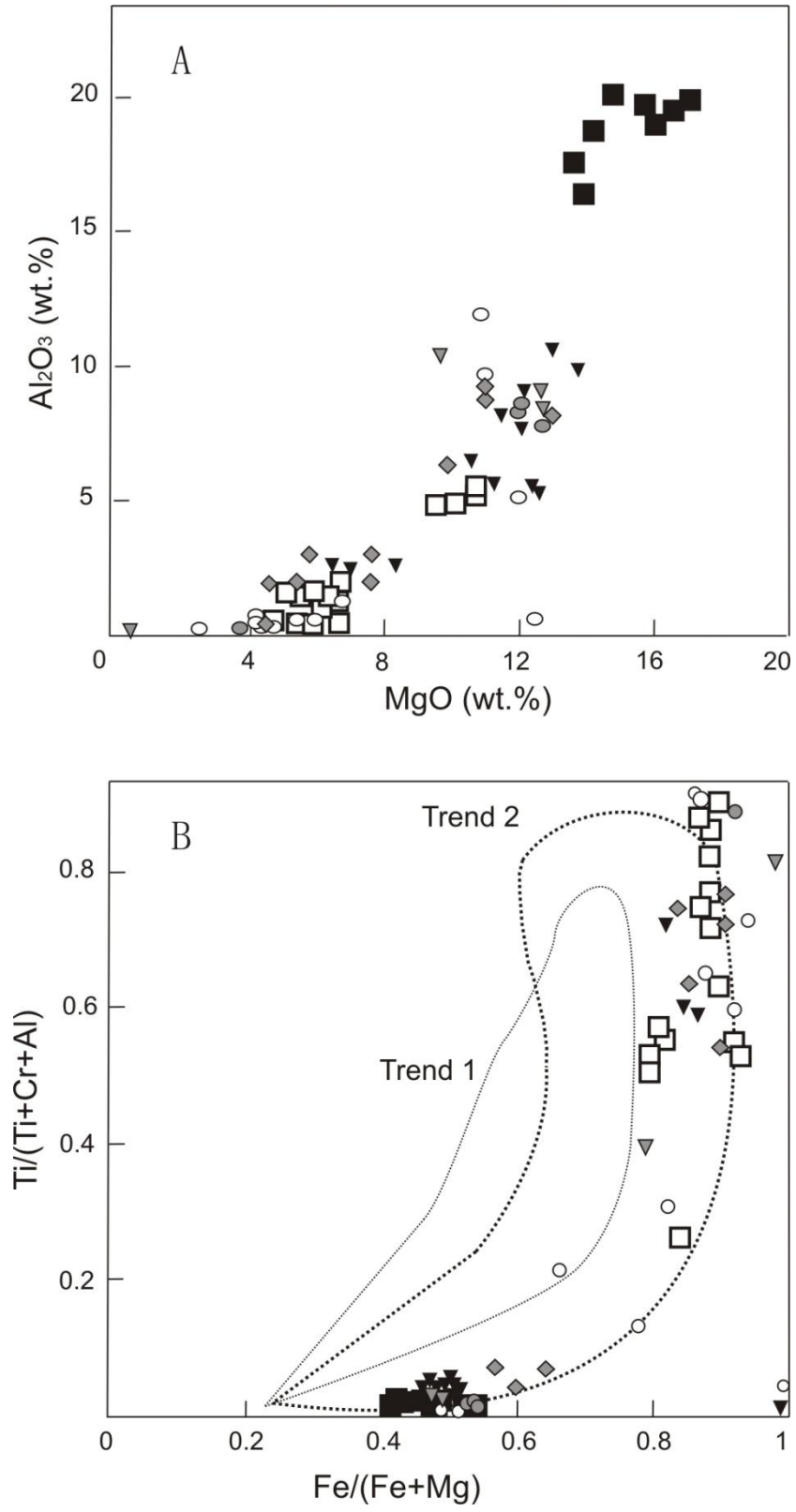

Fig. 4: A. Al_2O_3 *versus* MgO wt.% and B. Ti/(Ti+Cr+Al) *versus* $Fe^{2+}/(Fe^{2+}$ + Mg) (molar fractions). Filled squares are Rosário do Sul Mg-chromites and open squares are Rosário do Sul Mg-ulvöspinels. Spinels from Alto Paranaíba kimberlites and kamafugites, and

Arkhangelsk Field are shown as in figure 3. Trend 1 represents spinels from Group I kimberlites, and trend 2 represents spinels from Group II kimberlites (orangeites) and also lamproites Mitchell (1986).

Trace element compositions of Mg-chromites show V contents from 1042 to 1593 ppm, Ni contents from 694 to 7538 ppm, Ba contents from 15 to 1502 ppm, Rb contents from 2 to 32 ppm, Sr contents from 5.8 to 148 ppm, Zr contents from 33 to 176 ppm and Nb contents from 2 to 34 ppm. Mg-ulvöspinels have V contents from 735 to 1725 ppm, Ni contents from 709 to 2221 ppm, Ba contents from 6 to 10263 ppm, Rb contents from 2 to 713 ppm, Sr contents from 12 to 1697 ppm, Zr contents from 135 to 723 ppm and Nb contents from 2 to 316 ppm (Table 2). Compared to Cr-Fe-Ti oxides of Alto Paranaíba kimberlites and kamafugites (Melluso et al., 2008), Ni, Ba, Rb, Sr, Zr and Nb contents are higher in Rosário do Sul Mg-chromites and Mg-ulvöspinels, while only V contents are similar.

Phlogopite

Phlogopite occurs in Rosário do Sul kimberlite as microphenocrysts (<1.5 mm) (Fig. 1B, D and E) and in the groundmass (Fig. 1A, E and F), which is generally associated to melilite, calcite and the mesostasis. Phlogopite microphenocrysts have inclusions of $CaTiO_3$-perokskite, Mg-chromite, Mg-ulvöspinel and monticellite, and can be frequently altered to chlorite. Phlogopite also occurs as inclusions in the serpentinized olivine macrocryst rims and microphenocrysts, together with Mg-chromite and melt pockets.

Rosário do Sul phlogopites have SiO_2 content from 37.5 to 42 wt.%, MgO from 20.8 to 24 wt.%, K_2O from 9.5 to 10.4 wt.%, and FeO from 7 to 11 wt.%. Phlogopite microphenocrysts (Table 5) are enriched in TiO_2 (from 1.6 to 2.9 wt.%) but have less Al_2O_3 contents (from 3.3 to 9.6 wt.%) compared to groundmass phlogopites, that have lower TiO_2

contents (from 0.1 to 0.8 wt.%) and higher Al_2O_3 contents (from 12.2 to 16.6 wt.%). This variation can be related to the crystallization of $CaTiO_3$-perovskite that consumed Ti and left less amount of this element available in the melt. This evolution trend is observed in the diagram of figure 5, together with phlogopites compositions from Alto Paranaíba kimberlites and kamafugites (Brazil) (Melluso et al., 2008), Arkhangelsk kimberlite province and a calciocarbonatite of Mela Field (Russia) (Beard et al., 2000); Jacupiranga complex carbonatites (Brazil) (Brod et al., 2001), and others Canadian and Russian kimberlites and carbonatites (Reguir et al., 2009). The same tetraferriphlogopite-phlogopite trend is observed in phlogopites from Alto Paranaíba kimberlites and kamafugites, and Arkhangelsk kimberlites. The main phlogopites from carbonatites (Mela Field, Jacupiranga complex and the ones from Canada and Russia) have equal or higher Al and Fe contents than phlogopites from Rosário do Sul kimberlites.

Sample	*Phlogopite*					*$CaTiO_3$-Perovskite*				*Apatite*	
(n.o.a.)	CAR3A(3)	CA03D(7)	CAR301(2)	CAR3I(3)	CAR3F(2)	CAR3A(3)	CA03D(3)	CAR301(4)	CAR3I(3)	CAR-3A(3)	CA-03D(4)
SiO_2	42(1)	40(1)	37(1)	40(3)	37.5(0.6)	0.01(0.03)	0.06(0.03)	n.d.	0.05(0.02)	0.7(0.9)	0.5(0.4)
TiO_2	2.1(0.8)	1.1(0.9)	0.2(0.1)	1.3(0.7)	0.5(0.1)	56.3(0.4)	55.4(0.3)	56.9(0.4)	55.3(0.4)	0.02(0.01)	n.d.
Al_2O_3	6(2)	9(4)	16.3(0.4)	9(6)	13.8(0.6)	0.23(0.02)	0.36(0.02)	0.21(0.01)	0.27(0.07)	0.03(0.05)	0.02(0.02)
FeO*	11(2)	7(2)	7.6(0.7)	9.5(0.4)	10.2(0.5)	1.5(0.2)	2.24(0.09)	1.2(0.1)	1.5(0.4)	0.2(0.1)	0.1(0.05)
MnO	0.11(0.03)	0.1(0.1)	0.21(0.04)	0.2(0.2)	0.36(0.03)	0.02(0.02)	0.04(0.02)	0.01(0.01)	n.d.	0.03(0.02)	0.01(0.03)
MgO	24(2)	24(1)	22.8(0.4)	22(2)	20.8(0.5)	0.05(0.01)	0.045(0.005)	0.05(0.02)	0.04(0.02)	0.06(0.03)	0.05(0.04)
CaO	0.12(0.05)	0.14(0.06)	0.18(0.05)	0.06(0.04)	0.20(0.09)	38.5(0.8)	38.0(0.2)	37.9(0.4)	39.5(0.3)	53.2(0.6)	51(3)
Na_2O	0.5(0.2)	0.3(0.3)	0.04(0.04)	0.5(0.5)	0.10(0.05)	0.27(0.02)	0.22(0.03)	0.24(0.05)	0.27(0.07)	0.03(0.03)	0.4(0.5)
K_2O	9.5(0.2)	9.7(0.3)	9.5(0.3)	10.2(0.2)	10.4(0.3)	0.06(0.02)	0.054(0.006)	0.07(0.06)	0.07(0.02)	0.01(0.01)	0.03(0.05)
Cr_2O_3	0.09(0.05)	0.04(0.04)	0.03(0.05)	0.02(0.02)	n.d.	0.10(0.03)	0.04(0.05)	0.09(0.09)	0.09(0.08)	0.01(0.02)	n.d.
P_2O_5	n.d.	n.d.	n.d.	n.d.	n.d.	n.d.	n.d.	n.d.	n.d.	40.3(0.9)	39(2)
Total	96.4	93.1	93.8	92.3	93.9	97.1	96.5	96.7	97.1	94.7	91.9
Cations per formula unit based on 22 (phlogopite), 12 (perovskite) and 24 (apatite) oxygens.											
Si	6.215	5.994	5.403	6.007	5.611	0.001	0.006	0.001	0.005	0.087	0.114
Ti	0.233	0.128	0.025	0.151	0.063	3.971	3.936	4.015	3.904	0	0.002
Al	0.970	1.648	2.835	1.610	2.438	0.026	0.041	0.024	0.030	0.003	0.001
Fe	1.311	0.918	0.935	1.212	1.274	0.115	0.177	0.097	0.117	0.021	0.024
Mn	0.014	0.013	0.026	0.026	0.046	0.002	0.003	0.001	0	0.002	0.004
Mg	5.307	5.360	5.0	4.954	4.631	0.007	0.006	0.007	0.005	0.012	0.016
Ca	0.019	0.022	0.028	0.010	0.033	3.869	3.849	3.807	3.975	9.444	9.495
Na	0.141	0.095	0.013	0.144	0.030	0.048	0.040	0.043	0.049	0.138	0.010
K	1.822	1.835	1.783	1.983	1.991	0.007	0.006	0.008	0.009	0.007	0.002
Cr	0.011	0.005	0.004	0.003	0.001	0.007	0.003	0.007	0.007	0	0.001
P	0	0	0	0	0	0	0	0	0	5.708	5.688
Total	16.04	16.02	16.05	16.10	16.12	8.04	8.06	7.99	8.10	15.42	15.36

Table 5: Representative mineral compositions (wt.%) of phlogopite, $CaTiO_3$-perovskite and apatite of the Rosário do Sul kimberlite. *Total Fe reported as FeO. Notes: n.d., not detected; n.o.a., (x) number of analysis; all standard deviations are given in 1σ, as last significant digits in brackets.

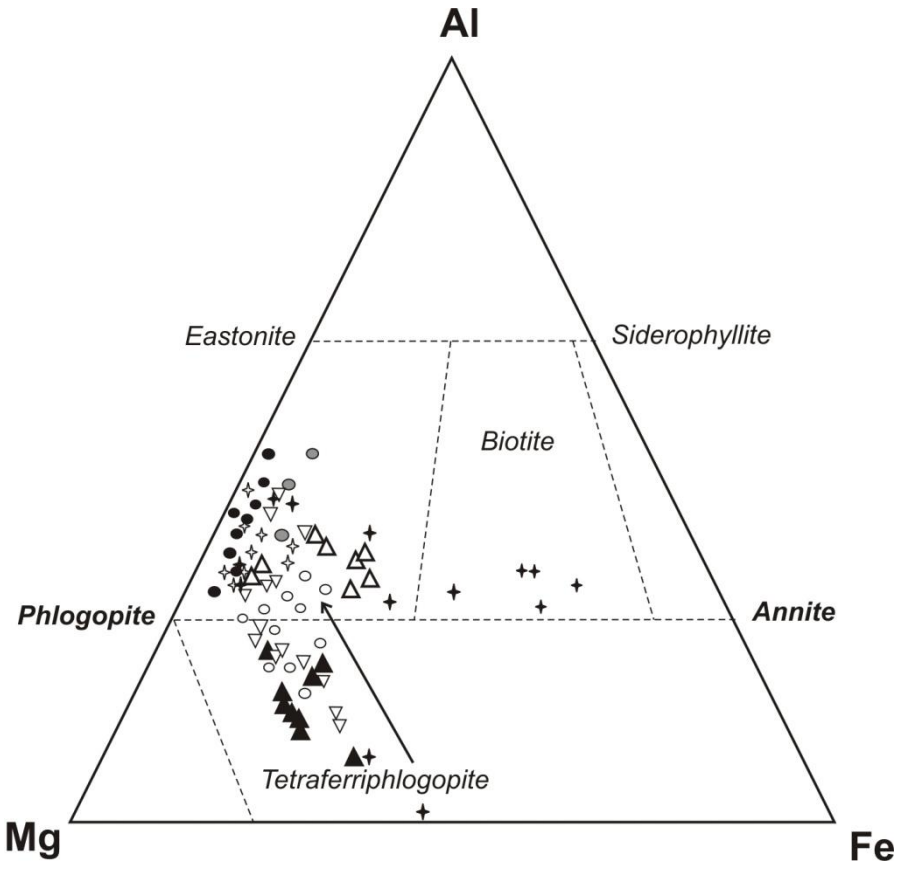

Fig. 5: Mg-Fe-Al diagram modified after Mitchell (1995), showing the compositions of Rosário do Sul phlogopite microphenocrysts (filled triangles) and groundmass phlogopites (open triangles). The tetraferriphlogopite-phlogopite evolution trend shows an Al enrichment and Ti depletion of the phlogopite compositions. For comparison, phlogopites from Alto Paranaíba kimberlites and kamafugites are shown by open circles (Melluso et al., 2008); phlogopites from Arkhangelsk kimberlite province are shown by open down-triangles, and from the calciocarbonatite of Mela Field are gray circles (Beard et al., 2000); phlogopites from Jacupiranga complex carbonatites (Brazil) are filled circles (Brod et al., 2001), and phlogopites from Canadian and Russian kimberlites and carbonatites are open and filled stars, respectively (Reguir et al., 2009).

Figure 6A shows the Ti depletion and Al enrichment of Rosário do Sul phlogopites, which is represented by the tetraferriphlogopite-phlogopite trend. This compositional

variation is also observed in phlogopites from other kimberlites and carbonatites. The octahedral sites of Rosário do Sul phlogopites are randomly occupied by Fe^{2+} and Mg, and the tetrahedral sites are occupied by Si and Al, as the trend observed in figure 6B.

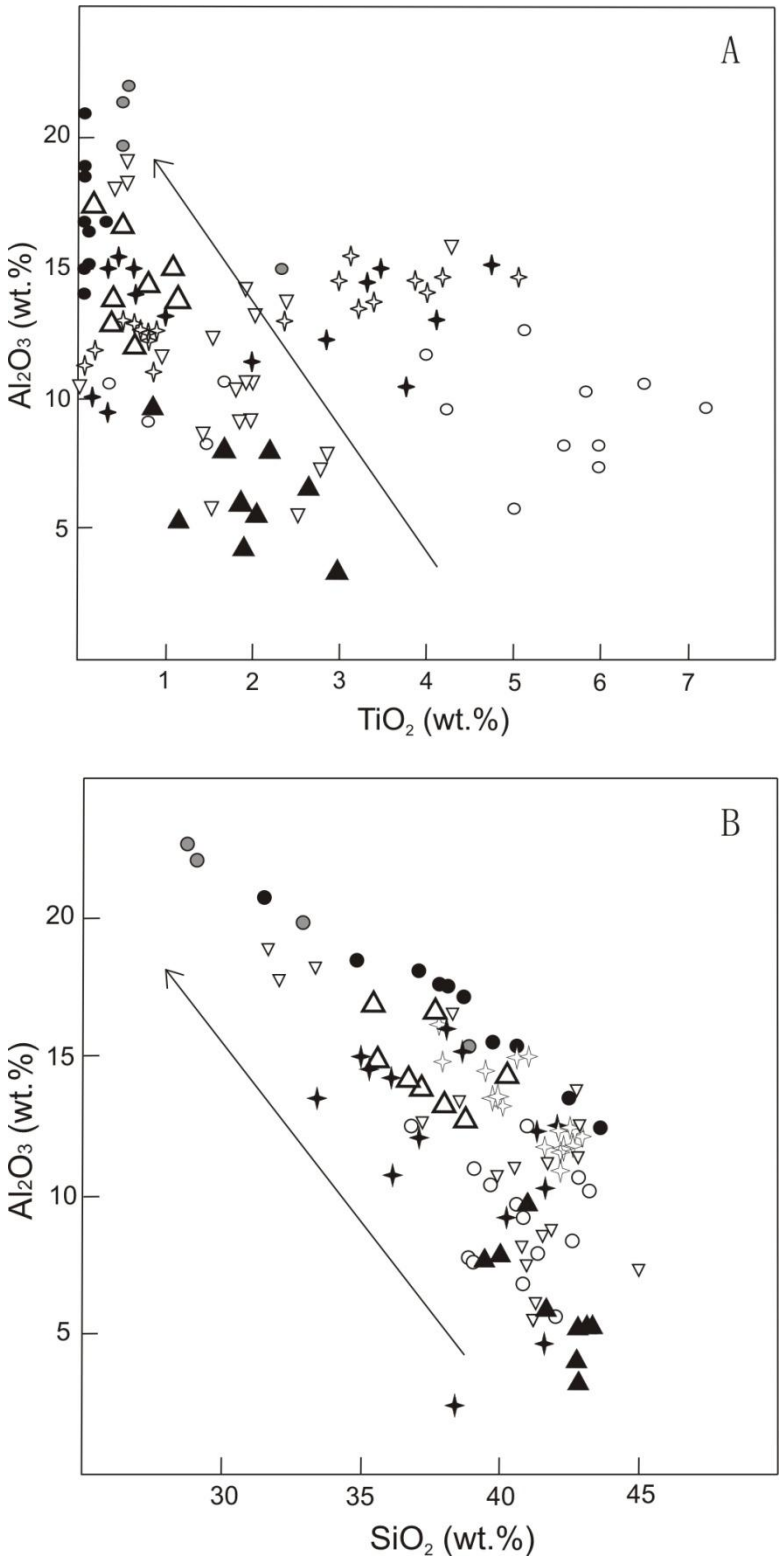

Fig. 6: A. Diagram comparing Al_2O_3 *versus* TiO_2 (wt.%) contents of phlogopite microphenocrysts and groundmass, and the evolution trend TiO_2 – Al_2O_3 observed in Rosário do Sul phlogopites compositions; B. Diagram comparing Al_2O_3 *versus* SiO_2 (wt.%)

contents of phlogopite microphenocrysts and groundmass, showing the substitutions in the tetrahedral site. Symbols legend identical to figure 5.

Trace element compositions of Rosário do Sul phlogopites (Table 2) have Rb contents from 4.6 to 1380 ppm, Sr contents from 4.1 to 1831 ppm, Zr contents from 37 to 5661 ppm and Ba contents from 342 to 21276 ppm. The chondrite normalized trace element compositions of the Ti-rich-Al-poor (microphenocrysts) (Fig.7A) and Ti-poor-Al-rich (groundmass) (Fig.7B) phlogopites of the Rosário do Sul kimberlite show positive anomalies of Li, Rb, Sr, Zr, Nb, Ba and Ta, and negative anomalies of Ni, Y, Ho, Yb and Th. There is an enrichment in LREE (La, Ce, Pr, Nd, Sm and Eu) related to the HREE (Y, Gd, Ho and Yb).

The carbonatitic phlogopites from Canada and Russia (Reguir et al., 2009), and kimberlitic and kamafugitic phlogopites from Alto Paranaíba (Melluso et al., 2008) (Fig.7A and B) have spidergrams very similar to Rosário do Sul phlogopites, with positive anomalies of Rb, Sr, Zr, Nb, Ba and Ta, and negative anomalies of Ni and Y. Phlogopites from Alto Paranaíba kimberlites and kamafugites also show negative anomalies of HREE and Th. The first crystallized phlogopite microphenocrysts have higher Ti, Sr and Ba contents and lower Al, Nb and La contents (Fig. 8A, B and C) than the later groundmass phlogopites (Fig. 8D).

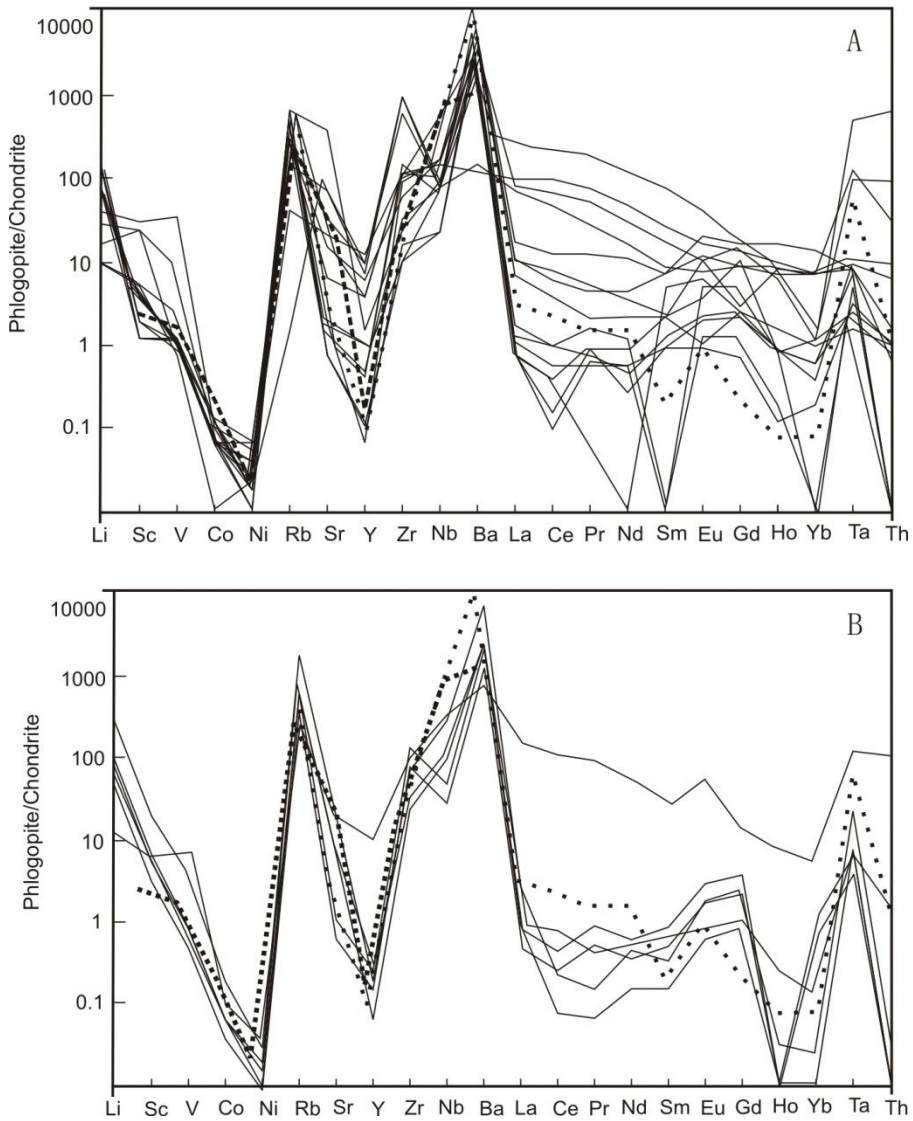

Fig. 7: Trace element diagrams of Rosário do Sul phlogopites normalized to chondrite from McDonough & Sun (1995): A. spidergrams of Ti-rich - Al-poor phlogopite microphenocrysts; B. spidergrams of Ti-poor – Al-rich phlogopites of the groundmass phlogopites. In both figures, chondrite normalized trace element average of phlogopites from Alto Paranaíba (Brazil) kimberlites and kamafugites are shown by the light dashed line (Melluso et al., 2008); and chondrite normalized trace element average of phlogopites from Canadian and Russian carbonatites are shown by the strong dashed line (Reguir et al., 2009).

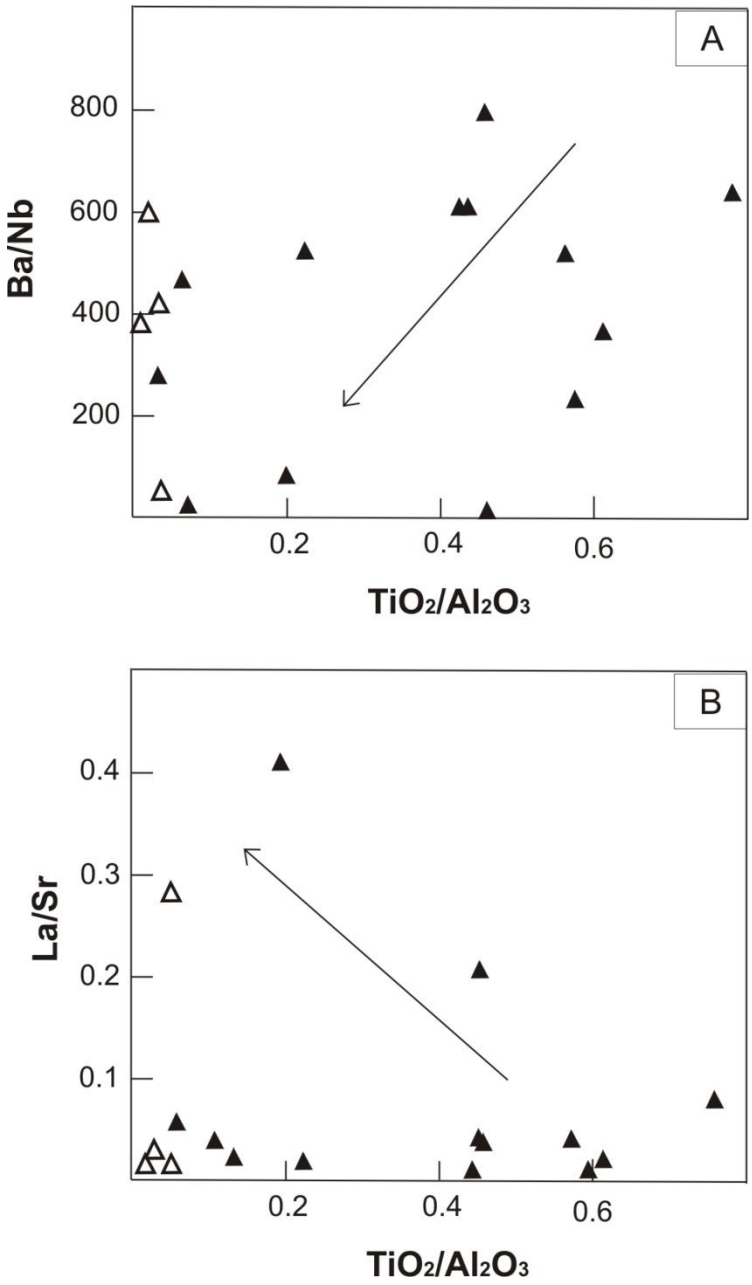

Fig. 8: Diagrams of Ba/Nb (A) and La/Sr (B) ratios *versus* TiO_2/Al_2O_3 ratio of Rosário do Sul phlogopite microphenocrysts (filled triangles) and groundmass (open triangles): Ba and Sr contents decrease, while Nb and La contents increase with TiO_2 depletion and Al_2O_3 enrichment of phlogopite compositions.

$CaTiO_3$-perovskite

$CaTiO_3$-perovskite is ubiquitous in Rosário do Sul kimberlite samples. They are small and euhedral (10 – 40 μm) (Fig. 1), and present a homogeneous chemical composition of around 55 wt.% TiO_2 and 38 wt.% CaO, with very little solid solution (Table 5). Inclusions of olivine and Mg-chromite are very common. The total FeO contents display slight variation from 1.2 and 2.24 wt.% and may be indicative of formation under low oxygen fugacities Kimura and Muan (1971a and b).

The Rosário do Sul perovskite composition is essentially $CaTiO_3$, without considerable substitution of Ca cations for Na + Ce and Sr + Ba cations in the dodecahedral site (Fig. 9A and B), but with substitution of Nb + Fe cations for Ti cation in the octahedral site (Fig. 9C).

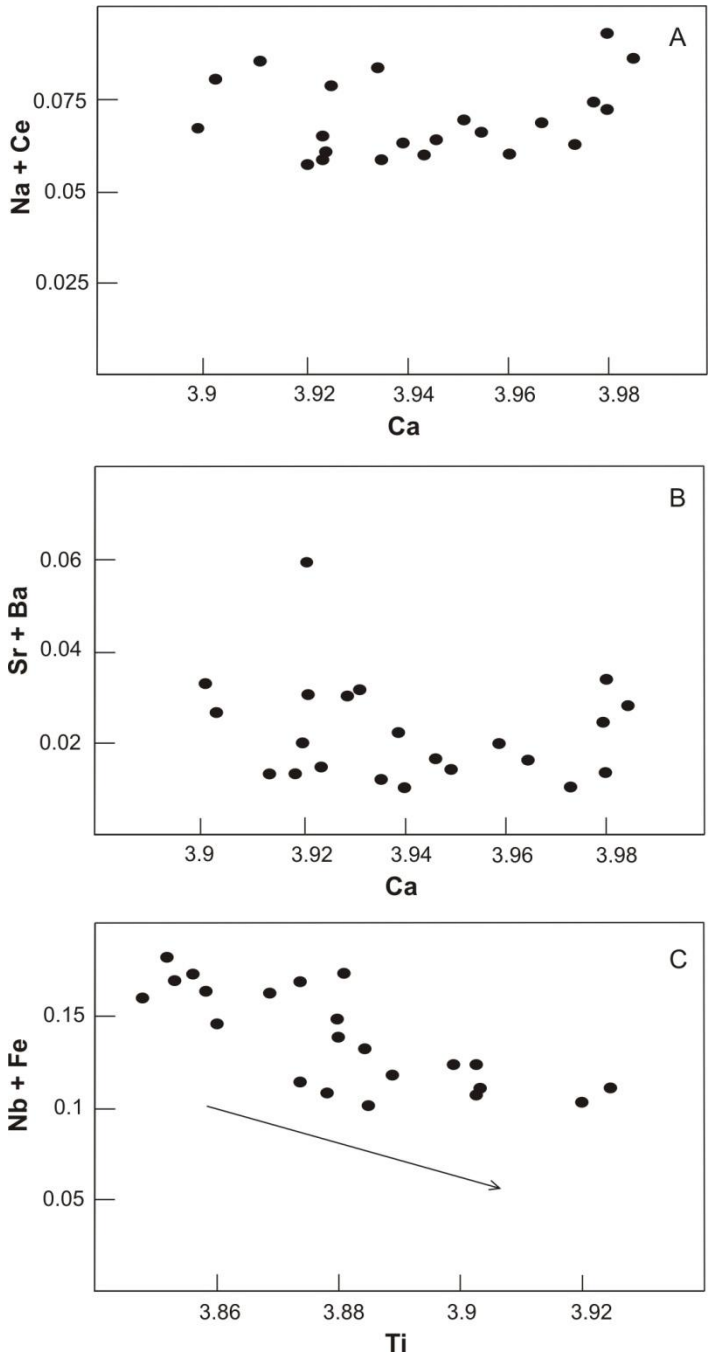

Fig. 9: Diagrams comparing: (A) Na + Ce cations plotted against Ca cations; (B) Sr + Ba cations plotted against Ca cations; (C) Nb + Fe cations *versus* Ti cations of Rosário do Sul perovskites. The only substitution observed is Nb + Fe *versus* Ti cations in the octahedral site.

The Rosário do Sul $CaTiO_3$-perovskites are the major REE mineral host, with Sr contents from 1883 to 5349 ppm, Nb contents from 2547 to 4283 ppm, Ba contents from 26

to 8502 ppm, La contents from 1760 to 3364 ppm, Ce contents from 3027 to 7745 ppm and Nd contents from 1273 to 3349 ppm (Table 2). Ni contents range from 160 to 914 ppm, Rb contents range from 2.5 to 899 ppm, Zr contents range from 432 to 992 ppm, Pr contents range from 322 to 911 ppm and Th contents range from 112 to 930 ppm. In the chondrite-normalized trace element diagram (Fig. 10A), the Rosário do Sul perovskites plot with positive anomalies of Sr, Nb, La and Ta, and negative anomalies of Sc, Co, Ni, Ba and Yb. For comparison, perovskites data from the Lucapa I kimberlite (Angole) (Castillo-Oliver et al., 2016), and from the West Kimberley lamproite Ellendale 4 (Western Australia) (Jaques, 2016) are also plotted. The chondrite-normalized REE distribution pattern (Fig. 10B) shows an enrichment of REE contents compared to chondrite composition, and an enrichment of LREE contents compared to HREE contents, with La/Yb ratio ranging from 234 to 794, which reflects the high partition coefficient of LREE for $CaTiO_3$-perovskite in silicate melts (Nagasawa et al., 1980). The diagram also shows this similar LREE enrichment in $CaTiO_3$-perovskites from Udachnaya East (Russia), Chicken Park (Colorado) and Iron Mountain (Wyoming) hypabyssal kimberlites, and Grizzly pipe (Canada) (Chakhmouradian et al., 2013); and from a sövitic carbonatite perovskite from Badberg Kaiserstuhl (Germany) (Hornig-Kjarsgaard, 1998). Carbonatitic perovskites from Kola carbonatites (Russia) (Chakhmouradian and Mitchell, 1997) have higher Nb (from 43100 to 140200 ppm), La (from 5800 to 17700 ppm) and Ta (from 2700 to 9400 ppm) contents than Rosário do Sul perovskites.

During the beginning of perovskite crystallization, the TiO_2 content in the Rosário do Sul melt is higher, and the melt is richer in Sr and Ba contents (Fig. 11A and B) than during the late stages of perovskite crystallization, when the Al_2O_3 content increase with the depletion of Ti, and La and Ta contents also increase (Fig. 11C and D).

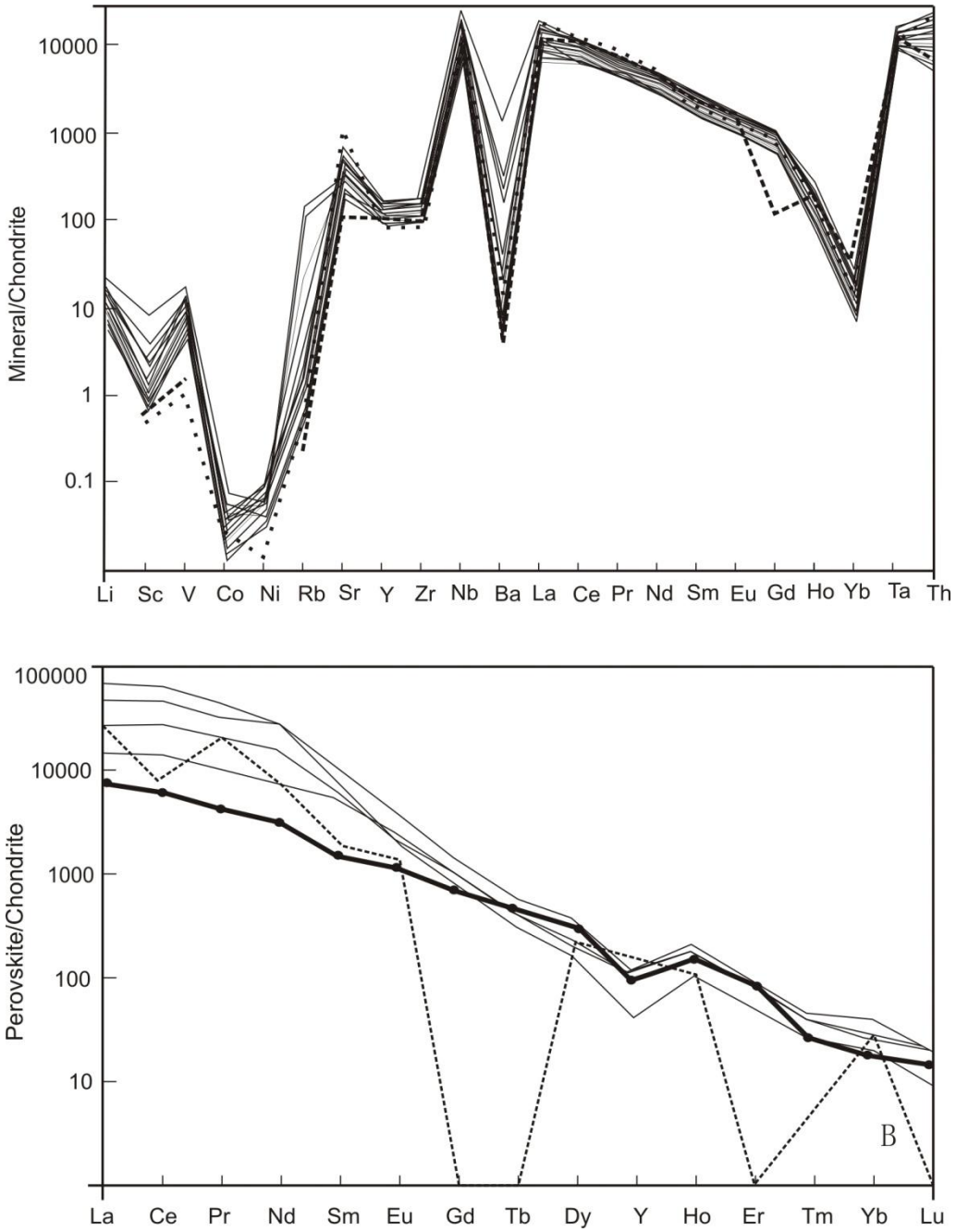

Fig. 10: A. Trace element compositions normalized to chondrite from McDonough & Sun (1995): Rosário do Sul perovskites are the simple lines; perovskite from Lucapa I kimberlite (Angole) is the strong dashed line (Castillo-Oliver et al., 2016); and perovskite from West Kimberley lamproite Ellendale 4 (Western Australia) is the light dashed line (Jaques, 2016). B. Chondrite-normalized REE distribution patterns for the most REE-enriched perovskite of each kimberlite. The bold line represents Rosário do Sul $CaTiO_3$-perovskite composition. The simple lines are from Udachnaya East, Chicken Park, Iron Mountain and Grizzly

perovskites (data from Chakhmouradian et al., 2013); and the dashed line is from Badberg Kaiserstuhl (Germany) mica sövite perovskite (data from Hornig-Kjarsgaard, 1998).

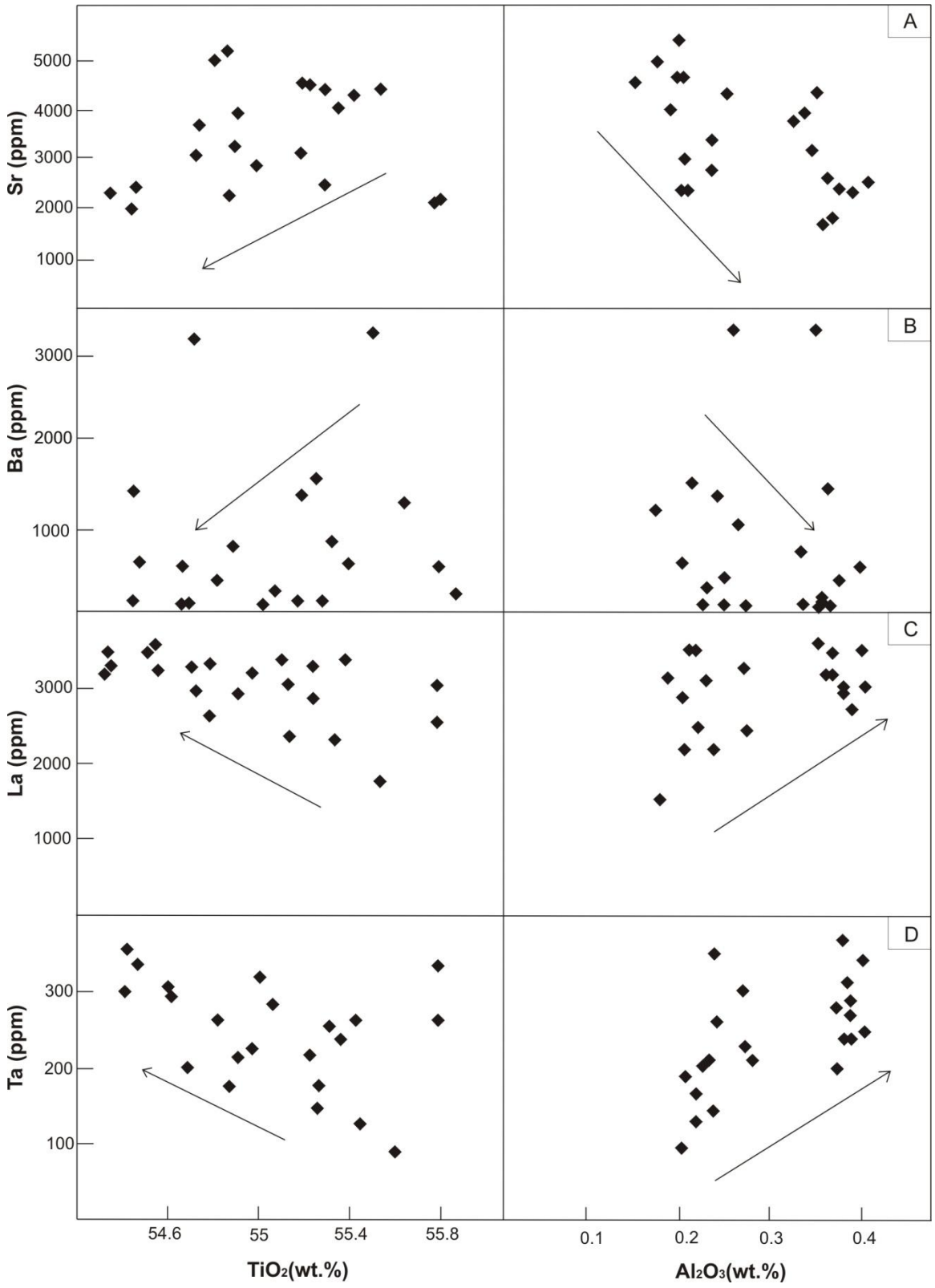

Fig. 11: Diagrams of Sr, Ba, La and Ta (ppm) *versus* TiO_2 (wt.%) and Al_2O_3 (wt.%) of Rosário do Sul perovskites: the Sr and Ba contents (A and B) decrease, while the La and Ta contents (C and D) increase, with TiO_2 depletion and Al_2O_3 enrichment of the melt.

Apatite

Apatite is present in the Rosário do Sul kimberlite, as euhedral to subhedral microphenocrysts (Fig. 1C, D and F), varying in size from 20 to 150 μm, or in the groundmass, generally with irregular shape. The CaO and P_2O_5 contents of Rosário do Sul apatites range from 51 to 53 wt.% and from 39 to 40 wt.%, respectively. The microphenocrysts are commonly zoned, with Si and Na-enriched borders and P and Ca-enriched cores, while the groundmass apatites show corroded borders surrounded by ulvöspinel and the mesostasis.

The trace-elements compositions of Rosário do Sul apatites show V contents from 619 to 4773 ppm, Sr contents from 8913 to 22168 ppm and Ba contents from 622 to 7684 ppm (Table 2). The apatite trace element distribution normalized to chondrite (Fig. 12A) show positive anomalies in V, Sr, Ba, and LREE. In the same diagram, Co, Ni, Nb and Ta have negative anomalies compared to chondrite. The apatite composition average from Belaya Zima carbonatite complex (Russia) (Doroshkevich et al., 2017) has a very similar trace element pattern (Fig. 12A). Figure 12B shows the REE content of Rosário do Sul apatites, compared to the average REE composition of apatites from Fen (Norway) and Jacupiranga (Brazil) carbonatites studied by Hornig-Kjarsgaard (1998), and REE composition of apatites from the Oka carbonatite complex (Quebec) (Eby, 1975). The REE contents of Rosário do Sul apatites are lower when compared to Fen, Jacupiranga and Oka carbonatitic apatites.

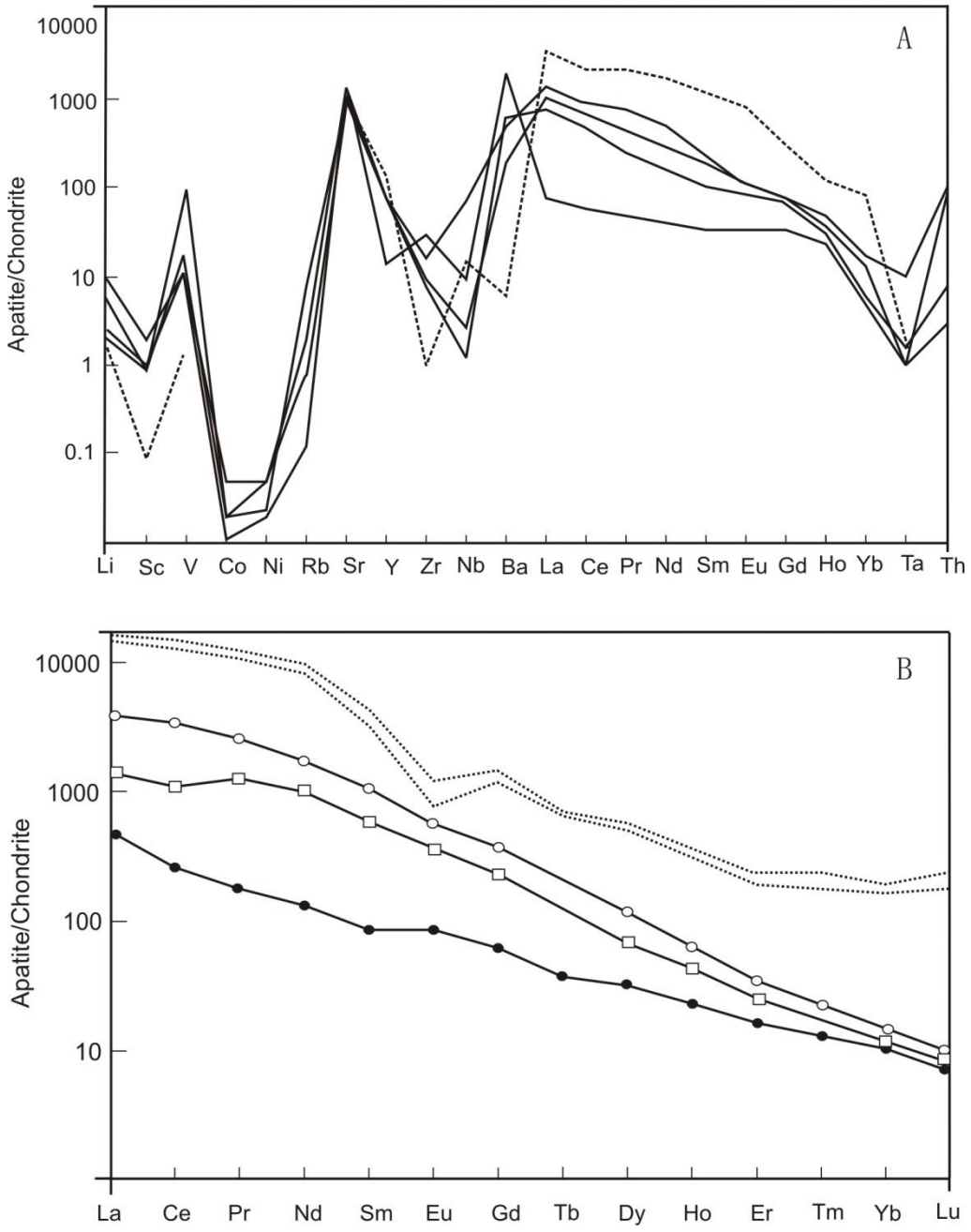

Fig. 12: A. Trace element compositions of apatites normalized to chondrite from McDonough & Sun (1995): simple lines are Rosário do Sul apatites; dashed line is the average of apatites compositions from Russian carbonatites Doroshkevich et al., 2017; B. Apatite normalized to chondrite REE diagram: filled circles represent Rosário do Sul apatites; open circles and squares represent average composition of carbonatitic apatites from Fen (Norway) and Jacupiranga (Brazil), respectively (data from Hornig-Kjarsgaard, 1998); and dashed lines are from Oka carbonatite complex apatites (Quebec) (Eby, 1974).

Mesostasis

Mesostasis is the last-formed interstitial material which comprises, in Rosário do Sul kimberlite, acicular microlites of segregated phlogopite, melilite (Fig. 13A), soda melilite ($CaNaAlSi_2O_7$), akermanite ($Ca_2MgSi_2O_7$), serpentine and calcium carbonate (Fig. 13B). In figures 13A-D, mesostasis is found percolating the olivine macrocrysts and microphenocrysts, the groundmass, and the pelletal lapilli components (Fig. 13C and D), which are widespread in the Rosário do Sul rocks and represent autholiths of previous crystalline components or liquid/gas pockets filled with an aphanitic material. The carbonate present is calcite, composed of 95 wt.% of CaO and with very low MgO and FeO concentrations, which corroborates the studies of Clement (1982) and Kobelski et al. (1979) that found calcite as the dominant carbonate present in kimberlites. The Rosário do Sul mesostasis is richer in Na than the Rosário do Sul mineral assemblage. This is evidenced by the occurrence of soda melilite, which is a mineral observed only in the mesostasis. This increase of the Na content in the residual kimberlitic liquid is due to this element remained in the melt and crystallizes together with the other minerals composing the mesostasis.

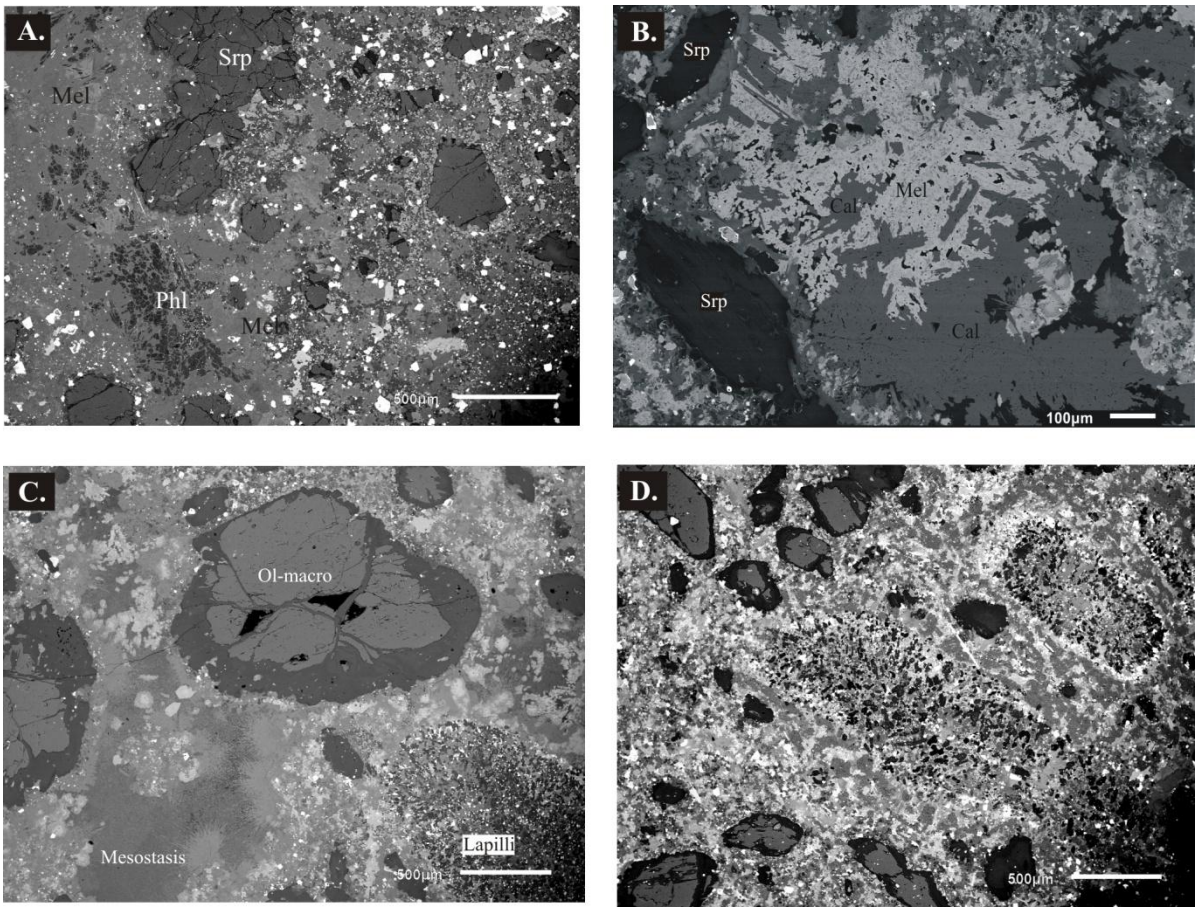

Fig. 13: Backscattered electron images of the thin sections from Rosário do Sul kimberlite. A. melilite and phlogopite mesostasis; olivine microphenocryst. B. melilite and calcite mesostasis; olivine microphenocrysts. C. and D. olivine macrocrysts; mesostasis and pelletal lapilli. Notes: serpentinized olivine microphenocryst (Srp), melilite (Mel), phlogopite (Phl), calcium carbonate (Cal).

5. Discussion

Calculations for melt source composition of Rosário do Sul kimberlite

In order to estimate the trace element concentrations of the Rosário do Sul melt source, we used the trace element compositions of phlogopite (~8 vol.%), $CaTiO_3$-perovskite (~8

vol.%) and apatite (~3 vol.%), which are the Rosário do Sul minerals that crystallize since the beginning of the kimberlite crystallization, as proposed by Conceição et al. (*in prep.*), and have higher trace element contents. Minerals as olivines, serpentines, monticellites and spinels have a minor influence on the trace element contents of the melt, except for V, Cr, Ni and Co elements. For calculations, we used the partition coefficient data between: phlogopite and kimberlitic (Fujimaki & Tatsumoto, 1984) or lamprophyric melt (Foley et al., 1996); $CaTiO_3$-perovskite and kimberlitic melt (Chakhmouradian et al., 2013); apatite and silicate melt (Prowatke & Klemme, 2006). The calculated melt composition based on Rosário do Sul phlogopites, $CaTiO_3$-perovskites and apatites trace element contents (Table 6 and Fig. 14), reflects important characteristics of the source of the Rosário do Sul melt as: high positive anomaly of Rb, Nb, Cs and Ba; moderately positive anomaly of Li, Sr, Zr, LREE, Hf, Ta, Th and U, and negative anomaly of V, Y, HREE and Pb. The Rosário do Sul source was probably enriched in elements as V, Cr, Ni and Co, however, these elements partition more easily in olivines, serpentines, monticellites and spinels crystals.

	Calculated Melt-phlo	Calculated Melt-pv	Calculated Melt-ap
Li	688(34)	n.c.	n.c.
K	n.c.	46883(2344)	n.c.
Ti	n.c.	17452(873)	n.c.
V	n.c.	326(16)	n.c.
Rb	166(8)	221462(11073)	3722(186)
Sr	1229(61)	1308(65)	10069(503)
Y	110(5)	26(1)	31(2)
Zr	4131(206)	615(31)	894(45)
Nb	384(19)	222(11)	4899(245)
Cs	12(0.6)	n.c.	4147(207)
Ba	2634(132)	65436(3272)	17823(891)
La	291(15)	112(6)	92(5)
Ce	539(27)	191(10)	107(5)
Pr	n.c.	17(0.9)	9.5(0.5)
Nd	314(16)	58(3)	n.c.
Sm	66(3)	10(0.5)	5.5(0.3)
Eu	31(2)	3.8(0.2)	n.c.
Gd	98(5)	9(0.5)	6.9(0.3)
Tb	n.c.	1.4(0.1)	n.c.
Dy	43(2)	5.8(0.3)	n.c.
Ho	n.c.	0.84(0.04)	n.c.
Er	25(1)	2.1(0.4)	n.c.
Tm	n.c.	0.29(0.01)	n.c.
Yb	13(0.7)	1.9(0.1)	n.c.
Lu	1.5(0.1)	0.2(0.1)	0.28(0.01)
Hf	68(3)	15(1)	30(2)
Ta	7(0.4)	3.8(0.2)	63(3)
Pb	n.c.	0.80(0.04)	2.2(0.1)
Th	85(4)	3.7(0.2)	4.9(0.2)
U	n.c.	3.8(0.2)	3.1(0.2)

Table 6: Melt composition is calculated from trace element compositions of phlogopite, $CaTiO_3$-perovskite and apatite from this study, and partition coefficients of phlogopites from Foley et al. (1996) and Fujimaki & Tatsumoto (1984), $CaTiO_3$-perovskites from

Chakhmouradian et al., (2013) and apatites from Prowatke & Klemme, (2006). Notes: n.c., not calculated; analytical uncertainties of 5%, as last significant digits given in brackets.

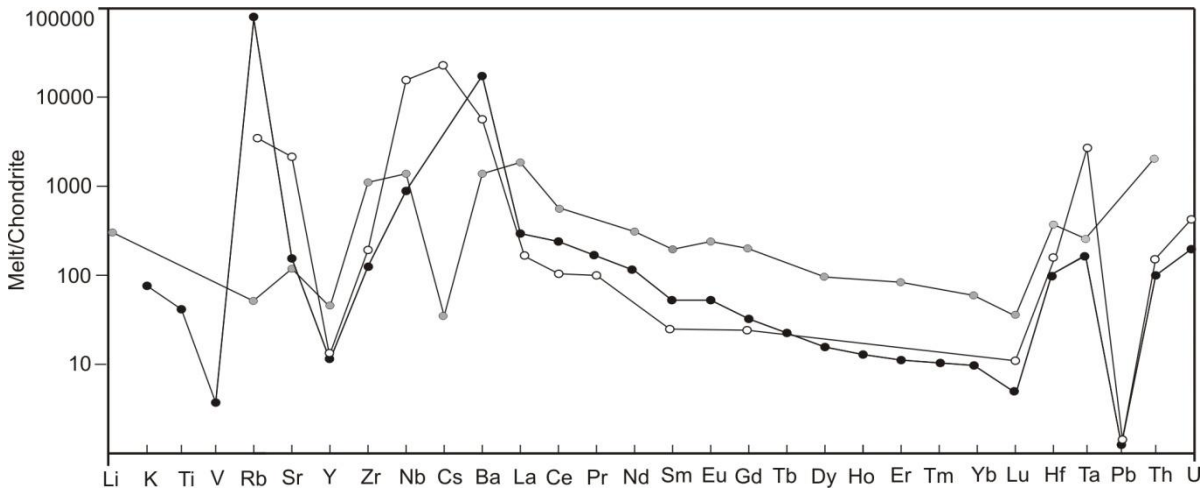

Fig. 14: A chondrite-normalized (values from McDonough & Sun, 1995) trace element distribution pattterns for Rosário do Sul melt calculated based on phlogopite (grey circles), $CaTiO_3$-perovskite (black circles), and apatite (white circles) partition coefficients and trace element compositions.

Implications for mantle composition

According to Carniel et al. (*submitted*), Rosário do Sul crystallization temperatures registered by olivine-chromite at an estimated pressure of 3 GPa, are around 1573°C. The fO_2 of coexisting olivine and $CaTiO_3$-perovskite at this temperature is 0.6 log units more oxidized than the nickel-nickel oxide buffer (NNO buffer) at a silica activity limited by the crystallization of monticellite. These estimates suggest that the Rosário do Sul kimberlite probably experienced oxidizing conditions during its ascent.

V/Sc ratio in olivines can also be used to characterize oxidation state during melting based on the principle that these two elements have similar compatibilities, but only

vanadium has two valence states, being less compatible in minerals under oxidizing conditions (Li and Lee, 2004; Lee et al., 2005 and Foley et al., 2011). According to a number of authors (Canil, 1997; Canil and Fedortchouk, 2001; Mallmann and O'Neill, 2009; Foley et al., 2011; Foley et al., 2013), the low V/Sc of the olivines (V/Sc < 3) corresponds to peridotites or silicate melts that suffered metasomatic enrichment events, whereas high V/Sc ratios (V/Sc > 3) characterize the least modified peridotites or silicate melts. Figure 15 shows Ni content *versus* V/Sc ratio from olivines microphenocrysts of the Rosário do Sul kimberlite. For comparison, olivines from Victor North Kimberlite olivines (Canada) and from orogenic peridotites (Norway) plot mainly in the oxidized area, whereas olivines from Kaalvallei kimberlite xenoliths (South Africa) (De Hoog et al., 2010) plot in the reduced area. The oxidizing characteristics of Rosário do Sul olivines, with V/Sc ratios lower than 3, probably reflects a metasomatic event of this melt during crystallization.

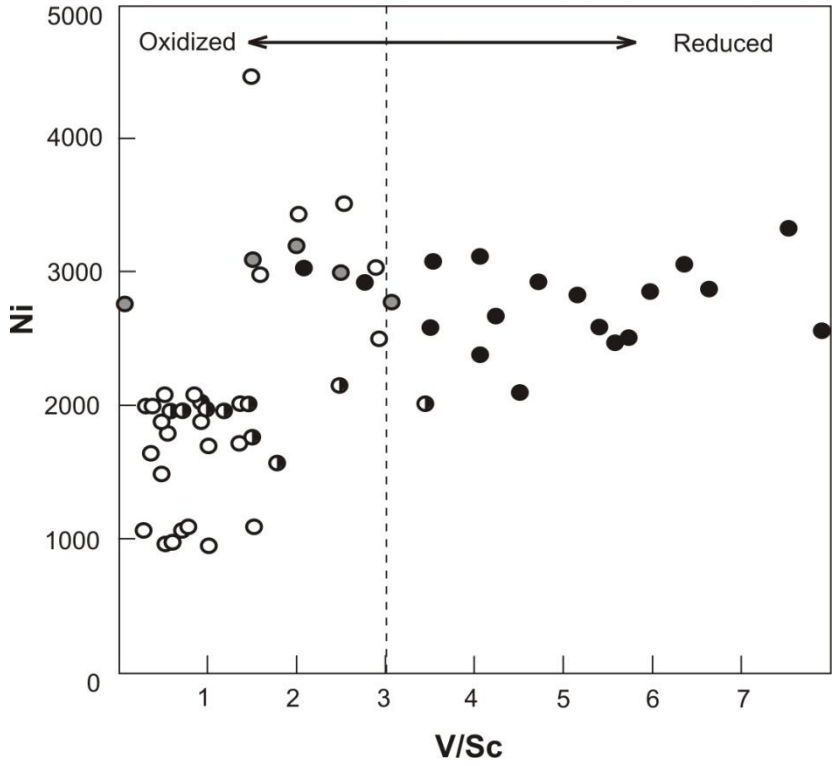

Fig. 15: Diagram Ni (ppm) *versus* V/Sc ratio (ppm) of olivines. The Rosário do Sul olivines microphenocrysts plotted as open circles in the oxidized field (Foley et al., 2013) limited by the dashed broken line. The metasomatized silicate melts have V/Sc ratios < 3 (high oxidation state), whereas least modified melts have V/Sc ratios > 3 (low oxidation state). The half filled circles are from Victor North Kimberlite olivines (Canada); the gray circles are from orogenic peridotites olivines (Norway); and the filled circles are from olivines of Kaalvallei kimberlite xenoliths (South Africa) (De Hoog et al., 2010).

The abundance of phlogopite and serpentinized olivines, in addition to low V/Sc ratios of olivine microphenocrysts of the Rosário do Sul kimberlite, are indicative of a metasomatized source. The high Ti content of the minerals as Mg-ulvöspinel, Mg-chromite, phlogopite and melilite, and the presence of $CaTiO_3$-perovskite, suggest that the source of Rosário do Sul kimberlite was Ti-enriched, however, after the consumption of Ti by $CaTiO_3$-perovskite crystallization, the melt becomes Ti-depleted. This is confirmed by the Fe-Ti zonation in Mg-ulvöspinel and melilite crystals, and the compositional variation of

early phlogopite microphenocrysts (high-Ti) and late groundmass phlogopite (low-Ti). $CaTiO_3$-perovskites, together with monticellites, are the most homogeneous minerals, suggesting that they crystallized in the beginning of the kimberlite crystallization. Rosário do Sul monticellites could be resultant of olivine alteration or dissolution due to CO_2 degassing, as proposed by Abersteiner et al. (*in press*). The olivine-serpentine-monticellite-melilite evolution trend, the phlogopite microphenocrysts and groundmass compositions, and the $CaTiO_3$-perovskites compositions, indicate that the Rosário do Sul melt undergone a Ti-depletion and Al-enrichment process, which reflects a variation of magma composition. During the beginning of perovskite and phlogopite microphenocrysts crystallization, the TiO_2 content in the Rosário do Sul melt is high, and the melt is probably richer in Rb, Sr and Ba contents. Throughout the late stages of perovskite crystallization and the beginning of groundmass phlogopite crystallization, the Ti content decreases and the Al content increases, followed by the increase of Nb, La and Ta contents, and the depletion of Rb, Sr and Ba.

The calcium carbonate present in the mesostasis, also indicates that the Rosário do Sul liquid was very rich in CO_2. The Rosário do Sul mesostasis is richer in Na than the Rosário do Sul mineral assemblage, evidenced by the occurrence of soda melilite. This increase of the Na content in the residual kimberlitic liquid is due to this element remained in the melt and crystallizes together with the other minerals to compose the mesostasis.

The Ti-enrichment and the positive anomalies of Nb, Ce, Ta and U, suggest that Rosário do Sul kimberlite source was enriched by recycled oceanic crust that caused fertilization of mantle peridotite by melts derived from former basaltic crust and subducted carbonates (Litasov et al., 2013). The positive anomalies of Rb, Ba and Sr, the enrichment in LREE, and the negative anomalies of HREE in the Rosário do Sul minerals, are also indicatives of a metasomatism process in the mantle source that could be caused by fluids from recycled oceanic crust. The similarities between the trace element contents of Rosário do Sul spinels,

phlogopites, $CaTiO_3$-perovskites and apatites, and the trace element contents of these minerals in carbonatites – carbonatitic spinels and phlogopites from calciocarbonatite of Mela Field (Russia), Jacupiranga complex carbonatites (Brazil), and others Canadian and Russian carbonatites; carbonatitic perovskites from Kola carbonatites (Russia); and carbonatitic apatites from Belaya Zima carbonatite complex (Russia), Fen (Norway) and Jacupiranga (Brazil) carbonatites, and Oka carbonatite complex (Quebec) - contribute to support the hypothesis that Rosário do Sul kimberlite source was associated to a carbonatitic melt originated from a mantle metasomatized by CO_2-rich fluids from recycled marine sediments.

In Rosário do Sul geological context, subducted slabs composed by carbonated sediments and basalts could be the responsible for oxidizing the mantle and producing carbonatitic and silicate magmas. This hypothesis is also proposed for the Paraná flood basalts source (Rocha-Júnior et al. 2012, 2013) and was experimentally proved by Gervasoni et al. (2017), who showed that the reaction of an ultramafic silicate-carbonate melt with peridotite, can produce Ca-rich carbonatite melt at lower temperature, or an alkali-rich carbonated silicate melt that is similar to Group I kimberlites, at higher temperature.

Based on our results, we can predict that Rosário do Sul kimberlite source could be linked to the Paraná flood basalts source and the Anitápolis alkaline-carbonatitic magmatism source. These occurrences are similar in age and could be product of a very similar mantle source and tectonic scenario. The alkaline events probably occurred in the early stages of the rifting, before and perhaps during the Africa - South America continental separation and during or just after the Paraná-Etendeka Igneous Province. The extension movements of the continental crust that produced the flood basalts, and events related to reorganization of continental plates during the rifting, could be responsible for triggered the alkaline-carbonatitic occurrences in the South of Brazil.

6. Conclusion

The Rosário do Sul kimberlite assemblage is composed of olivine, monticellite, melilite, Mg-chromite, Mg-ulvöspinel, $CaTiO_3$-perovskite, phlogopite and apatite. The high Ti content in Mg-chromite, Mg-ulvöspinel, phlogopite and melilite, and the presence of $CaTiO_3$-perovskite, suggest a Ti-rich source. $CaTiO_3$-perovskites, together with monticellites, are the most homogeneous minerals, indicating that they crystallized in the beginning of the kimberlite crystallization. The olivine-serpentine-monticellite-melilite evolution trend, the phlogopite microphenocrysts and groundmass compositional variations, and the $CaTiO_3$-perovskites compositions, indicate that the Rosário do Sul melt undergone an Al-enrichment process. With the crystallization process evolution (Ti-depletion and Al-enrichment), the trace element contents of Rb, Sr and Ba decrease, while Nb, La and Ta contents increase. The Rosário do Sul mesostasis is richer in Na and have calcium carbonate, indicating that the Rosário do Sul liquid was rich in CO_2.

The calculated melt composition based on Rosário do Sul phlogopites, $CaTiO_3$-perovskites and apatites trace element contents, shows high positive anomaly of Rb, Nb, Cs and Ba, however, the kimberlite source was probably also enriched in elements that partition more easily in olivines, serpentines, monticellites and spinels, as V, Cr, Ni and Co. The positive anomalies of Rb, Ba and Sr, the enrichment in LREE, and the negative anomalies of HREE in the Rosário do Sul minerals, and the positive anomalies of Nb, Ce, Ta and U, suggest a source that is product of a peridotite mantle enriched by recycled oceanic crust. The present study lead us to conclude that Rosário do Sul kimberlite was originated from a depleted mantle enriched and metasomatized by recycled slab material, that cause fertilization of this mantle by melts derived from basaltic crust and subducted carbonates.

Our evidences propose a mantle heterogeneity caused by the melt of slab materials in the peridotite mantle that also produced the Paraná flood basalts and other alkaline events that occurred concomitant to Rosário do Sul kimberlite eruption.

Acknowledgments

We are very grateful to Beate Schmitte and Maik Trogisch from Universität Münster, for their assistance and contributions in the microprobe and ICP-MS samples preparation and analysis. Thanks to Geol. Tamara R. Manfredi and Geol. Carlos A. S. Provenzano for their helpful suggestions. We also thank the financial support for this research, provided by CNPq (National Counsel of Technological and Scientific Development), the program "Science without Borders" from Brazil and the project "Diamonds from Brazil" of Geological Survey of Brazil (CPRM).

References

Abersteiner, A., Kamenetsky, V.S., Pearson, D.G., Kamenetsky, M., Goemann, K., Ehrig, K., Rodemann, T. (*in press*) Monticellite in group-I kimberlites: Implications for evolution of parental melts and post-emplacement CO_2 degassing. Chemical Geology (*article in press*).

Adrião, A. B. (2015) Heterogeneidade mantélica na fonte da Província Magmática Paraná: nova evidência de 128 Ma da Província kimberlítica Rosário do Sul, Brasil. Dissertation, 45 f. – Universidade Federal do Rio Grande do Sul. Porto Alegre.

Bailey, D. K. (1993) Carbonate magmas. Journal of the Geological Society, London v.150, pp. 637-651.

Beard, A.D., Downes, H., Hegner, E., Sablukov, S.M. (2000) Geochemistry and mineralogy of kimberlites from the Arkhangelsk Region, NW Russia : evidence for transitional kimberlite magma types. Lithos 51, 47-73.

Brod, J.A., Gaspar, J.C., de Araújo, D.P., Gibson, S.A., Thompson, R.N., Junqueira-Brod, T.C. (2001) Phlogopite and tetra-ferriphlogopite from Brazilian carbonatite complexes: petrogenetic constraints and implications for mineral-chemistry systematics. Journal of Asian Earth Sciences 19, 265-296.

Canil, D. (1997) Vanadium partitioning and the oxidation state of Archaean komatiite magmas. Nature 389, 842–845.

Canil, D., Fedortchouk,Y. (2001) Olivine-liquid partitioning of vanadium and other trace elements, with applications to modern and ancient picrites. The Canadian Mineralogist 39, 319–330.

Carniel, L.C., Conceição R.V., Klemme S., Provenzano C.A.S. *(submitted)* Origin and redox conditions of kimberlite occurrences in southernmost Brazil: implications for mantle conditions during Gondwana breakup.

Castillo-Oliver, M., Galí, S., Melgarejo, J.C., Griffin, W.L., Belousova, E., Pearson, N.J., Watangua, M., O'Reilly, S.Y. (2016) Trace-element geochemistry and U–Pb dating of perovskite in kimberlites of the Lunda Norte province (NE Angola): Petrogenetic and tectonic implications. Chemical Geology 426, 118-134.

Chakhmouradian, A.R. and Mitchell, R.H. (1997) Compositional variation of perovskite-group minerals from the carbonatite complexes of the Kola Alkaline Province, Russia. The Canadian Mineralogist 35, 1293-1310.

Chakhmouradian, A. R., Reguir, E. P., Kamenetsky, V. S., Sharygin, V. V., Golovin, A. V. (2013) Trace-element partitioning in perovskite: Implications for the geochemistry of

kimberlites and other mantle-derived undersaturated rocks. Chemical Geology 353, 112–131.

Chaves, M.L.S.C., Andrade, K.W., Azzi, A.A., Silveira, F.V. (2014) Minerais indicadores kimberlíticos e prospectividade diamantífera da intrusão Alfeu-01 (Canguçu, RS). Revista Brasileira de Geociências 33(4), 535-548.

Clement, C.R. (1982) A comparative geological study of some major kimberlite pipes in the Northern Cape and Orange Free State. PhD thesis. University of Cape Town, South Africa, 432pp.

Comin-Chiaramonti, P., Cundari, A., Piccirillo, E.M., Gomes, C.B., Castorina, F., Censi, P., De Min, A., Marzoli, A., Speziale, S., Velázquez, V.F. (1997) Potassic and sodic igneous rocks from Eastern Paraguay: their origin from the lithospheric mantle and genetic relationships with associated Paranáá flood tholeiites. Journal of Petrology 38 (4), 495-528.

Comin-Chiaramonti, P., Gomes, C.B., Castorina, F., Di Censi, P., Antonini, P., Furtado, S., Ruberti, E., Scheibe, L.F. (2002) Geochemistry and geodynamic implications of the Anitápolis and Lages alkaline-carbonatite complexes, Santa Catarina State, Brazil. Revista Brasileira de Geociências 32(I), 43-58.

Conceição, R.V. (*in prep.*) Mantle heterogeneity on the source of Paraná continental flood basalts: New evidence from 128Ma Rosário do Sul Kimberlitic Province, Southern Brazil.

Deer, W.A., Howie R.A., and Zussman J. (1992) An Introduction to the Rock Forming Minerals. Pearson Education Limited, 2nd ed., 696 pp.

De Hoog, J.C.M., Gall, L., Cornell, D.H. (2010) Trace-element geochemistry of mantle olivine and application to mantle petrogenesis and geothermobarometry. Chemical Geology 270, 196-215.

Doroshkevich, A.G., Veksler, I.V., Klemd, R., Khromova, E.A., Izbrodin, I.A. (2017) Trace-element composition of minerals and rocks in the Belaya Zima carbonatite complex (Russia): Implications for the mechanisms of magma evolution and carbonatite formation. Lithos 284-285, 91-108.

Eby, G.N. (1975) Abundance and distribution of the rare-earht elements and yttrium in the rocks and minerals of the Oka carbonatite complex, Quebec. Geochimica et Cosmochimica Acta 39, 597-620.

Edgar, A.D., Arima, M., Baldwin, D.K., Bell, D.R., Shee, S.R., Skinner, M.W., Walker, E.C. (1988) High-pressure-high-temperature melting experiments on a SiO_2-poor aphanitic kimberlite from the Wesselton mine, Kimberley, South Africa. American Mineralogist 73, 524-533.

Edler, E., Winter, F., Edwards, R. (1998) The Rosário do Sul Kimberlitic Province, Rio Grande do Sul State, Southern Brazil, 7° International Kimberlite Conference, Cape Town, South Africa, pp.202-204.

Ernesto, M., Marques, L.M., Piccirillo, E.M., Molina, E., Ussami, N., Comin-Chiaramonti, P. and Bellieni, G. (2002) Paraná Magmatic Province – Tristan da Cunha plume system: fixed versus mobile plume, petrogenetic considerations and alternative heat sources. Journal of Vulcanology and Geothermal Researches 118, 15-36.

Fedortchouk, Y., Canil, D. (2004) Intensive Variables in Kimberlite Magmas, Lac de Gras, Canada and Implications for Diamond Survival. Journal of Petrology 45(9), 1725-1745.

Foley, S.F., Jackson S.E., Fryer, B.J., Greenough J.D., Jenner, G.A. (1996) Trace element partition coefficients for clinopyroxene and phlogopite in an alkaline lamprophyre from Newfoundland by LAM-ICP-MS. Geochimica et Cosmochimica Acta 60(4), 629-638.

Foley, S.F., Jacob, D.E., O'Neill, H.S.C. (2011) Trace element variations in olivines from Ugandan potassic rocks as clues to the chemical characteristics of parental magmas. Contributions to Mineralogy and Petrology 162, 1–20.

Foley, S.F., Prelevic, D., Rehfeldt, T., Jacob, D.E. (2013) Minor and trace elements in olivines as probes into early igneous and mantle melting processes. Earth and Planetary Science Letters 363, 181-191.

Fujimaki, H. and Tatsumoto, M. (1984) Partition coefficients of Hf, Zr and REE between phenocrysts and groundmass. Journal of Geophysical Research 89, B662-B672.

Gervasoni, F., Klemme, S., Rohrbach, A., Grützner, T., Berndt, J. (2017) Experimental constraints on mantle metasomatism caused by silicate and carbonate melts. Lithos 282-283, 173-186.

Gibson, S.A., Thompson, R.N., Leonardos, O.H., Dickin, A.P., Mitchell, J,G. (1999) The limited extent of plume-lithosphere interactions during continental flood-basalt genesis: geochemical evidence from Cretaceous magmatism in southern Brazil. Contributions to Mineralogy and Petrology 137, 147-169.

Griffin, W.L., Powell, W.J., Pearson, N.J. and O'Reilly, S.Y. (2008) Glitter: Data reduction software for laser ablation ICP-MS; In Sylvester, P.J. (ed.), Laser Ablation ICP-MS in the Earth Sciences: Current Practices and Outstanding Issues, Mineralogical Association of Canada Short Course Series, Short Course 40, Vancouver, B.C., pp. 308-311.

Hasui, Y., Cordani, U.G. (1968) Idades potássio-argônio de rochas eruptivas mesozóicas do Oeste Mineiro e Sul de Goiás. In: XXII Congresso Brasileiro de Geologia. Belo Horizonte p. 139-143.

Hornig-Kjarsgaard, I. (1998) Rare Earth Elements in Sövitic Carbonatites and their Mineral Phases. Journal of Petrology 39, 2105-2121.

Jaques, A.L. (2016) Major and trace element variations in oxide and titanate minerals in the West Kimberley lamproites, Western Australia. Mineralogy and Petrology 110, 159-197.

Jochum, K.P., Nohl, L., Herwig, K., Lammel, E., Toll, B., Hofmann, A.W. (2005) GeoReM: a new geochemical database for reference materials and isotopic standards. Geostandards and Geoanalytical Research 29, 333–338.

Kaminsky, F.V., Khachatryan, G.K., Andreazza, P., Araujo, D., Griffin, W.L. (2009) Super-deep diamonds from kimberlites in the Juina area, Mato Grosso State, Brazil. Lithos 112S, 833-842.

Kimura, S., Muan, A. (1971a) Phase relation in the system CaO-iron oxide-TiO in air. American Mineralogist 56, 1332-1346.

Kimura, S., Muan, A. (1971b) Phase relations in the system CaO-iron oxide-TiO under strongly reducing conditions. American Mineralogist 56, 1347-1358.

Kobelski, B.J., Gold, D.P., Deines, P. (1979) Variations in stable isotope compositions for carbon and oxygen in some South African and Lesothan Kimberlites. SIKC 1, 252-271.

Lee, C.T.A., Leeman, W.P., Canil, D., Li, Z.X.A. (2005) Similar V/Sc systematics in MORB and arc basalts: implications for the oxygen fugacities of their mantle source regions. Journal of Petrology 46, 2313–2336.

Li, Z.X.A., Lee, C.T.A. (2004) The constancy of upper mantle fO_2 through time inferred from V/Sc ratios in basalts. Earth and Planetary Science Letters 228, 483–493.

Litasov, K.D., Shatskiy, A., Ohtani, E. and Yaxley, G.M. (2013) Solidus of alkaline carbonatite in the deep mantle. Geology 41, 79-82.

Mallmann, G., O'Neill, H.S.C. (2009) The crystal/melt partitioning of V during mantle melting as a function of oxygen fugacity compared with some other elements (Al, P, Ca, Sc, Ti, Cr, Fe, Ga, Y, Zr and Nb). Journal of Petrology 50, 1765–1794.

Marques, L.S., Dupré, B., Piccirillo, E.M. (1999) Mantle source compositions of the Paraná

Magmatic Province: evidence from trace element and Sr-Nd-Pb isotope geochemistry. Journal of Geodynamics 28, 439-459.

McDonough, W.F., Sun, S. (1995) The composition of the Earth. Chemical Geology 120, 223-253.

Melluso, L., Lustrino, M., Ruberti, E., Brotzu, P., Gomes, C.B., Morbidelli, L., Morra, V., Svisero, D.P., D'Amelio, F. (2008) Major- and trace-element composition of olivine, perovskite, clinopyroxene, Cr–Fe–Ti oxides, phlogopite and host kamafugites and kimberlites, Alto Paranaíba, Brazil. The Canadian Mineralogist 46, 19-40.

Mitchell, R.H. (1986) Kimberlites: mineralogy, geochemistry and petrology. Plenum Press, New York, 442 pp.

Mitchell, R.H. (1995) Kimberlites, Orangeites, and Related Rocks. Plenum, New York, 410 pp.

Nagasawa, H., Schreiber, H.D., Morris, R.V. (1980) Experimental mineral/liquid Ds of REE, Si and Sr for perovskite, spinel and melilitite. Earth and Planetary Science Letters 46, 431-437.

Peate, D., Hawkesworth, C.J. (1996) Lithospheric to astenospheric transition in low-Ti flood basalts from Southern Paraná, Brazil. Chemical Geology 127, 1-24.

Peate, D.W., Hawkesworth, C.J., Mantovani, M.S.M., Rogers, N.W., Turner, S.P. (1999) Petrogenesis and stratigraphy of the high-Ti/Y Urubici magma type in the Paraná flood basalt province and implications for the nature of 'Dupal'- type mantle in the South Atlantic region. Journal of Petrology 40 (3), 451-473.

Provenzano, C.A.S. (2016) Caracterização petrográfica, química mineral e petrogênese do kimberlito Alfeu I – Canguçu/RS e uma revisão conceitual de Magmatismo e rochas kimberlíticas. Dissertation, 215 f. – Universidade Federal do Rio Grande do Sul. Porto Alegre.

Prowatke, S., and Klemme, S. (2006) Trace element partitioning between apatite and silicate melts. Geochimica et Cosmochimica Acta 70(17), 4513–4527.

Reguir, E.P., Chakhmouradian, A.R., Halden, N.M., Malkovets, V.G., Yang P. (2009) Major- and trace-element compositional variation of phlogopite from kimberlites and carbonatites as a petrogenetic indicator. Lithos 112S, 372-384.

Renne, P.R., Ernesto, M., Pacca, I.G., Coe, R.S., Glen, J., Prev, M., Perrin, M. (1992) The age of Paraná flood volcanism, rifting of Gondwanaland, and the Jurassic - Cretaceous boundary. Science 258, 975-979.

Renne, P.R., Glen, J..M., Milner, S.C., Duncan, A.R. (1996) Age of Etendeka flood volcanism and associated intrusions in southwestern Africa. Geology 24, 659-662.

Rocha-Júnior, E.R.V., Marques, L.S., Babinski, M., Nardy, A.J.R., Figueiredo, A.M.G., Machado, F.B. (2013) Sr-Nd-Pb isotopic constraints on the nature of the mantle sources involved in the genesis of the high-Ti tholeiites from northern Paraná Continental Flood Basalts (Brazil). Journal of South American Earth Sciences 46, 9-25.

Rocha-Júnior, E.R.V., Puchtel, I.S., Marques, L.S., Walker, R.J., Machado, F.B., Nardy, A.J.R., Babinski, M., Figueiredo, A.M.G. (2012) Re-Os isotope and highly siderophile element systematics of the Paraná Continental Flood Basalts (Brazil). Earth and Planetary Science Letters 337-338, 164-173.

Sonoki, I.K. and Garda G.M. (1988) Idades K/Ar de rochas alcalinas do Brasil Meridional e Paraguai Oriental: compilação e adaptação às novas constantes de decaimento. Boletim IG-USP, Série Científica, 19, 63-87.

Turner, S., Hawkesworth, C.J. (1995) The nature of the continental mantle lithosphere: constraints from the major-element compositions of continental flood basalts. Chemical Geology 120, 295-314.

Turner, S., Regelous, M., Kelley, S., Hawkesworth, C.J., Mantovani, M. (1994) Magmatism and continental break-up in the South Atlantic: high precision 40Ar-39Ar geochronology. Earth and Planetary Science Letters 121, 333-348.

Van Achterbergh, E., Ryan, C.G., Jackson, S.E. and Griffin, W.L. (2001) Data reduction software for LA-ICP-MS: appendix; In Sylvester, P.J. (ed.), Laser Ablation –ICP-Mass Spectrometry in the Earth Sciences: Principles and Applications, Mineralogical Association of Canada Short Course Series, Ottawa, Ontario, Canada v. 29, pp. 239-243.

Wedepohl, K. H. and Muramatsu, Y. (1979) The chemical composition of kimberlites compared with the average composition of three basaltic magma types. In F. R. Boyd and H. O. A. Meyer, Eds., Kimberlites, Diatremes, and Diamonds: Their Geology, Petrology and Geochemistry, 300-312.

Suplementary data:

Rosário do Sul - Serpentinized olivine microphenocrysts:

wt.(%)	CAR-3I-1-3	CAR-3I-1-4	CAR-3I-1-5	CAR-3I-1-14	CAR-3I-1-18	CAR-3I-1-22	CAR-3I-1-23	CAR-3I-1-26	CAR-3I-1-35	CAR-3I-1-38	CAR-3I-1-40	CAR-3I-1-42	CAR-3I-1-49	CAR-3I-1-55	CAR-3I-1-57	CAR-3I-1-59	CAR-3I-2-7	CAR-3I-2-13	CAR-3I-2-17	CAR-3I-2-23	CAR-3I-2-27	CAR-3I-2-31	CAR-3I-2-32	CAR-3I-2-33
SiO_2	38.9	39	38.5	38.8	39.2	38	39.1	39.4	38.8	38.9	37.9	38	38.5	39.4	38.1	38	40.1	39	40	39.1	39.5	39.9	39.9	39.8
TiO_2	0.042	0.034	0.003	0.045	0.04	0.017	0.059	0.062	0.031	0.031	0.017	0.063	0.057	0.048	0.04	0	0	0	0.054	0.037	0.06	0.037	0.03	0.02
Al_2O_3	1.9	1.85	2.19	1.98	1.88	1.63	1.87	1.69	2.22	1.68	2.08	1.87	1.86	1.48	1.66	1.83	0.94	2.05	0.99	1.66	1.53	1.7	1.57	1.16
FeO	4.84	4.89	4.44	4.38	4.67	3.44	4.72	4.66	4.59	3.89	3.68	3.95	4.94	4.73	4.29	4.51	5.03	3.72	4.85	4.13	4.48	3.58	4.3	4.11
MnO	0.18	0.195	0.16	0.169	0.225	0.202	0.196	0.201	0.195	0.216	0.223	0.243	0.186	0.19	0.1414	0.16	0.212	0.137	0.202	0.198	0.159	0.248	0.221	0.241
MgO	35.5	35.6	36	36.2	35.	27.8	36.5	36	36.4	34.7	30.9	30.3	36.2	35.3	36.8	36.8	36.8	33.1	34.6	37	36.7	35.5	36.8	36.2
CaO	0.459	0.546	0.533	0.545	0.502	0.996	0.348	0.380	0.433	0.916	0.954	0.895	0.55	0.681	0.467	0.538	0.368	1.54	0.888	0.496	0.426	0.926	0.535	0.561
Na_2O	0.012	0.004	0.012	0.0186	0.013	0.078	0.009	0.009	0	0	0.056	0.095	0.029	0.036	0.019	0.037	0.036	0.044	0.067	0.023	0.03	0.02	0.03	0.03
K_2O	0.017	0.015	0.002	0.008	0.013	0.069	0.006	0.01	0	0.005	0.082	0.096	0.03	0.035	0.012	0.046	0	0.068	0.015	0.028	0.009	0.057	0.014	0.02
Cr_2O_3	0.056	0.052	0.064	0.16	0.102	0.262	0.072	0.065	0	0.126	0.009	0.035	0.007	0.027	0.059	0.014	0.06	0	0.038	0.043	0.004	0	0.022	0.131
Total	81.9	82	81.9	82.3	82.2	72.4	82.9	82.5	82.6	80.5	75.9	75.6	82.4	81.9	81.6	81.8	83.6	79.7	81.6	82.7	82.9	81.9	83.4	82.3
ppm																								
Li	3.38	3.37	3.4	12.5	3.45	11.2	3.83	3.83	3.93	3.74	6.72	3.94	4.03	9.23	8.77	4.07	3.63	19.4	3.61	3.94	8.43	8.78	8.7	4.25
Sc	8.1	3.62	6.01	28.3	4.34	19.7	12.3	23.9	3.72	25.2	13.8	16.2	29.6	27.2	2.33	6.61	12.9	30.6	36.4	29.6	37.3	28.3	32.6	3.78
V	13.8	7.24	8.11	17.4	11.9	18.2	8.85	15.8	11.2	10.8	11.6	24.1	5.6	11.2	7.09	4.83	8.2	16.6	11.3	7.36	13	14.6	14.5	5.87
Co	149	29.4	19.3	22.6	12.5	68.2	17.9	29.2	38.7	16.2	64.9	113	33.4	17.8	111	18.2	9.95	49.9	19.6	16.5	13.5	27.2	37.5	10.6

Ni	3095	3379	1997	1022	3382	901	1205	2130	2373	1113	1719	1154	2035	1751	3010	1859	1168	1017	1671	2014	1873	1491	2124	4518
Rb	0.37	0.37	0.37	65.4	0.52	1.77	1.33	0.4	0.39	0.46	1.47	53.3	0.38	0.89	0.81	0.46	1.78	1.95	0.65	0.39	0.78	35.7	18.2	0.37
Sr	28.7	21.2	22.6	30.7	27.5	29.9	47.9	25.1	23.9	33.5	26.8	29.6	28.4	29.9	26.3	30	29.2	32	32.3	22	25.9	28.4	29.2	22.9
Y	0.842	0.771	0.963	0.36	0.828	1.17	1.04	1.22	0.657	1.66	0.38	0.89	1.06	1.75	0.69	0.94	2.3	7.6	1.83	1.2	1.57	0.97	0.83	0.424
Zr	4.59	1.19	1.06	12.7	2.28	8.73	4.42	1.83	1.71	4.33	4.28	9.89	2.78	2.64	2.11	2.01	4.19	15.9	4.51	1.87	2.13	10.5	4.45	1.02
Nb	0.168	0.173	0.155	1.57	0.266	0.79	0.519	0.187	0.13	0.113	0.214	0.79	0.092	0.152	0.175	0.066	0.083	0.23	0.104	0.151	0.173	0.92	4.73	0.144
Mo	0.32	0.26	0.131	0.93	0.38	1.4	0.35	0.19	0.38	0.29	0.56	0.38	0.9	0.51	0.4	0.93	0.28	1.29	0.23	0.32	0.55	0.67	0.39	0.19
Cs	0.166	0.172	0.167	0.8	0.161	0.58	0.17	0.17	0.226	0.17	0.29	0.62	0.167	0.38	0.36	0.161	0.168	0.81	0.149	0.157	0.34	0.58	0.35	0.177
Ba	6.04	1.96	2.17	474	6.92	15.6	31.1	4.77	4.78	7.78	12.2	452	3.06	27.9	1.72	1.04	21.8	5.96	4.1	2.24	1.96	455	120	2.85
La	1.6	1.42	1.21	2.22	2.57	4.31	4.3	1.22	0.862	2.11	4.54	3.54	0.589	0.742	0.49	0.408	0.983	1.62	1.23	2.3	0.635	10.65	9.61	4.17
Ce	1.76	1.35	1.05	2.68	2.75	4.01	4.9	0.944	0.565	2.12	6.18	3.24	0.693	0.773	0.691	0.546	1.21	2.21	1.57	1.21	0.668	10	17.5	4.25
Pr	0.12	0.107	0.063	0.117	0.21	0.501	0.455	0.092	0.037	0.113	0.799	0.333	0.107	0.148	0.046	0.073	0.085	0.164	0.07	0.054	0.052	0.768	1.55	0.321
Nd	0.474	0.342	0.374	0.91	1.08	0.98	1.63	0.27	0.137	0.5	2.42	1.62	0.147	0.37	0.36	0.162	0.47	2.29	0.64	0.21	0.21	3.09	5.71	1.4
Sm	0.309	0.082	0.166	0.27	0.186	0.43	0.55	0.078	0.028	0.215	0.46	0.25	0.055	0	0.162	0.074	0.23	0.53	0.122	0.082	0	0.43	0.36	0.161
Eu	0.037	0.035	0.063	0.161	0.02	0.072	0.036	0.055	0.029	0.034	0.061	0.042	0.135	0.12	0.105	0.069	0.122	0.26	0.148	0.057	0.073	0.081	0.184	0.071
Gd	0.296	0.176	0.178	0.63	0.33	0.43	0.64	0.114	0.182	0.254	0.48	0.22	0.29	0.39	0.38	0.203	0.25	1.16	0.24	0.149	0.32	0.35	1.09	0.19
Tb	0.026	0.021	0.028	0.041	0.029	0.054	0.056	0.013	0.009	0.031	0.02	0.061	0.033	0.036	0.024	0.011	0.07	0.216	0.019	0.028	0.061	0.07	0.093	0.016
Dy	0.159	0.183	0.254	0.116	0.076	0.32	0.233	0.093	0.069	0.254	0.27	0.194	0.09	0.4	0.107	0.146	0.407	0.85	0.199	0.183	0.144	0.179	0.272	0.04
Ho	0.054	0.056	0.05	0.049	0.061	0.013	0.041	0.035	0.018	0.053	0.028	0.031	0.018	0.039	0.024	0.033	0.077	0.178	0.03	0.0313	0.076	0.043	0.023	0.022
Er	0.097	0.048	0.105	0.17	0.165	0.21	0.114	0.102	0.113	0.169	0	0.036	0.038	0.193	0.101	0.059	0.194	0.93	0.121	0.103	0.146	0.125	0.109	0.101
Tm	0.013	0.02	0.047	0.046	0.015	0.039	0.015	0.019	0.008	0.019	0.008	0.024	0.024	0.034	0.017	0.004	0.029	0.091	0.02	0.018	0.031	0	0.038	0.015
Yb	0.173	0.052	0.097	0	0.071	0.16	0.162	0.096	0.099	0.113	0.09	0.084	0.135	0.116	0.156	0.018	0.251	0.44	0.203	0.05	0.174	0.131	0.12	0.073

Lu	0.016	0.019	0.006	0.007	0.012	0.062	0.009	0.033	0.013	0.019	0.015	0.016	0.024	0.036	0.042	0.006	0.03	0.171	0.027	0.026	0.031	0.036	0.044	0.017
Hf	0.062	0.034	0.049	0.59	0.059	0.212	0.097	0.046	0.046	0.099	0.094	0.259	0.068	0.098	0.122	0.066	0.045	0.21	0.028	0.03	0.086	0.309	0.14	0.043
Ta	0.018	0.014	0.009	0.077	0.013	0.094	0.024	0.014	0.017	0.01	0.128	0.052	0.018	0.022	0.036	0.013	0.013	0.081	0.019	0.023	0.028	0.03	0.161	0.023
Pb	4.58	2.03	1.62	2.77	0.679	6.38	2.79	1.92	4.75	1.87	4.14	5.76	1.65	0.352	2.28	0.036	0.058	0.94	0.367	1.95	0.478	0.656	1.64	0.173
Th	0.007	0.002	0.007	0.045	0.003	0.35	0.027	0.011	0.003	0.003	1.09	0.187	0	0	0.006	0	0.007	0	0.007	0.004	0	0.028	0.764	0
U	0.073	0.033	0.059	0.089	0.075	0.224	0.118	0.057	0.026	0.101	0.26	0.289	0.022	0.065	0.014	0.004	0.03	0.228	0.048	0.034	0.031	0.156	0.128	0.025

Rosário do Sul - Spinels:

wt.(%)	**CAR-3I-1-9**	**CAR-3I-1-19**	**CAR-3I-1-21**	**CAR-3I-1-36**	**CAR-3I-1-66**	**CAR-3I-2-10**	**CAR-3I-2-16**	**CAR-3I-2-34**	**CAR-3I-1-29**	**CAR-3I-1-30**	**CAR-3I-1-32**	**CAR-3I-1-33**	**CAR-3I-1-45**	**CAR-3I-1-53**	**CAR-3I-1-62**	**CAR-3I-2-5**
SiO_2	0.173	0.138	0.145	0.155	0.156	0.151	0.123	0.146	0.04	0.084	0.048	0.045	0.019	0.056	0.07	0.068
TiO_2	1.27	1.37	1.35	1.25	1.42	1.52	1.61	1.09	10.9	10.7	9.3	10.0	10.2	11.0	10.8	9.8
Al_2O_3	19.5	19.2	19.9	18	19.4	20.7	18.7	16.7	3.59	3.35	4.7	3.99	4.19	3.56	3.17	3.84
FeO	20.3	19.8	20.6	22.6	19.2	18.9	19.4	24.2	66.1	66.9	61.9	63.3	63.5	65.5	67.3	62.7
MnO	0.27	0.398	0.402	0.428	0.374	0.372	0.439	0.456	0.524	0.517	0.536	0.497	0.491	0.550	0.534	0.498
MgO	13.5	14.3	13.9	13.4	14.3	14.1	13.7	13.3	9.3	8.8	10.3	9.6	9.88	9.42	8.12	9.47
CaO	0.032	0.016	0.04	0.02	0.034	0.11	0.036	0.02	0.21	0.12	0.181	0.108	0.082	0.023	0.133	0
Na_2O	0.07	0	0.029	0.04		0.009	0.014	0.003	0.024	0.012	0.018	0.01	0	0.016	0	0.004
K_2O	0.001	0.023	0.001	0.007	0	0.004	0	0.025	0	0	0.013	0.003	0.01	0.03	0.064	0.005
Cr_2O_3	41.2	40.8	40.9	40.3	41.7	40.9	43.3	39.7	2.43	2.23	6.22	5.88	4.7	2.89	2.37	6.57
Total	96.3	96	97.3	96.3	96.7	97	97.6	95.7	93.4	92.8	93.3	93.6	93.2	93.2	92.6	93.1
ppm																
Li	172	117	46.9	67.5	64.3	22.7	20.5	125	32.2	24.5	48	21.8	16.7	45.7	81.7	45.5
Sc	61.4	57.3	28	59.9	49.2	26.4	54.5	30.4	122	134	111	85.6	119	65.6	99.7	94.3
V	1179	1514	1072	1042	1770	1267	1593	1133	983	945	1724	1347	810	734	922	2509

Co	497	592	265	248	438	262	393	407	125	155	387	253	170	115	168	502
Ni	5498	3843	694	1794	4925	1351	2573	7538	1361	1160	1862	2220	1985	1249	709	2940
Rb	16.6	12.3	5.29	7.01	26.4	7.2	2.06	32.3	3.4	22.2	4.9	2.2	3.28	201	712	4.29
Sr	40.2	219	24.2	5.79	74.2	10	13.2	148	96.2	72.7	23.7	40.3	69.5	681	1697	11.9
Y	5.12	2.81	1.04	1.12	1.23	0.57	0.43	2.34	1.29	6.32	1.19	2.28	0.98	23.2	26.04	0.88
Zr	53.4	80.3	41.7	65	175	33.2	99.7	137	288	341	147	229	286	541	722	135
Nb	3.39	5.85	2.01	2.01	34	4.25	4.53	2.88	20.1	8.34	4.22	7.66	11.6	316	278	4.86
Mo	17.7	4.33	2.77	2.33	5.3	1.82	1.32	8.73	1.45	2.42	2.32	1.61	1.07	1.47	2.05	4.32
Cs	7.79	5.45	2.31	2.92	2.36	0.87	0.83	4.83	1.4	1.12	1.96	0.93	0.66	1.59	9.41	1.74
Ba	53	101	37.2	15.3	1502	20.6	24.6	162	60.3	207	25	8.9	9.6	3910	10262	6.66
La	1.41	8.93	0.6	0.44	0.75	1.66	0.68	12.3	3.03	1.17	2.33	1.16	0.34	274	262	0.55
Ce	2.41	11.9	1.1	0.71	0.79	2.38	1.01	16	5.62	2.01	2.76	1	0.25	451	435	0.78
Pr	0.89	1.21	0.2	0.4	0.38	0.271	0.209	2.08	0.53	0.4	0.31	0.057	0.046	50.4	52	0.2
Nd	1.21	1.19	0.81	1.17	0.99	0.6	0.56	3.86	2.47	0.49	1.44	0.62	0.47	205	197	0.65
Sm	0.69	0	0.93	2.33	1.14	0.18	0	1.99	0.99	0.28	0.96	0	0.17	29	22.6	0.79
Eu	0.18	0.67	0.43	0.5	0.68	0.42	0.171	1.49	0.27	0.48	0.44	0.175	0.14	8.67	10.5	0.62
Gd	0	4.01	2.35	1.38	1.66	0.75	1.02	2.75	1.38	1.02	2.13	0	0.72	22.3	23.8	1.63
Tb	0.1	0	0.191	0	0.44	0.089	0.056	0.49	0.074	0.169	0.088	0.053	0.093	2.45	1.69	0.117
Dy	0.41	0.8	0.15	0.24	0.72	0	0.079	2.85	0.77	0.27	0.8	0	0.3	10.77	9.55	0.65
Ho	0	0	0.198	0	0	0.123	0.056	0.43	0.149	0.26	0.204	0.082	0.047	1.87	1.53	0.167
Er	4.57	2.49	0.34	0.59	0.71	0.32	0.25	0.88	0.38	0.35	0	0.45	0.075	0.93	2.33	0.17
Tm	0	0.19	0.073	0.059	0	0.039	0.053	0.4	0.149	0.065	0.127	0.055	0.045	0.106	0.065	0.226
Yb	1.4	0	0.17	0	0.79	0.5	0	1.39	0.58	0.58	0	0.37	0	1.04	1.56	1.09
Lu	0	0	0.153	0.048	0.096	0.07	0.097	0.52	0.14	0.066	0.069	0.063	0.067	0.088	0.2	0.22
Hf	0.28	2.78	0.63	1.86	6.75	1.06	3.16	3.36	10.2	11.8	6.28	8.85	8.1	17.6	23.1	6.2
Ta	0.76	0.45	0.119	0.21	0.58	0.121	0.068	0.26	0.46	0.082	0.38	0.098	0.181	17.02	18.01	0.25
Pb	6.91	10.34	1.36	3.31	11.8	0.45	0.162	4.87	0.38	1.93	0.86	0.62	0.53	1.28	3.17	0.37
Th	0.34	0.27	0.025	0.133	0.16	0.1	0.013	0	0.244	0.045	0.175	0	0	31.7	31.6	0
U	0.056	0.44	0.08	0	0.57	0.12	0.2	0.41	0.34	0.228	0.024	0.4	0.206	9	9.8	0.27

Rosário do Sul - Phlogopites:

wt.(%)	CAR-3I-1-2	CAR-3I-1-12	CAR-3I-1-13	CAR-3I-1-17	CAR-3I-1-34	CAR-3I-1-37	CAR-3I-1-44	CAR-3I-1-46	CAR-3I-1-50	CAR-3I-1-54	CAR-3I-1-60	CAR-3I-1-61	CAR-3I-2-9	CAR-3I-2-12	CAR-3I-2-14	CAR-3I-2-22	CAR-3I-2-24	CAR-3I-2-28	CAR-3I-2-35
SiO_2	41.5	36.8	38.9	35	37.8	41	40	40	40.1	36.2	39.5	40.5	36.6	42.1	40.1	40.4	36.4	40.2	39.3
TiO_2	2.15	0.149	3.22	0.536	1.33	0.252	0.715	0.714	2.96	0.562	2.7	3.1	0.343	1.82	3.03	1.59	0.05	2.61	0.372
Al_2O_3	4.92	14.3	6.59	13	5.54	7.6	9.06	9.07	5.16	15	5.66	4.08	14.4	4	5.49	8	9.27	4.3	8.33
FeO	9.59	8.23	9.36	14.3	10.6	6.9	5.74	5	10.5	9.98	10.3	10.6	8.71	9.54	9.67	9.09	11.2	11.8	8.83
MnO	0.052	0.234	0.068	0.384	0.225	0.063	0.117	0.119	0.131	0.404	0.070	0.129	0.305	0.056	0.087	0.143	0.192	0.125	0.099
MgO	22.5	21.4	21.8	17	25.2	25.2	24.4	24.4	21.8	20.2	22	21.8	20.7	23.4	22.1	22.1	25.5	21.5	23.9
CaO	0.016	0.073	0.082	0.061	0.345	0.007	0.474	0.474	0.207	0.091	0.090	0.054	0.043	0.013	0.064	0.083	0.54	0.036	0.097
Na_2O	0.838	0.043	0.483	0.038	0.240	0.112	0.233	0.233	0.694	0.034	0.643	0.95	0.059	0.968	0.818	0.462	0.091	0.834	0.179
K_2O	10.2	10.3	9.68	9.63	6.78	10.4	10.1	10	9.77	10.4	9.83	9.88	9.9	10	9.66	10.3	3.87	9.9	10.4
Cr_2O_3	0.012	0.260	0.01	0	0.006	0	0	0	0.008	0.045	0.005	0.011	0.029	0.005	0	0.015	0.036	0.016	0.01
Total	91.9	91.7	90.1	89.8	88.1	91.6	90.7	90.6	91.3	92.8	90.8	91.2	91.1	91.9	91	92.1	87.2	91.3	91.5
ppm																			
Li	111	139	8.41	164	54.8	120	180	15.7	35.4	18.4	101	101	96.7	95.3	185	175	81.3	182	14.3
Sc	27.2	27.3	19.2	26.9	111	8.11	12.4	26.1	163	30.1	10.2	18.6	21.2	45.1	14.9	30.4	29.7	31.2	34.5
V	100	75.7	220	73	107	67.7	91.6	40.9	564	318	68.7	59.8	44.6	69.3	42.7	85.1	71	70.2	162
Co	37.1	40.4	38.2	30.5	46.1	41.1	69.3	4.74	23	65	34.5	74.1	32.9	67.8	31.5	39.1	46.3	41	75.1
Ni	215	123	184	69.3	105	365	198	216	504	274	144	557	284	585	379	315	568	178	288
Rb	1206	863	91.3	1042	779	748	1104	4.56	447	384	1329	836	1099	1198	1380	1211	810	1055	719
Sr	1830	69.8	156	43.5	294	144	18.5	736	406	191	4.06	56.5	8.23	23.5	5.65	226	25	30.7	4.87
Y	3.98	0.502	28.3	0.062	16.4	10.6	0.089	10.1	43.2	16.2	0.21	6.9	0.33	1.04	0.54	6.11	1.76	1.53	0.23
Zr	94.9	222	451	152	2077	180	281	5661	3760	359	56.8	345	672	143	821	237	36.5	439	95.3
Nb	19.2	29.6	56.4	23	17.4	47	36.4	16.8	27.7	75.1	14.9	33.5	10	24.6	12	140	7.84	25.2	4.93
Mo	0.32	0.53	1	0.236	0.52	1.3	0.179	0.89	0.83	0.6	0.72	0.66	1.14	2.08	0.21	0.54	2.04	0.43	0.77
Cs	10.7	8.6	0.88	7.65	9.5	7.45	9.36	0.63	2.98	2.17	13	8.68	8.99	11.1	12.9	11.4	5.93	8.84	1.66
Ba	11526	11089	342	9815	9292	12547	16529	363	6489	2367	12033	21275	6038	14635	6218	8869	6298	9151	9264
La	1.69	0.298	32.3	0.152	4.19	20.8	0.348	10.6	4.81	54.6	0.162	4.75	0.102	0.715	0.119	92.2	0.221	0.497	0.126

Ce	2.6	0.487	73.5	0.043	6.02	33.5	0.23	17.4	5.92	107	0.071	7.75	0.137	0.61	0.163	208	0.26	0.667	0.097
Pr	0.251	0.032	8.32	0.0056	0.505	3.6	0.041	1.62	0.63	10.6	0.062	0.79	0.069	0.16	0.08	21.6	0.205	0.061	0.053
Nd	1.47	0.203	31	0.104	1.61	14	0.178	6.91	2.48	40.5	0.254	3.35	0.281	0.59	0.33	71.4	0	0.146	0.133
Sm	0.37	0.118	6.31	0.038	0.54	2.46	0.134	1.27	0.96	6.88	0	0.7	0.12	0	0.39	10.8	0.74	0.17	0.155
Eu	0.063	0.049	2.03	0.034	0.558	0.78	0.049	0.39	0.83	3.02	0.11	0.45	0.192	0.38	0.27	3	0.41	0.112	0.16
Gd	0.61	0.189	6.34	0.142	0.92	3.38	0.113	2.27	7	3.87	0.43	1.23	0.75	1.22	1.05	6.67	0.93	0.43	0.63
Tb	0.145	0.01	1.02	0.015	0.144	0.269	0.019	0.213	0.29	0.66	0.041	0.112	0.068	0.12	0.088	0.542	0.077	0.044	0
Dy	0.67	0.042	4.92	0.022	1.36	1.55	0.013	1.59	4.92	2.46	0.133	1.73	0.191	0.17	0.23	2.13	0.3	0.32	0.146
Ho	0.111	0.019	1.011	0	0.468	0.42	0.01	0.49	1.37	0.73	0.01	0.198	0	0.126	0.058	0.4	0.111	0.051	0.053
Er	0.425	0.027	2.61	0.025	1.38	1.01	0.028	0.66	4.33	1.11	0.15	0.28	0.104	0.37	0.42	0.61	0.59	0.13	0.085
Tm	0.046	0.007	0.338	0.01	0.137	0.13	0.018	0.088	0.78	0.126	0.02	0.046	0.046	0.069	0.017	0.101	0.084	0.024	0.062
Yb	0.202	0.031	1.37	0	1.65	0.33	0.044	1.29	4.11	1.14	0	0.65	0.39	0.51	0	0.34	0.13	0.095	0.107
Lu	0.051	0.008	0.179	0.011	0.17	0.107	0.015	0.059	0.23	0.08	0.008	0.038	0	0.097	0.04	0.032	0.148	0.028	0.031
Hf	4.25	6.19	12.4	5.95	37.4	4.62	7.48	94.9	74.3	8.64	1.74	7.97	25.9	3.97	29.8	9.28	0.69	12.9	2.17
Ta	0.056	0.069	2.04	0.067	0.153	1.02	0.051	0.203	0.253	3.22	0.06	0.192	0.072	0.038	0.11	6.65	0.163	0.037	0.071
Pb	0.601	0.138	1.19	0.172	0.124	1.49	6.14	0.081	0.23	1.81	0.051	1.87	0.099	5.04	0.185	0.519	0.224	0.402	0.083
Th	0.059	0.049	0.946	0	0.015	1.91	0.032	0.221	0.074	4.62	0	0.291	0	0.044	0	15.23	0	0.018	0
U	0.2	0.622	1.41	0.154	1.306	1.02	0.688	6.66	1.36	1.69	0.0171	0.518	1.61	0.086	1.84	2.44	0.043	0.857	0.032

Rosário do Sul - Perovskites:

wt.(%)	**CAR-3I-1-7**	**CAR-3I-1-8**	**CAR-3I-1-10**	**CAR-3I-1-11**	**CAR-3I-1-15**	**CAR-3I-1-16**	**CAR-3I-1-20**	**CAR-3I-1-27**	**CAR-3I-1-28**	**CAR-3I-1-43**	**CAR-3I-1-48**	**CAR-3I-1-63**	**CAR-3I-2-1**	**CAR-3I-2-2**	**CAR-3I-2-3**	**CAR-3I-2-6**	**CAR-3I-2-8**	**CAR-3I-2-15**	**CAR-3I-2-20**	**CAR-3I-2-21**	**CAR-3I-2-25**	**CAR-3I-2-26**
SiO_2	0.026	0.028	0.022	0.029	0.034	0.014	0.035	0.06	0.039	0.037	0.05	0.07	0.034	0.052	0.048	0.079	0.061	0.047	0.068	0.082	0.032	0.014
TiO_2	55.5	55.1	54.7	55.4	54.9	55.2	55.2	55.4	54.7	55.3	55	54.7	55.8	55.3	54.9	54.4	54.5	54.9	55.2	55.7	55	54.5
Al_2O_3	0.177	0.265	0.215	0.207	0.198	0.219	0.215	0.355	0.339	0.266	0.271	0.355	0.228	0.365	0.381	0.367	0.391	0.354	0.241	0.234	0.365	0.358
FeO	1.18	1.57	1.11	1.12	1.27	1.25	1.2	1.94	2.01	1.35	1.42	2.12	1.26	1.99	1.92	2.01	1.88	1.95	1.39	1.32	1.73	1.78
MnO	0.007	0	0.01	0.002	0.02	0.019	0	0	0.017	0	0	0	0.009	0	0.031	0.032	0.011	0	0	0	0.006	0.006
MgO	0.011	0.033	0.026	0.023	0.039	0.04	0.023	0.04	0.024	0.041	0.037	0.03	0.032	0.037	0.049	0.047	0.043	0.062	0.035	0.026	0.036	0.035
CaO	39.2	39.5	39.4	39.7	38.9	39	40	39.2	39.4	38.8	39	39.4	39.1	39.2	39.2	39.2	39.5	39.4	39	39	39.3	39.3

Na_2O	0.249	0.224	0.339	0.312	0.259	0.25	0.317	0.25	0.183	0.294	0.312	0.215	0.308	0.214	0.209	0.233	0.225	0.208	0.249	0.288	0.213	0.182
K_2O	0.1	0.039	0.053	0.052	0.076	0.114	0.047	0.068	0.018	0.067	0.048	0.050	0.010	0.044	0.049	0.034	0.071	0.092	0.163	0.079	0.049	0.05
Cr_2O_3	0.102	0.016	0.061	0.156	0.103	0.120	0.185	0.013	0.007	0.097	0.071	0.023	0.021	0	0.016	0.043	0.003	0.051	0.095	0.05	0.029	0.07
Total	96.5	96.8	95.9	97	95.7	96.2	97	97.3	96.8	96.3	96.1	97	96.7	97.2	96.7	96.4	96.7	97.1	96.3	97.2	96.8	96.3
ppm																						
Li	21.4	17.5	43.1	13.9	68.6	14.7	32.5	48.5	30.2	30.5	32	28	11	10.7	12.5	31.6	25.9	19.3	30.7	21.6	11.4	19.5
Sc	18.1	9.51	25.3	5.89	27.9	11.1	10.8	32.1	9.36	9.05	50.6	10.1	7.39	9.15	13.3	14	7.14	20	20.3	7.83	4.59	5.16
V	334	250	360	365	387	301	312	273	274	294	339	254	287	280	284	246	234	393	278	250	193	193
Co	50.4	5.18	12.2	3.74	29.6	7.48	4.83	9.47	3.51	4.32	98.4	2.87	3.7	4.1	26.8	25.5	3.03	32.3	46.2	3.65	1.29	2.29
Ni	914	212	684	166	679	193	380	564	350	433	429	409	166	160	325	545	447	346	585	425	220	373
Rb	140	12.3	28	36.7	898	144	11.4	366	3.09	58.3	224	2.54	17.7	19.7	91.9	130	74.3	55.1	91	17.4	1.61	9.24
Sr	4483	2892	5349	3985	5001	4621	4674	4418	3678	4408	3230	3074	2414	2411	2296	2348	2540	3742	3026	2378	1938	1883
Y	203	164	239	183	207	230	255	222	202	222	132	176	146	151	149	163	173	195	153	180	142	150
Zr	736	640	827	599	991	673	791	774	712	974	679	647	532	588	564	662	548	821	666	548	432	458
Nb	2747	3171	4282	3106	3468	3497	4087		3441	3604	3250	3365	2547	2713	2766	2779	3016	3382	3152	2943	2640	2691
Mo	1.35	1.5	1.65	0.99	3.62	0.73	3.17	4.05	1.83	1.94	3.51	2.18	0.64	0.42	0.77	1	0.94	1.11	1.54	1.46	0.7	1.18
Cs	1.04	0.88	2.06	0.71	5.92	0.76	1.53	4.37	1.31	1.35	1.4	1.16	0.45	0.41	0.49	2.43	1.22	1.11	1.25	0.86	0.49	0.79
Ba	1224	167	367	680	8502	140	134	3252	58.1	919	3209	55.3	105	100	260	1255	425	615	1256	397	26.2	55.5
La	1760	3146	3342	2283	3097	2877	3300	3226	3363	3144	2628	3133	2564	2709	2897	2995	3244	3134	2296	3040	2928	3112
Ce	3027	6899	6713	4393	5273	5400	5726	6416	7125	6160	6026	6704	6585	6778	6842	6692	7610	6692	4765	7186	7214	7745
Pr	321	844	659	481	595	583	674	756	751	687	641	824	708	730	796	751	894	720	555	858	849	910
Nd	1273	3046	2559	1639	2009	2292	2510	2878	2927	2540	2409	2958	2592	2652	2858	2804	3234	2539	1729	3303	3189	3349
Sm	211	417	420	283	313	383	413	379	411	374	328	427	358	370	399	386	462	396	290	442	420	454
Eu	74.9	95.4	118	91.4	106	114	111	119	110	100	77.3	109	93.3	98.6	96.6	96.7	116	110	88.2	111	103	100
Gd	160	221	246	176	194	244	243	261	234	229	172	232	179	198	183	200	232	229	167	222	207	217
Tb	19.9	20	23	19.7	21.8	25.4	26.1	25.9	24.2	25.3	16.8	22.1	17.7	18.7	18.6	20.2	21.9	21.6	17.1	21.7	19	19.8
Dy	83.5	75.5	106	81.9	104	110	116	105	96.6	91.7	56.7	90.8	69	68.5	71.2	80.2	91.2	80.7	57.2	81.1	71.8	71.8
Ho	11.6	10.4	12.9	11.1	12.1	11.9	14.3	11.4	11.1	11.3	8.9	10.6	9	8.61	9.49	8.49	10.9	9.91	7.84	10.1	9.41	8.76
Er	17.4	17.9	20.1	17.6	21.3	18.9	24.3	18.7	22	20	10.4	18.8	14.3	14.3	15.5	16.9	19	18.2	16.7	16.2	13.6	14.2
Tm	1.59	1.08	1.88	1.8	1.14	1.79	1.86	1.51	1.78	1.92	1.26	1.34	1.0	1.23	1.1	1.39	1.61	1.81	1.53	1.31	1.19	1.17

Yb	7.53	5.22	6.7	5.71	7.49	8.7	5.47	6.96	7.06	8.5	3.31	6.8	5.35	6.02	5.18	5.52	6.38	6.36	4.17	5.74	5.1	5.67
Lu	0.414	0.712	0.4	0.407	0.24	0.559	0.94	0.45	0.33	0.443	0.48	0.71	0.538	0.422	0.38	0.527	0.84	0.7	0.47	0.469	0.412	0.353
Hf	29.2	30	31	24.3	38.8	30.3	32.5	38.1	30	37	25.8	30.6	26.1	27.4	28.4	31.9	27.3	37.7	35.3	23	20	24.8
Ta	101	283	201	128	187	169	207	248	285	232	212	276	246	246	259	290	322	218	138	324	310	339
Pb	9.41	13.2	12.8	5.87	8.2	7.41	9.37	12.6	11.4	10.8	10.2	11.3	10.2	10.2	10.8	10.9	13.2	11.9	11.3	14.5	11.5	13
Th	112	765	326	186	288	292	374	580	701	468	484	702	657	618	655	702	866	476	272	929	842	925
U	59.2	43.8	83.2	66.8	78.4	76.5	74.2	64	60	60	57.6	52	38.3	41.1	38.9	37.6	41.4	60.8	50.8	40.4	35.4	31.9

Rosário do Sul - Apatites:

wt.(%)	**CAR-3A-10**	**CAR-3A-31**	**CAR-3A-50**	**CA-03D-12**
SiO_2	0.229	0.104	1.71	0.653
TiO_2	0.029	0.007	0.024	0
Al_2O_3	0.009	0	0	0
FeO	0.232	0.035	0.24	0.114
MnO	0.034	0	0.044	0
MgO	0.055	0.04	0.098	0.07
CaO	53.1	52.7	53.8	53.8
Na_2O	0.044	0	0.05	0.06
K_2O	0.023	0	0.008	0.01
P_2O_5	40.3	41.2	39.4	40.8
SO_3	0.095	0.109	0.182	0.158
Total	94.2	94.2	95.6	95.7
ppm				
Li	15.1	4.27	3.34	9.01
Sc	11.8	5.38	3.76	3.81
V	827	618	4773	984
Co	13.4	0.5	1.32	1.07
Ni	255	64.3	58	178
Rb	5.52	0.36	12.2	0.82

Sr	9084	8912	22168	15232
Y	78	96.2	37.3	89.8
Zr	34.3	16.9	151	21.3
Nb	16.6	0.694	2.7	0.392
Mo	1.46	0.24	0.182	0.68
Cs	0.74	0.164	0.138	0.34
Ba	1388	621	7684	1197
La	392	251	15	132
Ce	536	346	22.4	158
Pr	51.9	35.9	2.8	16.5
Nd	195	142	12.2	58.7
Sm	37.4	30.9	4.92	13.5
Eu	14.5	10.7	1.82	6.25
Gd	36	35.7	6.68	24.9
Tb	4.13	3.9	1.32	3.24
Dy	19.7	19.9	7.03	16
Ho	2.67	3.4	1.4	2.84
Er	5.71	6.61	2.61	5.49
Tm	0.441	0.637	0.257	0.595
Yb	2.78	3.36	1.27	2.82

Lu	0.268	0.36	0.135	0.329
Hf	0.55	0.096	1.62	0.265
Ta	0.146	0.015	0.015	0.029
Pb	1.55	0.46	0.159	0.594
Th	2.59	1.72	0.12	0.556
U	2.4	1.0	1.349	1.015

Rosário do Sul - Monticellites:

wt.(%)	CAR-3I-2-18	CAR-3I-2-19
SiO_2	36.8	37
TiO_2	0.104	0.098
Al_2O_3	0.002	0.015
FeO	7.4	6.72
MnO	0.308	0.318
MgO	22	22
CaO	32.7	32.9
Na_2O	0.094	0.154
K_2O	0.018	0.069
Cr_2O_3	0	0
NiO	0	0
Total	99.4	99.3
ppm		
Li	30.5	30.2
Sc	12.6	12.8
V	28.4	54.8
Co	81.7	73.6
Ni	552	555
Rb	45.3	30.3
Sr	174	588
Y	20.6	41.1
Zr	30.3	63.5
Nb	0.71	137
Mo	2.47	1.98
Cs	1.31	1.22
Ba	161	191
La	3.19	167
Ce	7.29	349
Pr	0.92	36.6
Nd	4.72	141
Sm	1.41	28
Eu	1.35	7.75
Gd	4	16.6
Tb	0.42	2.06
Dy	3.31	11.4
Ho	0.9	2.13
Er	2.03	3.96
Tm	0.177	0.44
Yb	1.09	2.37
Lu	0.164	0.377
Hf	0.87	3.61
Ta	0.163	11
Pb	0.86	0.54
Th	0.053	22.2
U	0.131	2.34

3.3 Manuscrito: "Origin and redox conditions of the Rosário do Sul and Alfeu-I kimberlites, Southern Brazil: implications for diamond preservation"

Submetido à revista científica *Journal of South American Earth Sciences*

Assunto: Successfully received: submission Origin and redox conditions of kimberlite occurrences of southernmost Brazil: implications for mantle conditions during Gondwana breakup for Journal of South American Earth Sciences

Remetente: Journal of South American Earth SciencesAdd contact

Para: larissa.colombo@ufrgs.br

Responder para: j.bakthavachalam.1@elsevier.com

Data: Seg 22:09

This message was sent automatically. Please do not reply.

Ref: SAMES_2017_332

Title: Origin and redox conditions of kimberlite occurrences of southernmost Brazil: implications for mantle conditions during Gondwana breakup

Journal: Journal of South American Earth Sciences

Dear Mrs. Colombo Carniel,

Thank you for submitting your manuscript for consideration for publication in Journal of South American Earth Sciences. Your submission was received in good order.

To track the status of your manuscript, please log into EVISE® at: http://www.evise.com/evise/faces/pages/navigation/NavController.jspx?JRNL_ACR=SAMES and locate your submission under the header 'My Submissions with Journal' on your 'My Author Tasks' view.

Thank you for submitting your work to this journal.

Kind regards,

Journal of South American Earth Sciences

Origin and redox conditions of kimberlite occurrences of southernmost Brazil: implications for mantle conditions during Gondwana breakup

L.C. Carniel[1], R.V. Conceição[1], S. Klemme[2], C.A.S. Provenzano[3]

[1] Programa de Pós-Graduação em Geociências (PPGGEO), Universidade Federal do Rio Grande do Sul

Bento Gonçalves 9500, Porto Alegre, Brazil

[2] Institut für Mineralogie, Westfälische Wilhelms-Universität Münster

Corrensstraße 24, Münster, Germany

[3]CPRM – Geological Survey of Brazil

Banco da Província 105, Porto Alegre, Brazil

*Corresponding author: larissa.colombo@ufrgs.br; Tel: +1551996990296

Abstract

The Rosário do Sul and Alfeu-I are two kimberlite occurrences situated in the Rio Grande do Sul State, South of Brazil. Crystallization temperatures, pressures and oxygen fugacities (fO_2) of Rosário do Sul and Alfeu-I kimberlite magmas are estimated using different methods from olivines, spinels, $CaTiO_3$-perovskites, garnets, orthopyroxenes and clinopyroxenes compositions. Rosário do Sul crystallization temperatures registered by olivine-chromite geothermobarometer, are around 1556°C at a pressure of 2 GPa, and 1573°C at 3 GPa. The fO_2 conditions at these temperatures are around 3.1 log units more oxidized than the NNO buffer, at a silica activity limited by the crystallization of monticellite (2 GPa and 3 GPa). Applying the new $CaTiO_3$-perovskite oxygen barometer of Carniel et al. (*submitted*), we obtained less oxidized values of ΔNNO (1.2 at 2 GPa and 0.6 at 3 GPa). Alfeu-I kimberlite crystallization temperatures recorded by olivine-chromite geothermobarometer are around 1617°C at 4 GPa, and 1636°C at 5 GPa. The fO_2 calculated

from coexisting olivine and chromite at this temperature is ΔNNO 3.0 (4 GPa) and 3.2 (5 GPa). The Rosário do Sul kimberlite melt conditions can provide valuable information about the mantle conditions during the eruption of Paraná flood basalts and the Gondwana breakup. The high fO_2 conditions of Rosário do Sul and Alfeu-I kimberlites show that this mantle was very oxidized by slab materials from old subductions and denote their low potential to carry and preserve diamonds.

Keywords: redox mantle conditions; kimberlite melts; $CaTiO_3$-perovskite oxygen barometer; diamond preservation

1. Introduction

The estimations of pressure, temperature and redox conditions (fO_2) of a kimberlite magma source is very helpful to better understand the primary composition of a kimberlite melt formed in the mantle. This is a very complex study, considering the hybrid nature of the kimberlite rocks that are formed by minerals crystallized in the melt phase, but also xenoliths derived from the mantle and crust, in addition to high amounts of volatiles (CO_2 and H_2O). Nevertheless, the knowledge of such kimberlite conditions is very useful to better understand the mantle pressure, temperature and fO_2 in a specific tectonic context, and also contributes to specify the possibility of occurrence and the quality of the diamonds that may be carried to the surface by these rocks.

The application of mineral thermobarometers and oxygen barometers in kimberlite rocks is permeated by difficulties regarding the low preservation grade of these rocks, that is usually the main obstacle, but also due to the diversified kimberlitic mineral assemblage, that sometimes do not contain all potential minerals required for such calculations.

Nonetheless, some kimberlitic primary magma can be partially represented by aphanitic kimberlites, such as Jericho, Canada (Price et al., 2000) and those from Kimberley, South Africa (Shee, 1986; Edgar et al., 1988; Edgar & Charbonneau, 1993; Le Roex et al., 2003).

In order to determine the temperature, pressure and redox conditions of the mantle in the south of South America, we choose Rosário do Sul and Alfeu-I kimberlites, as the only kimberlites studied in this region. Rosário do Sul is a very well preserved hypabyssal kimberlite located in the southeastern edge of the Paraná Basin, while Alfeu-I is an intrusive volcanic chimney which occurs in the southeastern portion of the Rio Grande do Sul Shield, South of Brazil. The geochemical, mineral chemistry and trace element data suggest that the Rosário do Sul kimberlite is a transitional kimberlite very rich in Ti and CO_2, which indicates that this kimberlite is the product of a silicate-carbonate liquid reaction in the mantle (Conceição et al., *in prep.*; Carniel et al., *submitted*). Despite the petrography and mineralogy of Alfeu-I be similar to Group II kimberlites, the mineral chemistry indicates transitional characteristics among Group I and II kimberlites and lamproites, which suggests similar petrogenesis of Alfeu-I and other potassic magmas without a strong affinity with a particular group (Provenzano, 2016).

Geochronology determination was performed in Rosário do Sul kimberlite, based on U-Pb isotope ratios in perovskite, which resulted in ages of ~ 128 Ma (Conceição et al., *in prep.*), which indicates the eruption of Rosário do Sul just after the volcanism of Paraná-Etendeka Province (between 133 and 132 Ma; Renne et al., 1992, 1996; Turner et al., 1994; Ernesto et al., 2002) and very close to the opening of the South Atlantic Ocean, during Early Cretaceous (Piccirillo and Melfi, 1988; Hawkesworth et al., 1992).

The Gondwana breakup probably initiated in the mid-Jurassic, however, the exact timing is uncertain, considering that the oldest magnetic anomalies on South Atlantic

oceanic crust have associated ages from 131 and 126 Ma (Turner et al., 1994; Nürnberg and Müller, 1991). The Paraná flood basalts are one of the most important events that occurred during the beginning of the South America and South Africa separation, and they provide significant information about the sub-continental mantle in the Rosário do Sul kimberlite context. They are geochemically divided in low-Ti basalts and high-Ti basalts, the last with higher Fe, P, Ti, Zr, Ce, La, Ba and Sr concentrations. This compositional variation is interpreted by Bellieni et al. (1984) as an evidence of a large scale heterogeneous mantle source. In addition to previous studies (Peate et al., 1999; Marques et al., 1999) that proposed a heterogeneous lithospheric mantle melting as the source of the Paraná flood basalts, Rocha-Júnior et al. (2012, 2013) demonstrated, based on Re-Os and Sr-Nd-Pb isotopic data, that the asthenospheric source of the basalts was enriched by fluids or magmas related to the Neoproterozoic subduction processes. The authors also suggest that a mantle plume (Tristan da Cunha) could have acted as a heat source that may triggered the Paraná flood basalts generation, but without any role in the Paraná flood basalt source.

According to Conceição et al.(*in prep.)* and Carniel et al. (*submitted),* extensional movements that caused the Gondwana breakup and contributed to the eruption of Paraná flood basalts that covered the Paraná basin sediments, may have been also responsible for Rosário do Sul event. The carbonated material and basalts from subducted slabs may have oxidized the mantle and caused alkaline events as Rosário do Sul kimberlite, with similar age to the Paraná basalts, in southern Brazil.

In this study, we estimated temperatures, pressures and fO_2 conditions for Rosário do Sul and Alfeu-I kimberlites, applying different thermobarometers and oxygen barometers. We used our results to discuss the possibility of Rosário do Sul kimberlite composition be a representative melt of a mantle contaminated by old subductions. Furthermore, our goal is to

constrain the potential of these kimberlites to carry and preserve diamonds, since no diamonds were found in both of them until today.

2. Samples

The Rosário do Sul transitional kimberlite investigated in this study is a hypabyssal body from the Rosário do Sul Kimberlitic Province, embedded in Phanerozoic sandstones of the Piramboia formation in the Paraná Basin, South of Brazil (Conceição et al., *in prep.*). Mineralogy and chemistry of minerals were well described in Carniel et al. (*submitted*). Olivine megacrysts from peridotite mantle xenoliths and pelletal lapilli are spread in the rock immersed in the heterogeneous and segregated matrix of Rosário do Sul kimberlite. The Rosário do Sul mineral assemblage consists of macrocrysts and microphenocrysts of olivine, and microphenocrysts of phlogopite and apatite, all immersed in a groundmass composed of serpentinized olivine, monticellite, melilite, phlogopite, $CaTiO_3$-perovskite, Mg-chromite, Mg-ulvöspinel and apatite, in addition to a mesostasis composed of phlogopite, soda melilite, akermanite and carbonate (Conceição et al., *in prep.*). Olivine, spinel and perovskite compositions were used to determine the temperature and oxygen fugacity of the Rosário do Sul magma source (Table 1).

The Alfeu-I kimberlite is an intrusive volcanic chimney in Pinheiro Machado Suite of the Pelotas Batholith domain, and occurs in the eastern portion of the Rio Grande do Sul Shield in the South of Brazil, about 200 km far from Rosário do Sul kimberlite. According to Provenzano (2016), the Alfeu-I kimberlite has petrographic and mineralogical characteristics compatible with kimberlites from Group II, although the mineral chemistry interpretation indicates a transitional composition between Group I and II kimberlites, and lamproites. The Alfeu-I rocks are composed of megacrysts/macrocrysts and phenocrysts

with different compositions (mica, spinel, garnet, ilmenite and pyroxene) in an interstitial matrix with some imbricated pelletal lapilli, rock autoliths and mantle xenoliths. The olivine, garnet, orthopyroxene and clinopyroxene compositions used in this study were acquired by Provenzano (2016), while spinel compositions are from Chaves et al. (2014) (Table 2).

Olivines	**3A-21**	**3A-30**	**3A-37**	**3D-55***	**3D-67**	**3D-74**	**3D-86**	**3D-93**	**3I-1-3***	**3I-1-4***	**3I-1-5***	**3I-1-6***	**3I-1-14***	**301-15***	**301-42**	**301-43**	**301-44**	**301-63**
SiO_2	41	42	42	45	39	40	41	40	39	39	39	39	39	41	41	40	41	41
Al_2O_3	0.005	0	0.01	0.04	0.01	0.1	0.01	0.01	1.9	1.8	2.2	1.9	2.0	0.9	0.05	0.02	0.02	0.03
FeO	9.6	8.8	7.9	5.4	11	10	10	11	4.8	4.9	4.4	4.6	4.4	5.8	11	10	11	10
MgO	50	49	49	29	49	50	49	48	35	35	36	35	36	38	49	46	48	49
CaO	0.14	0.26	1.31	1.6	0.22	0.11	0.11	0.69	0.46	0.55	0.53	0.65	0.54	0.53	0.10	0.32	0.1	0.13
TiO_2	0.02	0.02	0.03	0.01	0.1	0.04	0	0.04	0.04	0.03	0.003	0.1	0.04	0.02	0.03	0.05	0	0
K_2O	0	0.03	0.01	0.02	0.01	0.004	0	0.02	0.02	0.01	0.002	0.033	0.01	0.002	0.02	0.01	0	0
Na_2O	0.03	0.02	0.01	0.003	0	0.05	0	0.03	0.01	0.004	0.01	0.01	0.02	0.02	0.002	0.04	0.005	0.04
Cr_2O_3	0.04	0.1	0.03	0.05	0.1	0.02	0.05	0	0.06	0.05	0.06	0.03	0.16	0.01	0.01	0	0.1	0.1
MnO	0.15	0.15	0.28	0.41	0.16	0.12	0.14	0.28	0.18	0.20	0.16	0.18	0.17	0.18	0.15	0.16	0.11	0.13
Total	101	101	100	81	100	100	101	100	82	82	82	81	82	86	102	98	100	101

Chromites	**R-3A-36**	**R-3A-37**	**R-3A-38**	**R-3D-67**	**R-3D-68**	**R-3D-69**	**R-3D-70**	**R-3D-71**	**R-3I-1-21**	**R-3I-1-36**	**R-3I-1-66**	**R-3I-2-16**	**R-3I-2-34**	**R-301-27**
SiO_2	0.16	0.16	0.16	0.17	0.12	0.15	0.12	0.15	0.14	0.15	0.16	0.12	0.15	0.16
Al_2O_3	18	17	18	19	19	18	19	18	20	18	19	19	17	19
FeO	23	24	23	20	19	23	19	24	21	23	19	19	24	19
MgO	13	13	12	15	15	13	15	13	14	13	14	14	13	15
CaO	0.02	0.01	0.02	0.06	0.1	0.02	0.06	0	0.04	0.02	0.03	0.04	0.02	0.14
TiO_2	1.3	1.2	1.2	1.7	1.5	1.1	1.7	1.1	1.4	1.3	1.4	1.6	1.2	1.5
K_2O	0	0.01	0.01	0	0	0	0	0.03	0	0.01	0	0	0.03	0.02
Na_2O	0.04	0.06	0.06	0.01	0	0	0	0	0.03	0.04	0	0.01	0.003	0.004
Cr_2O_3	40	40	39	44	42	40	42	39	41	40	42	43	40	43
MnO	0.4	0.2	0.2	0.5	0.5	0.5	0.5	0.4	0.4	0.4	0.4	0.4	0.5	0.4
Total	96	96	96	100	99	96	99	96	97	96	97	98	96	99

Pvks	**R-3A-6**	**R-3A-38**	**R-3A-51**	**R-3D-11**	**R-3D-56**	**R-3D-63**	**R-3I-1-20**	**R-3I-1-27**	**R-3I-1-63**	**R-3I-2-15**	**R-3I-2-21**	**R-301-28**	**R-301-46**	**R-301-47**	**R-301-55**
SiO_2	0.05	0	0	0.1	0.03	0.05	0.04	0.06	0.1	0.05	0.1	0	0	0.02	0
Al_2O_3	0.2	0.2	0.2	0.3	0.4	0.4	0.22	0.36	0.36	0.35	0.23	0.2	0.2	0.2	0.2
FeO	1.3	1.7	1.4	2.1	2.3	2.3	1.2	1.9	2.1	2.0	1.3	1.2	1.2	1.4	1.1
MgO	0.04	0.04	0.06	0.05	0.05	0.04	0.02	0.04	0.03	0.06	0.03	0.04	0.03	0.1	0.05
CaO	39	38	38	38	38	38	40	39	39	39	39	38	38	37	38
TiO_2	56	57	57	56	55	55	55	55	55	55	56	57	57	57	57
K_2O	0.03	0.1	0.06	0.06	0.06	0.05	0.05	0.1	0.05	0.1	0.1	0.01	0.03	0.14	0.1
Na_2O	0.3	0.3	0.3	0.2	0.2	0.2	0.3	0.3	0.2	0.2	0.3	0.17	0.24	0.29	0.25
Cr_2O_3	0.06	0.1	0.1	0	0.1	0.02	0.2	0.01	0.02	0.05	0.05	0.23	0.05	0.05	0.03
MnO	0.002	0.05	0.01	0.06	0.02	0.04	0	0	0	0	0	0.02	0	0.03	0.01
Total	97	97	97	97	96	97	97	97	97	97	97	98	96	96	97

Table 1: Rosário do Sul olivines, chromites and perovskites compositions used in calculations; (*) are serpentinized olivine microphenocrysts. Mineral data are from Carniel et al. (*submitted*).

Olivines	**Ol-1**	**Ol-2**	**Ol-3**	**Ol-4**	**Ol-5**	**Ol-6**	**Ol-7**	**Ol-8**	**Ol-9**
SiO_2	41	41	41	40	41	41	41	41	41
Al_2O_3	0	0	0	0	0	0	0	0	0
FeO	9	10	9	10	10	10	9	10	9
MgO	49	49	49	49	48	49	49	48	48
MnO	0.1	0	0	0.2	0.2	0.2	0.2	0	0
NiO	0.4	0.4	0.4	0.4	0.4	0.4	0.4	0.4	0.4
Total	100	99	99	99	99	100	100	100	100

Chromites	**Alf-Cr-01**	**Alf-Cr-02**	**Alf-Cr-04**	**Alf-Cr-05**	**Alf-Cr-06**	**Alf-Cr-07**	**Alf-Cr-08**	**Alf-Cr-11**	**Alf-Cr-12**
Al_2O_3	28	17	42	34	37	36	23	26	34
FeO	13	28	12	14	13	13	19	14	13
MgO	17	13	17	16	17	18	14	15	18
TiO_2	1.2	4.4	0.2	0.1	0.1	0.2	2	0.4	0.1
Cr_2O_3	41	38	30	36	33	32	41	44	35
MnO	0.2	0.2	0.1	0.2	0.2	0.2	0.2	0.2	0.2
Total	101	101	101	99	100	100	100	99	100

Garnets	**Grt-1**	**Grt-2**	**Grt-3**	**Grt-4**	**Grt-5**	**Grt-6**	**Grt-7**	**Grt-8**	**Grt-9**	**Grt-10**	**Grt-11**	**Grt-12**	**Grt-13**	**Grt-14**	**Grt-15**	**Grt-16**	**Grt-17**	**Grt-18**	**Grt-19**	**Grt-20**	**Grt-21**	**Grt-22**	**Grt-23**	**Grt-24**
SiO_2	42	42	42	42	42	41	41	42	42	42	42	41	42	42	41	42	42	42	41	41	41	40	41	41
Al_2O_3	24	24	23	24	23	23	24	23	23	23	23	23	23	23	23	23	23	23	22	22	22	22	22	22
FeO	8.7	8.5	7.3	7.7	11	11	12	11	9.2	9.4	10	10	9.6	9.4	10	11	10	10	16	16	17	17	17	17
MgO	21	21	21	22	19	19	19	18	20	20	20	19	20	19	20	20	20	20	15	16	14	14	15	15
CaO	44	4.3	4.6	4.5	4	4	4.8	4.7	4.1	4.1	4.5	4.6	4.2	4.2	4	4.1	4.3	4.2	4.6	4.6	4.9	5	4.9	4.8

TiO_2	0.2	0.3	0.3	0.3	0.3	0.3	0.2	0.2	0.2	0.3	0.3	0.3	0.3	0.3	0.2	0.3	0.4	0.3	0.5	0.5	0.6	0.6	0.6	0.6
Cr_2O_3	0.2	0.2	0.4	0.4	0.2	0.2	0.4	0.3	0.3	0.3	0.1	0.1	0.5	0.6	0.5	0.5	0.6	0.5	0.02	0.02	0	0.01	0.01	0.01
MnO	0.3	0.4	0.4	0.4	0.4	0.4	0.4	0.4	0.4	0.4	0.3	0.4	0.2	0.4	0.4	0.3	0.3	0.3	0.4	0.4	0.4	0.5	0.4	0.4
Total	101	101	99	100	100	100	100	99	100	99	99	98	100	99	99	101	101	100	100	100	100	98	101	101

Opx	**Px-34**	**Px-35**	**Px-36**	**Px-37**	**Px-38**	**Px-39**	**Px-40**	**Px-41**	**Px-42**	**Px-43**	**Px-44**	**Px-45**	**Px-46**	**Px-47**	**Px-48**	**Px-49**	**Px-50**	**Px-51**	**Px-52**	**Px-53**	**Px-54**	**Px-55**	**Px-56**	**Px-57**
SiO_2	55	55	55	55	55	56	56	55	55	54	55	54	55	55	56	55	56	56	54	55	55	55	55	55
Al_2O_3	3.4	3.4	3.4	3.2	3.2	3.2	4.4	3.5	3.4	3.4	3.4	3.5	3.4	3.3	3.3	3.4	3.3	3.3	3.2	3.3	3.2	3.0	3.2	3.0
FeO	4.5	4.5	4.6	4.5	4.5	4.5	5.7	6.0	5.8	7.5	7.4	7.4	5.0	5.0	5.0	5.4	5.5	5.5	6.8	7.2	6.9	6.2	6.3	6.5
MgO	34	35	34	35	35	35	32	34	34	33	33	32	34	34	34	34	34	34	33	33	33	34	34	34
CaO	0.9	0.9	0.9	0.9	0.9	0.9	0.8	0.6	0.7	0.7	0.7	0.8	0.9	0.9	0.9	0.8	0.8	0.8	0.8	0.8	0.8	0.6	0.7	0.6
TiO_2	0.1	0.1	0.1	0.05	0.1	0.03	0.4	0.1	0.1	0.2	0.2	0.2	0	0.1	0	0.1	0.1	0.1	0.2	0.1	0.1	0.2	0.2	0.2
K_2O	0.01	0	0	0	0.02	0	0.1	0	0	0.01	0	0.02	0	0	0	0	0	0	0	0	0	0	0	0
Na_2O	0.2	0.1	0.2	0.1	0.1	0.1	0.2	0.1	0.1	0.1	0.1	0.1	0.2	0.2	0.2	0.2	0.2	0.2	0.1	0.1	0	0	0.1	0.1
Cr_2O_3	0.8	0.9	0.8	0.8	0.8	0.9	0.4	0.4	0.4	0.7	0.7	0.7	0.9	0.9	0.9	0.8	0.8	0.8	0.6	0.6	0.6	0.6	0.7	0.7
MnO	0.1	0.1	0.1	0.1	0.1	0.1	0.1	0.1	0.1	0.1	0.1	0.1	0	0	0	0.1	0	0.1	0.1	0.1	0.1	0.1	0.1	0.1
Total	100	100	99	100	100	100	100	100	100	100	101	99	100	100	100	100	100	101	99	100	100	100	100	100

Cpx	**Px-01**	**Px-02**	**Px-03**	**Px-04**	**Px-05**	**Px-06**	**Px-07**	**Px-08**	**Px-09**	**Px-13**	**Px-14**	**Px-15**	**Px-22**	**Px-23**	**Px-24**	**Px-25**	**Px-26**	**Px-28**	**Px-29**	**Px-30**	**Px-31**	**Px-32**	**Px-33**	**Px-70**
SiO_2	52	52	52	52	52	52	53	53	53	53	53	53	53	53	53	52	52	53	53	53	53	54	53	52
Al_2O_3	4.8	4.7	4.8	4.7	4.8	4.8	4.2	4.3	4.1	3.2	3.2	3.1	6.3	6.1	6.2	8.0	8.1	6.1	6	6	6.4	6.4	6.4	4.5
FeO	2.3	2.4	2.4	2.7	2.6	2.6	9	9.1	8.8	8.8	8.7	8.4	7.6	7.5	7.4	8.4	8.2	7.5	7.6	7.5	8.3	8.3	7.9	9.7
MgO	16	17	16	16	16	16	13	13	13	15	15	15	16	16	16	13	13	16	16	16	16	16	15	13
CaO	19	19	19	19	19	20	17	17	17	16	16	16	14	14	14	14	14	14	13	13	13	13	13	17
TiO_2	0.3	0.3	0.3	1	1	1	0.9	0.9	0.9	0.7	0.7	0.7	0.6	0.6	0.6	0.5	0.6	0.6	0.6	0.5	0.6	0.7	0.6	1.0

K_2O	0.01	0	0	0	0	0	0.02	0.01	0	0.01	0.01	0	0	0	0	0	0	0	0	0	0	0	0	0
Na_2O	1.7	1.6	1.6	1.3	1.5	1.5	2.7	2.6	2.6	2.1	2	2.1	2.3	2.3	2.3	2.8	2.8	2.2	2.1	2.2	2.3	2.4	2.3	2.8
Cr_2O_3	1.8	1.8	1.8	1.2	1.3	1.2	0.03	0	0.01	0.02	0.01	0.01	0.1	0.1	0.1	0.1	0.1	0.1	0.1	0.1	0.1	0.1	0.1	0
MnO	0.2	0.1	0.05	0.1	0.1	0.1	0.2	0.1	0.1	0.2	0.2	0.2	0.1	0.2	0	0.1	0.2	0.2	0.2	0.1	0.2	0.1	0.2	0.2
Total	98	99	99	99	99	99	99	99	98	99	98	98	99	100	99	99	100	99	100	99	99	100	98	100

Table 2: Alfeu-I olivines, chromites, garnets, clinopyroxenes and orthopyroxenes compositions used in calculations. Mineral data are from Chaves et al. (2014) and Provenzano (2016).

3. Methods

The determination of the crystallization temperatures and oxygen fugacities (fO_2) of Rosário do Sul kimberlite was made using the olivine-spinel oxygen geothermobarometer of O'Neill & Wall (1987) and Ballhaus et al., (1991), which is applicable to the entire spectrum of spinel compositions occurring in mantle rocks and mantle-derived melts, and gives reasonable results to temperatures as low as 800°C. The $CaTiO_3$-perovskite oxygen barometer of Carniel et al., (*submitted*) was also used in Rosário do Sul samples, in order to predict the redox conditions of the Rosário do Sul parental melt. In this method, the Fe content and modes of perovskites and olivines are used as an important tool to estimate the redox conditions of the kimberlite rocks. The pv-ol oxygen barometer equation can be applied in kimberlite rocks that contain perovskite and olivine from different fO_2 conditions. Fe^{3+}/Fe^{2+} ratio of the Rosário do Sul kimberlitic melt was calculated using Fe^{3+}/Fe^{2+}(melt) equation from Carniel et al., (*submitted*), to better understand the oxidation state of the magma source and the consequent preservation of diamonds.

The determination of crystallization temperature and fO_2 of Alfeu-I kimberlite was made using the same olivine-spinel oxygen geothermobarometer used in Rosário do Sul samples, from O'Neill & Wall (1987) and Ballhaus et al., (1991), since there is neither perovskite nor monticellite in Alfeu-I kimberlite mineral assembly. The temperatures and pressures of Alfeu-I kimberlite were also estimated with the orthopyroxene-clinopyroxene geothermometer of Wells (1977), and the garnet-orthopyroxene geothermobarometer of Nickel and Green (1985), respectively. Wells (1977) developed a semi-empirical equation of state extracted from the available experimental data for the diopside-enstatite miscibility gap. This equation

successfully reproduces the miscibility gap over a temperature range of 800°C to 1700°C. Nickel and Green (1985) used mineral assemblages containing garnet and orthopyroxene (±clinopyroxene) to deduce pressure and temperature conditions of crystallization. The pressure and temperature estimation equations are applicable to rocks in which MgO, FeO, CaO, Al_2O_3 and SiO_2 are significant components.

4. Geothermometry and oxygen barometry results

4.1. Olivine-spinel geothermobarometer and oxygen barometer

Temperatures of the Rosário do Sul and Alfeu-I kimberlites were determined applying the olivine-spinel $FeMg_{-1}$ exchange thermometer of equation (1) from O'Neill & Wall (1987) improved by Ballhaus et al. (1991):

$$T = (6530 + 280P + 700 + 108P) * (1 - 2X_{Fe}^{ol}) - 1960 * \left(X_{Mg}^{sp} - X_{Fe^{2+}}^{sp}\right) + 16150 * X_{Cr}^{sp} + 25150 * (X_{Fe^{3+}}^{sp} + X_{Ti}^{sp})/(R \ln K_{D^{ol-sp}}^{Mg-Fe} + 4.705) \quad (1)$$

where T is in K, X_{Fe}^{ol} are the number of Fe cations in olivine, X_{Mg}^{sp} , $X_{Fe^{2+}}^{sp}$, X_{Cr}^{sp} , $X_{Fe^{3+}}^{sp}$ and X_{Ti}^{sp} are the number of Mg, Fe^{2+}, Cr, Fe^{3+} and Ti cations in spinel calculated based on 4 oxygens, $K_{D^{ol-sp}}^{Mg-Fe}$ is the ratio $(X_{Mg}^{ol} * X_{Fe^{2+}}^{sp})/(X_{Fe}^{ol} * (X_{Mg}^{sp})$. For calculations, we used chromites and olivines analyses of Rosário do Sul (Carniel et al., *submitted*) and Alfeu-I (Chaves et al., 2014; Provenzano, 2016) kimberlites. Fe^{2+} and Fe^{3+} contents of chromites were

calculated with the method of Droop (1987) that is a general equation for estimating Fe^{3+} concentrations in ferromagnesian silicates and oxides from microprobe analyses, based on stoichiometric criteria, assuming that iron is the only element present with variable valence, and oxygen is the only anion.

Temperatures were calculated in different pressures: 2 and 3 GPa for Rosário do Sul, based on silica activity limit constrained by the presence of monticellite (Edgar et al., 1988), and 4 and 5 GPa for Alfeu-I. Based on these calculations, the estimated mean temperature of Rosário do Sul kimberlite source is 1556(±60)ºC at 2 GPa, and 1573(±60)ºC at 3 GPa (Table 3), whereas Alfeu-I kimberlite source is 1617(±62)ºC at 4 GPa and 1636(±63)ºC at 5GPa (Table 4). The Alfeu-I mineral assembly suggests a crystallization pressure higher than the pressure of Rosário do Sul, which was later proved by garnet-orthopyroxene geothermobarometer.

The oxygen barometer developed by Ballhaus et al., (1991) from equation (2) can be applied to a variety of mantle-derived rocks and spinel-bearing primitive melts. However, the equation is only valid if silica activity (a_{SiO_2}) is buffered by the presence of both olivine and orthopyroxene:

$$\Delta\log(fO_2)^{FMQ} = 0.27 + 2505/T - 400P/T - 6\log\left(X_{Fe}^{ol}\right) - 3200\left(1 - X_{Fe}^{ol}\right)^2/T + 2\log(X_{Fe^{2+}}^{sp}) + 4\log(X_{Fe^{3+}}^{sp}) + 2630(X_{Al}^{sp})^2/T \quad (2)$$

The silica activity (a_{SiO_2}) of Rosário do Sul kimberlite is lower than that required to stabilize orthopyroxene. In this case, the Ballhaus et al., (1991) barometer can be used if a correction (equation 3) is applied:

$$\Delta \log(fO_2)^{\mathrm{FMQ}} = \Delta \log(fO_2)^{\mathrm{FMQ}}\ (\text{calculated}) + 3 * (\log a_{SiO_2}^{\mathrm{rock}} - \log a_{SiO_2}^{\mathrm{Fo-En\ buffer}}) \quad (3)$$

Applying the corrected fO_2 values from equation (2) and (3), the calculated mean of oxygen fugacity relative to the nickel-nickel oxide (ΔNNO) of Rosário do Sul kimberlitic melt at 2 GPa and 3 GPa is 3.1(±0.2) and 3.2(±0.2), respectivelly. These values represent the average of fresh olivine macrocrysts cores. Considering the serpentinized olivine macrocrysts rims and olivine microphenocrysts, the results are slightly higher, with 3.8(±0.3) at 2 GPa and 3.9(±0.3) at 3 GPa (Table 3). The calculated means of Alfeu-I oxygen fugacity (ΔNNO) using equation (2) at 4 GPa are 3.0 (±0.3), and at 5 GPa are 3.2 (±0.3) (Table 4).

Sample		Ol-sp T(°C)		Ol-sp Δlog(fO_2)		log(fO_2)		Ol-sp ΔNNO			
		2 GPa	3 GPa	2 GPa	3 GPa	2 GPa	3 GPa	2 GPa		3 GPa	
Ol	R-3A-21	1578	1596	3.1	2.9	-0.5	0.0	3.1		3.2	
Chr	R-3A-36										
Ol	R-3A-30	1559	1576	3.3	3.1	-0.5	0.0	3.3		3.4	
Chr	R-3A-37										
Ol	R-3A-37	1530	1547	3.5	3.3	-0.5	0.1	3.5		3.6	
Chr	R-3A-38										
Ol	R-3D-55*	1640	1658	3.0	2.8	-0.2	0.3	3.0*		3.1*	
Chr	R-3D-67										
Ol	R-3D-67	1613	1630	2.8	2.6	-0.6	-0.1	2.8		2.9	
Chr	R-3D-68										
Ol	R-3D-74	1585	1602	3.2	2.9	-0.4	0.1	3.1		3.3	
Chr	R-3D-69										
Ol	R-3D-86	1597	1615	3.0	2.8	-0.5	0.0	3.0		3.1	
Chr	R-3D-70										
Ol	R-3D-93	1626	1643	2.8	2.6	-0.5	0.0	2.8		2.9	
Chr	R-3D-71										
Ol	R-3I-1-3*	1496	1513	3.8	3.5	-0.4	0.1	3.8*		3.9*	
Chr	R-3I-1-21										
Ol	R-3I-1-4*	1485	1502	3.8	3.6	-0.5	0.1	3.8*		4.0*	
Chr	R-3I-1-36										
Ol	R-3I-1-5*	1509	1527	3.9	3.7	-0.2	0.3	3.9*		4.0*	
Chr	R-3I-1-66										
Ol	R-3I-1-6*	1513	1530	3.8	3.6	-0.3	0.2	3.8*		3.9*	
Chr	R-3I-2-16										
Ol	R-3I-1-14*	1444	1461	4.1	3.9	-0.5	0.1	4.2*		4.3*	
Chr	R-3I-2-34										
Ol	R-301-15*	1603	1621	3.4	3.2	-0.1	0.4	3.4*		3.5*	
Chr	R-301-27										
Mean		1556	1573					3.1	3.8*	3.2	3.9*
(stdev)		(60)	(60)					(0.2)	(0.3)	(0.2)	(0.3)

Table 3: Rosário do Sul kimberlite equilibrium temperatures and oxygen fugacities calculated based on olivine-spinel geothermobarometer and oxygen barometer of Ballhaus et al. (1991). Notes: olivines (Ol), chromites (Chr), ΔNNO (fO_2 relative to the nickel-nickel oxide – NNO buffer), (stdev) standard deviations as last significant digits in brackets. (*) Calculations based on serpentinized olivine macrocrysts rims and serpentinized olivine microphenocrysts.

Sample		Ol-sp T(°C)		Ol-sp Δlog(fO_2)		log(fO_2)		Ol-sp ΔNNO	
		4 GPa	5 GPa	4 GPa	5 GPa	4 GPa	5 GPa	4 GPa	5 GPa
Ol	01	1736	1756	2.2	2.0	0.7	1.1	2.8	2.9
Chr	Alf-Cr-01								
Ol	02	1553	1569	2.8	2.6	0.2	0.7	3.5	3.6
Chr	Alf-Cr-02								
Ol	03	1545	1565	2.4	2.1	-0.3	0.2	3.0	3.2
Chr	Alf-Cr-04								
Ol	04	1581	1600	2.4	2.1	-0.1	0.4	3.0	3.2
Chr	Alf-Cr-05								
Ol	05	1578	1598	2.3	2.1	-0.1	0.4	3.0	3.1
Chr	Alf-Cr-06								
Ol	06	1608	1628	2.3	2.1	0.1	0.6	3.0	3.1
Chr	Alf-Cr-07								
Ol	07	1623	1641	2.5	2.3	0.4	0.8	3.2	3.3
Chr	Alf-Cr-08								
Ol	08	1669	1688	2.3	2.1	0.4	0.8	2.9	3.0
Chr	Alf-Cr-11								
Ol	09	1662	1682	2.3	2.1	0.3	0.8	2.9	3.0
Chr	Alf-Cr-12								
Mean		1617	1636					3.0	3.2
(stdev)		(62)	(63)					(0.2)	(0.2)

Table 4: Alfeu-I equilibrium temperatures and oxygen fugacities calculated based on olivine-spinel geothermobarometer and oxygen barometer of Ballhaus et al. (1991). Notes: olivines (Ol), chromites (Chr), ΔNNO (fO_2 relative to the nickel-nickel oxide – NNO buffer), (stdev) standard deviations as last significant digits in brackets.

4.2. $CaTiO_3$-perovskite oxygen barometer and Fe^{3+}/Fe^{2+} ratio in the melt

In order to calculate the ΔNNO (fO_2 relative to the nickel-nickel oxide – NNO buffer) of the melt of Rosário do Sul kimberlite, we used the Fe content and modal proportions of olivines (40 vol.%) and perovskites (8 vol.%), additionally to the estimated temperature and pressure calculated above, and the equation (4), proposed by Carniel et al. (*submitted*) as a perovskite oxygen barometer:

$$\Delta NNO = - 0.648 \times Fe(ol) + 0.591 \times Fe(pv) - 0.036 \times n(ol) - 0.023 \times n(pv) + 0.006 \times T - 0.767 \times P \quad (4)$$

where Fe(ol) is the total Fe in olivine (Fe^{2+}), Fe(pv) is the total iron in perovskite (Fe^{3+}), n(ol) is the modal quantity of olivine, n(pv) is the modal quantity of perovskite, T is temperature (°C) and P is pressure (GPa).

The product of the equation (4) for Rosário do Sul melt is ΔNNO (mean) = 1.2 (±0.6) at 2 GPa and ΔNNO (mean) = 0.6 (±0.6) at 3 GPa. These results are based on fresh olivine macrocrysts cores data. The mean of oxygen fugacities based on serpentinized olivine macrocrysts rims and serpentinized olivine microphenocrysts, are significantly higher (ΔNNO = 4.1 ±0.4 at 2 GPa and ΔNNO = 3.5 ±0.4 at 3 GPa).

Another important source of information on oxidation states is the ferric/ferrous iron ratio in the melt, which can be calculated from the amount of Fe in perovskite (Fe^{3+}) and in olivine (Fe^{2+}). The following equation from Carniel et al., (*submitted*) considers that perovskite mainly concentrates Fe^{3+}, while olivine concentrates mainly Fe^{2+}:

$$\frac{Fe^{3+}}{Fe^{2+}}(melt) = \frac{Fe^{3+}(pv) * D(\frac{ol}{melt})}{Fe^{2+}(ol) * D(\frac{pv}{melt})} \quad (5)$$

where ol is olivine, pv is perovskite, D(ol/melt) is the distribution coefficient of Fe^{2+} between olivine and melt, and D(pv/melt) is the distribution coefficient of Fe^{3+} between perovskite and melt. D(ol/melt) and D(pv/melt) (Table 5) were calculated from the molar fractions of Fe in perovskites, olivines and in the bulk rock from Rosário do Sul kimberlite (Conceição et al., *in prep.*). The average of Fe^{3+}/Fe^{2+} ratio of Rosário do Sul kimberlite melt is 0.69 using fresh olivines and 0.89 using serpentinized olivines for calculation, indicating that there is higher Fe^{3+} content in the melt after serpentinization. The Fe^{3+}/Fe^{2+} ratio average of 0.76 (Table 5) suggest that Rosário do Sul melt may have undergone some oxidation process, increasing the Fe^{3+} content in the melt.

Sample		FeO (wt.%)	D(pv/melt)	D(ol/melt)	Fe^{3+}/Fe^{2+} ratio	Ol-pv ΔNNO 2 GPa		3 GPa	
Ol	R-3A-21	1.34	0.13	0.65	0.70	1.2		0.6	
Pv	R-3A-6	9.62							
Ol	R-3A-30	1.67	0.16	0.59	0.69	1.9		1.2	
Pv	R-3A-38	8.75							
Ol	R-3A-37	1.38	0.14	0.53	0.69	2.1		1.4	
Pv	R-3A-51	7.88							
Ol	R-3D-74	2.14	0.21	0.66	0.69	1.7		1.0	
Pv	R-3D-11	9.71							
Ol	R-3D-86	2.31	0.23	0.69	0.69	1.5		0.9	
Pv	R-3D-56	10.2							
Ol	R-3D-93	2.28	0.22	0.76	0.70	1.2		0.5	
Pv	R-3D-63	11.0							
Ol	R-3I-1-3*	1.20	0.12	0.41	0.88	3.7*		3.1*	
Pv	R-3I-1-20	4.84							
Ol	R-3I-1-4*	1.94	0.19	0.42	0.88	4.1*		3.4*	
Pv	R-3I-1-27	4.89							
Ol	R-3I-1-5*	2.12	0.21	0.38	0.88	4.6*		4.0*	
Pv	R-3I-1-63	4.44							
Ol	R-3I-1-6*	1.95	0.19	0.40	0.89	4.5*		3.8*	
Pv	R-3I-2-15	4.6							
Ol	R-3I-1-14*	1.32	0.13	0.41	0.96	3.8*		3.1*	
Pv	R-3I-2-21	4.38							
Ol	R-301-42	1.18	0.12	0.74	0.69	0.4		-0.3	
Pv	R-301-28	10.9							
Ol	R-301-43	1.24	0.12	0.73	0.71	0.81		0.2	
Pv	R-301-46	10.4							
Ol	R-301-44	1.4	0.14	0.76	0.69	0.45		-0.2	
Pv	R-301-47	11.1							
Ol	R-301-63	1.10	0.11	0.67	0.69	1.1		0.4	
Pv	R-301-55	9.83							
Mean						1.2	4.1*	0.6	3.5*
(stdev)						(0.6)	(0.4)	(0.6)	(0.4)

Table 5: Rosário do Sul kimberlite oxygen fugacities and Fe^{3+}/Fe^{2+} ratio in the melt calculated based on $CaTiO_3$-perovskite oxygen barometer and Fe^{3+}/Fe^{2+} ratio in the melt of Carniel et al., (*submitted*). Contents of Fe^{3+} in perovskite, Fe^{2+} in olivine, in wt.%; D(pv/melt) and D(ol/melt) calculated from Fe molar fractions in perovskite, olivine and in the bulk rock (melt) from Rosário do Sul kimberlite. Rosário do Sul melt composition data from Conceição

et al. (*in prep.*); perovskite and olivine composition from Carniel et al. (*submitted*). Notes: olivines (Ol), $CaTiO_3$-perovskites (Pv), ΔNNO (fO_2 relative to the nickel-nickel oxide – NNO buffer), (stdev) standard deviations as last significant digits in brackets. (*) Calculations based on serpentinized olivine macrocrysts rims and serpentinized olivine microphenocrysts.

4.3. Orthopyroxene-clinopyroxene thermometer

We calculated Alfeu-I crystallization temperatures with the orthopyroxene-clinopyroxene thermometer of Wells (1977) (equation 6), updated from Wood and Banno (1973), which successfully reproduces the diopside-enstatite miscibility gap over a temperature range of 800°C to 1700°C:

$$T = \frac{7341}{3.355 + 2.44X_{Fe}^{opx} - ln\,K} \quad (6)$$

with T in °C, X_{Fe}^{opx} as the molar fraction of Fe in the orthopyroxene and K= $a_{Mg_2Si_2O_6}^{cpx}$/ $a_{Mg_2Si_2O_6}^{opx}$, where:

$$a_{\mathrm{Mg_2Si_2O_6}} = \left(\frac{\mathrm{Mg^{2+}}}{\mathrm{Ca^{2+} + Mg^{2+} + Fe^{2+} + Mn^{2+} + Na^{+}}}\right)_{\mathrm{M2}} * \left(\frac{\mathrm{Mg^{2+}}}{\mathrm{Fe^{3+} + Fe^{2+} + Al^{3+} + Ti^{4+} + Cr^{3+} + Mg^{2+}}}\right)_{\mathrm{M1}}$$

Temperatures of Alfeu-I kimberlite (Table 6) vary from 2108 to 2141°C, which is higher than the temperatures calculated with the method of Ballhaus et al.(1991) (from 1545 to 1756°C) (Table 4). These results can be useful to think about the conditions of Alfeu-I

kimberlite formation, but their use require caution due to the high degree of alteration of Alfeu-I samples.

4.4. Garnet-orthopyroxene geobarometer

We applied a garnet-clinopyroxene geobarometer in Alfeu-I minerals using the experimentally calibrated barometric equation from Nickel and Green (1985):

$$P = \{1/-[183.3 + 178.98\, X_{Al}^{M1}(1 - X_{Al}^{M1})]\}\ x\ \{-RTln[[(1 - X_{Ca}^{gt})^3 (X_{Al}^{gt})^2\ x\ [X_{Mg,Fe}^{M1} (X_{Mg,Fe}^{M2})^2\ X_{Al}^{M1}]^{-1}] - 9000(X_{Ca}^{gt})^2 - 3400\left[2(X_{Cr}^{gt})^2 - X_{Mg}^{M1} X_{Cr}^{M1}\right] - X_{Ca}^{gt} X_{Cr}^{gt}(90853 - 52.1T) - 7590 X_{Fe}^{gt} X_{Ca}^{gt} + 5157 X_{Mg}^{M1} X_{Fe}^{M1} + 6047 - 3.23T\} \quad (7)$$

where P is pressure (kbar), T is temperature (K), X is the molar fraction of the elements (Al, Ca, Mg, Fe and Cr) in the minerals (garnet and M1-M2-sites in orthopyroxene) and R is the gas constant. Calculated average of Alfeu-I pressure is 5.4(±0.2) GPa (Table 6) calculated from a mean temperature of 1627°C (Ballhaus et al., 1991).

Sample			Opx-cpx	Gt-opx
Gt	**Opx**	**Cpx**	**T(°C)[a]**	**P(GPa)[b]**
Grt-1	Px-34	Px-01	2128	5.3
Grt-2	Px-35	Px-02	2128	5.4
Grt-3	Px-36	Px-03	2127	5.2
Grt-4	Px-37	Px-04	2129	5.4
Grt-5	Px-38	Px-05	2129	5.5
Grt-6	Px-39	Px-06	2129	5.5
Grt-7	Px-40	Px-07	2136	5.0
Grt-8	Px-41	Px-08	2132	5.0
Grt-9	Px-42	Px-09	2133	5.2
Grt-10	Px-43	Px-13	2108	5.5
Grt-11	Px-44	Px-14	2110	5.4
Grt-12	Px-45	Px-15	2107	5.3
Grt-13	Px-46	Px-22	2142	5.1
Grt-14	Px-47	Px-23	2140	5.5
Grt-15	Px-48	Px-24	2141	5.3
Grt-16	Px-49	Px-25	2137	5.4
Grt-17	Px-50	Px-26	2136	5.4
Grt-18	Px-51	Px-28	2133	5.4
Grt-19	Px-52	Px-29	2112	5.6
Grt-20	Px-53	Px-30	2108	5.5
Grt-21	Px-54	Px-31	2114	5.6
Grt-22	Px-55	Px-32	2125	5.9
Grt-23	Px-56	Px-33	2121	5.8
Grt-24	Px-57	Px-70	2128	5.7
Mean			2126	5.4
(stdev)			(11)	(0.2)

Table 6: Alfeu-I equilibrium temperatures and pressures calculated based on garnets (Gt) and orthopyroxenes (Opx) compositions (equation 7): [a] Orthopyroxene-clinopyroxene thermometer of Wells (1977); [b] Garnet-orthopyroxene geothermobarometer of Nickel and Green (1985). Notes: ΔNNO is the fO_2 relative to the nickel-nickel oxide (NNO) buffer; stdev is the standard deviations given as last significant digits in brackets.

5. Discussion

5.1.Mantle conditions during Gondwana breakup

To constrain the mantle conditions during the formation of Rosário do Sul kimberlite, we compared the fO_2 calculated in the present study with the compositional variations of Rosário do Sul perovskites and olivines (Carniel et al., *submitted*). Based on olivine compositions (Fig. 1A and B), the fO_2 increasing of the kimberlite melt is followed by the serpentinization process, with the Fe decreasing and Al increasing in serpentinized olivines. Fresh olivines crystallized at lower fO_2 and have higher Fe content and lower Al content than serpentinized olivines. Figure 2 shows the effects of fO_2 of the kimberlite melt in $CaTiO_3$-perovskite compositional variation. Perovskites that crystallized at higher fO_2 have higher CaO/TiO_2 ratio than perovskites that crystallized at lower fO_2. The correlation between the fO_2 variations of the kimberlite melt and the compositional variations of the minerals confirms that the Rosário do Sul kimberlite melt undergone a Ti depletion, Al enrichment and fO_2 increasing during the evolution of its crystallization, which is also observed in the major element patterns of Rosário do Sul minerals. Trace element contents (Sr, Nb, Ce and Ta) from Carniel et al. (*submitted*) compared to ΔNNO (Fig. 3), show that fO_2 increasing follows Ce and Ta, but not Sr and Nb concentrations.

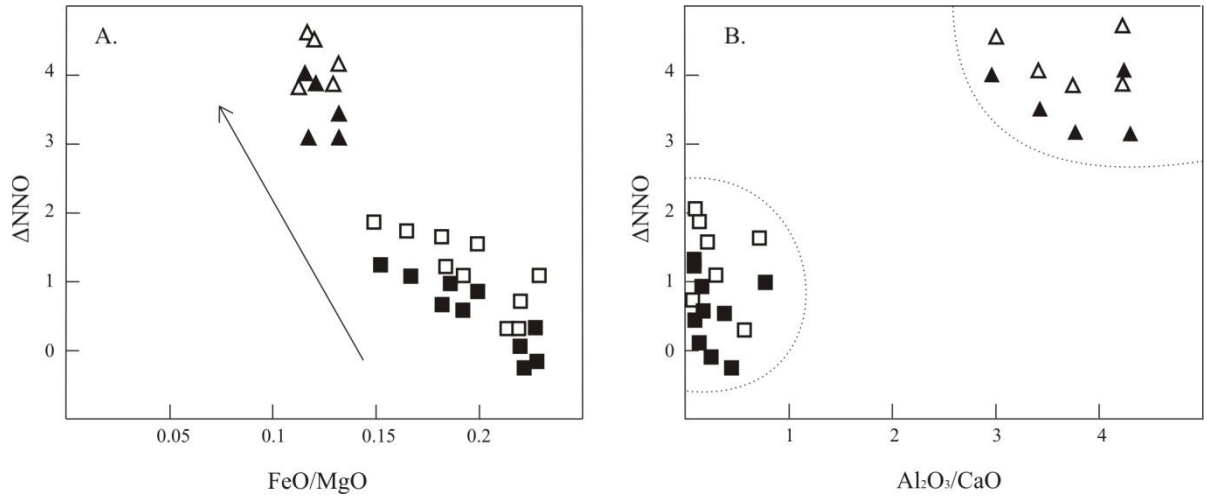

Fig. 1: Diagrams of Rosário do Sul olivines compositions: A. ΔNNO *versus* FeO/MgO (wt.%); and B. ΔNNO *versus* Al_2O_3/CaO(wt.%). Note: squares are results of calculations using perovskites and fresh olivines, while triangles are results using perovskites and serpentinized olivine microphenocrysts; open symbols are the results at 2 GPa, and filled symbols at 3 GPa.

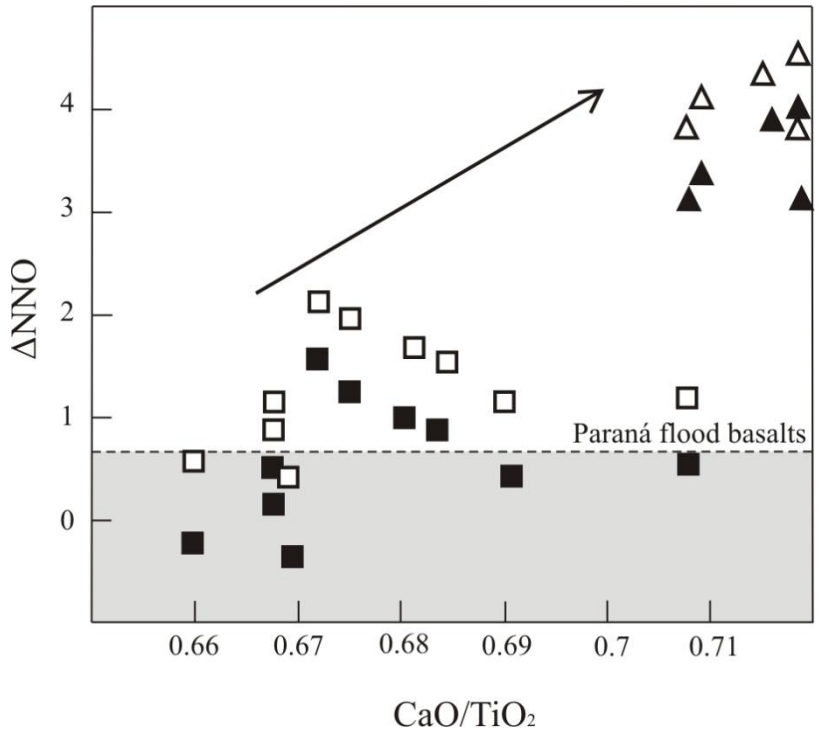

Fig. 2: Diagram of Rosário do Sul calculated ΔNNO *versus* CaO/TiO_2 (wt.%) of perovskites. Note: squares are results of calculations using fresh olivines, while triangles are results using perovskites and serpentinized olivine microphenocrysts; open symbols are the results at 2 GPa, and filled symbols at 3 GPa. Paraná flood basalts fO_2 conditions from Bellieni et al. (1984) are represented by the gray field.

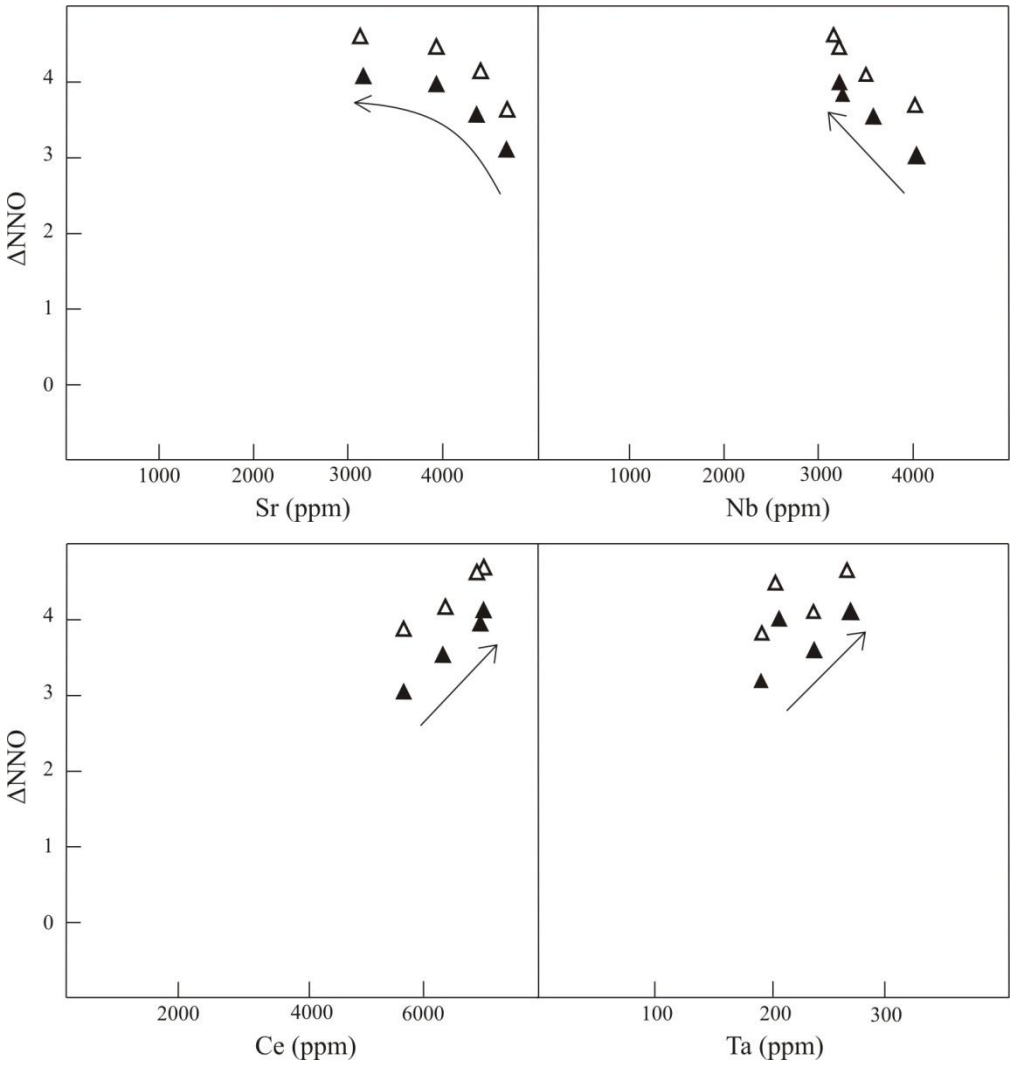

Fig. 3: Trace elements Sr, Nb, Ce and Ta (ppm) contents of Rosário do Sul $CaTiO_3$-perovskites compared to calculated oxygen fugacity (ΔNNO) of Rosário do Sul kimberlite melt. Trace element data from Carniel et al. (*submitted*). Note: fO_2 results were calculated using perovskites and serpentinized olivine microphenocrysts; open symbols are the results at 2 GPa, and filled symbols at 3 GPa.

The average of Fe^{3+}/Fe^{2+} ratio of Rosário do Sul kimberlite indicates that there was higher Fe^{3+} content in the melt during the serpentinization. This could be explained by a H_2O-rich fluid that percolates the magma, causing hydration of olivine and the partial oxidation of Fe^{2+} to Fe^{3+} (e.g. Evans et al., 2013). The Fe^{3+}/Fe^{2+} ratio of the melt *versus* oxygen fugacity (ΔNNO) are plotted in figure 4. Calculations using $CaTiO_3$-perovskite and fresh olivine

megacryst cores compositions resulted in a lower Fe^{3+}/Fe^{2+} ratio in the melt and lower oxygen fugacity than the calculations using $CaTiO_3$-perovskite and serpentinized olivine megacrysts rims and microphenocrysts compositions. This pattern occurs due to the increasing of the Fe^{3+} content in the melt with the increasing of fO_2 in the system, which is affected by olivine serpentinization. Such a melt oxidation process can be caused by H_2O-rich fluids from the kimberlite melt source, that are probably related to slab materials from subduction processes, in accordance with what has been suggested by Rocha-Júnior et al. (2012, 2013) for the Paraná flood basalts source. The carbonated material and basalts may have enriched and oxidized the mantle, causing alkaline events as Rosário do Sul kimberlite.

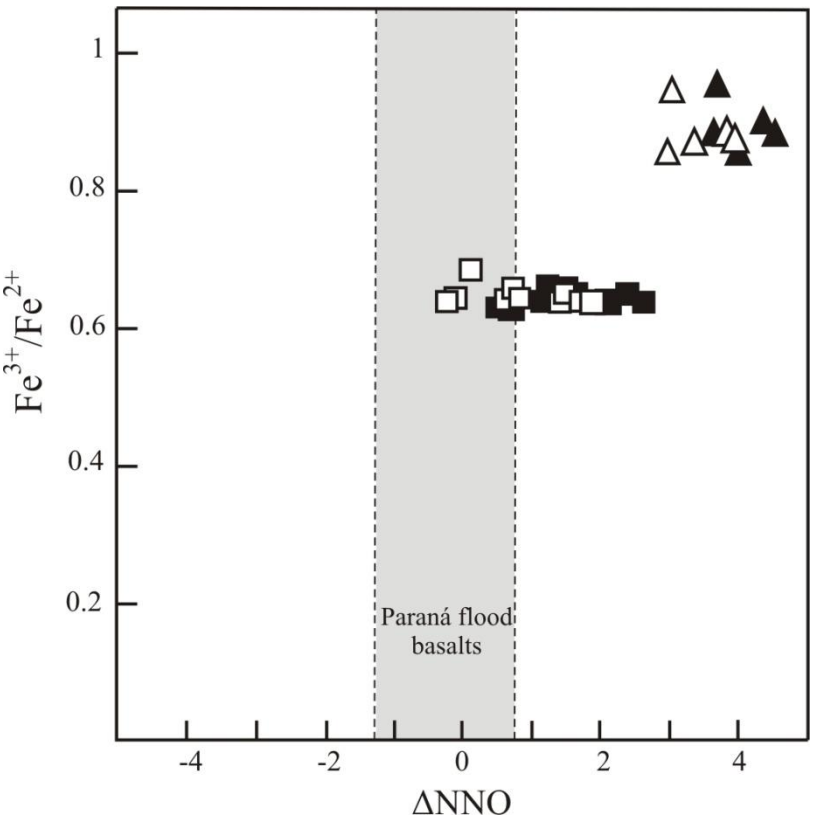

Fig. 4: The diagram shows a comparison between Fe^{3+}/Fe^{2+} ratio of the melt and the oxygen fugacity (ΔNNO). Notes: open symbols are from ΔNNO calculations based on estimated

pressure of 2 GPa, and filled symbols are from ΔNNO calculations based on 3 GPa; squares are calculated with perovskites and fresh olivine megacryst cores compositions, and triangles are calculated with perovskites and serpentinized olivine megacryst rims and serpentinized olivine microphenocrysts compositions. Paraná flood basalts fO_2 conditions from Bellieni et al. (1984) are represented by the gray field.

The Paraná flood basalts fO_2 conditions are representative of the mantle redox conditions in this region. As the most expressive event that occurs during the Gondwana breakup, its redox conditions may contribute to evaluate how oxidized is the Rosário do Sul kimberlite compared to the mantle source. The fO_2 of Rosário do Sul kimberlite is significantly higher than the fO_2 of the Paraná flood basalts, described by Bellieni et al. (1984) (Fig. 5). The authors determined the fO_2 of the Serra Geral basalts based on ilmenites and Ti-magnetites compositions, using the method of Buddington and Lindsley (1964). They found that high-Ti basalts, that have fO_2 values close to NNO-QFM buffers (NNO – nickel-nickel oxide; QFM – quartz-fayalite-magnetite), are slightly more oxidized than the low-Ti basalts, with fO_2 values close to QFM-WM buffers (QFM – quartz-fayalite-magnetite; WM – wüstite- magnetite). Rosário do Sul and high-Ti basalts fO_2 conditions are closer, which can be correlated to the Ti-enrichment and the source depth of these rocks. High-Ti basalts have been derived from greater depths (90 - 120 km depth), with lower degree of melting than the low-Ti basalts (30 - 60 km depth) (Garland et al., 1996).

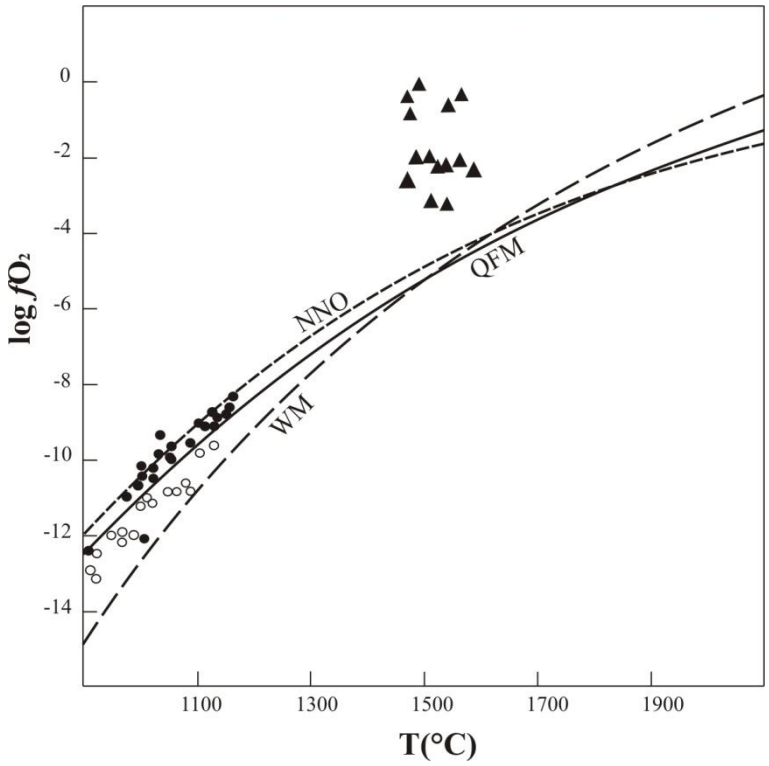

Fig. 5: Diagram of logfO_2 *versus* temperature (°C) with Rosário do Sul results (triangles); high-Ti Serra Geral basalts (filled circles); and low-Ti Serra Geral basalts (open circles) (Bellieni et al., 1984). Buffers: NNO (nickel-nickel oxide); QFM (quartz-fayalite-magnetite); WM (wüstite-magnetite). All buffer curves and results at 0.2 GPa.

5.2. Application to diamond preservation

The Rosário do Sul results indicate that this kimberlite crystallized at low pressures (from 2 to 3 GPa, which represents 60-90km depth), high temperatures (from 1556°C to 1573°C), and at ΔNNO = 1.2 - 3.1, while Alfeu-I kimberlite crystallized deeper in the mantle (from 4 to 5 GPa, around 120-150km depth), at higher temperatures (from 1617°C to 1636°C), and at ΔNNO = 3.0 – 3.2. Both kimberlite melts crystallized at high oxygen fugacities, with CO_2-rich mantle fluids that act as metasomatic agents in the kimberlite melt.

The Rosário do Sul and Alfeu-I temperatures and fO_2 are plotted in the diagrams of figure 6 (Rosário do Sul) and figure 7 (Alfeu-I), where: D/GCO is the diamond/graphite-carbon oxide buffer from Frost & Wood (1997); EMOD/G is the enstatite-magnesite-olivine-diamond/graphite buffer from Zhao et al. (1999); and NNO is the nickel-nickel oxide buffer from Ballhaus et al. (1991). All buffer curves at 2 GPa and 3 GPa. The GCO and DCO oxygen buffers describe the upper fO_2 stability of graphite or diamond with respect to a free C-O fluid (Frost & Wood, 1997). The EMOD/G curve defines the stability field between diamond/graphite and magnesite ($MgCO_3$) in the mantle. Considering this, the area below to this curve represents the oxygen fugacity for melts in equilibrium with diamond or graphite.

Rosário do Sul oxygen fugacity plots above the graphite stability area (Fig. 6), but some results at 3 GPa plot very close to the graphite stability curve. In the field of CO_2, fluids with CO_2 may react with mantle silicates to produce carbonate-rich melts.

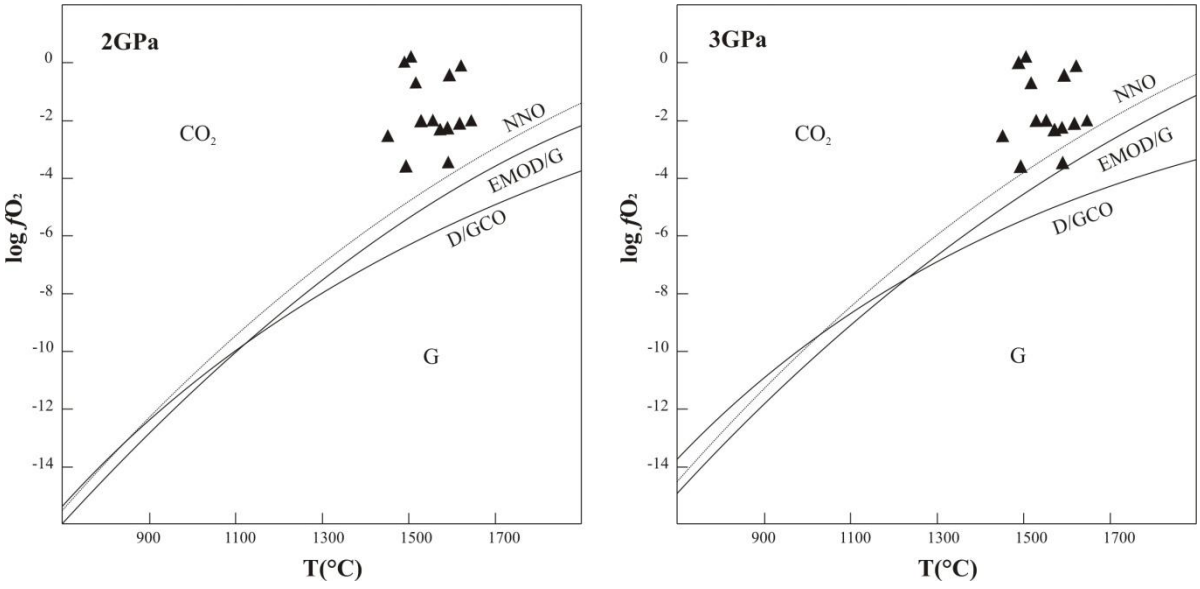

Fig. 6: Diagrams comparing logfO_2 and temperature (°C) with Rosário do Sul plots (filled triangles). D/GCO is the diamond/graphite-carbon oxide buffer at 2 and 3 GPa from Frost & Wood (1997). EMOD/G is the enstatite-magnesite-olivine-diamond/graphite buffer at 2 and 3

GPa from Zhao et al. (1999). NNO is the nickel-nickel oxide buffer at 2 and 3 GPa from Ballhaus et al. (1991).

Alfeu oxygen fugacity plots above the graphite stability curve (Fig. 7). At the fO_2 of Alfeu-I kimberlite, carbon can be oxidized to produce carbonate melt through the reduction of Fe^{3+} in silicate minerals during upwelling (Stagno et al., 2013). From 4 to 5 GPa (from 120 to 150 km depth), diamonds can survive but at very low oxygen fugacities and temperatures (see D/G limit of figure 7). For comparison, we also plotted the Lac de Gras kimberlites (Canada) data from Fedortchouk and Canil (2004). According the authors, the T–fO_2 values obtained from Lac de Gras diamondiferous kimberlites show that the diamonds of these kimberlites ascended in the stability field of graphite.

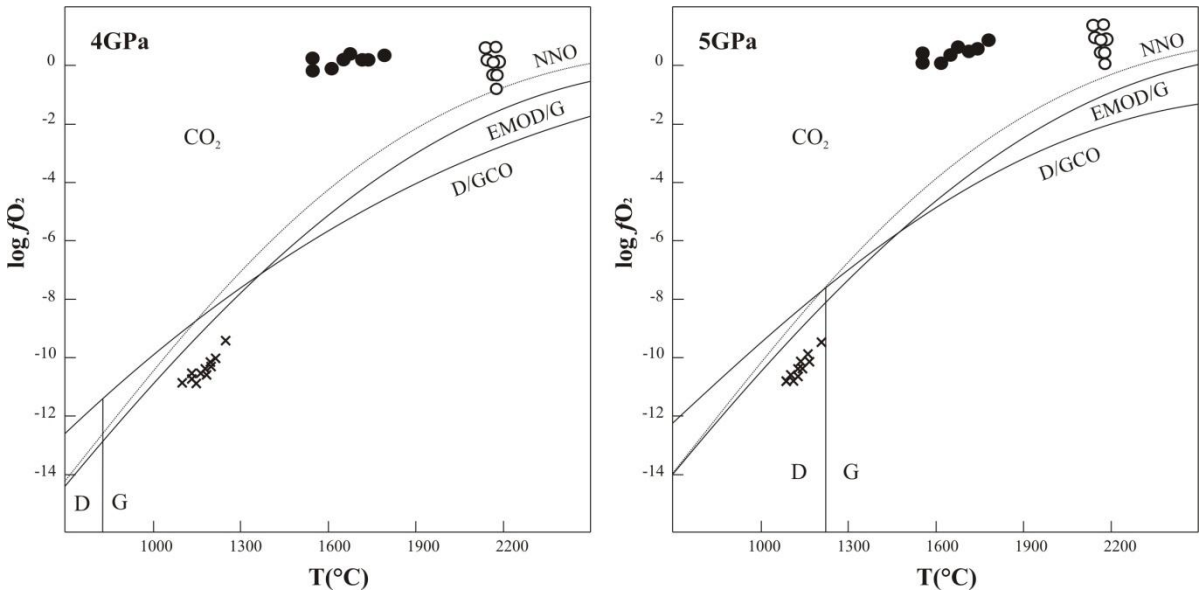

Fig. 7: Stability fields of graphite and CO_2 in logfO_2 *versus* temperature (°C) diagram at 4 GPa. D/GCO buffer from Frost & Wood (1997); EMOD/G buffer from Zhao et al. (1999); and NNO buffer from Ballhaus et al. (1991). D/G (diamond/graphite) limit is from Kennedy and Kennedy (1976). Alfeu-I results are plotted as filled circles (using temperatures calculated from Ballhaus et al., 1991) and open circles (using temperatures calculated from Wells, 1977).

Lac de Gras kimberlites data are crosses (Fedortchouk and Canil, 2004). All buffer curves limit and results at 4 and 5 GPa.

Canil and Bellis (2007), based on kimberlite samples from Lac de Gras area (Canada), shown that, estimates of kimberlite fO_2 may be useful in predicting the quality or properties of their diamonds, considering that the kimberlite pipe with the highest fO_2 has the highest proportion of highly resorbed diamonds, whereas pipes with lower estimated fO_2 have lower proportions of highly resorbed diamonds. Figure 8 shows a comparison between our fO_2 results for Rosário do Sul and Alfeu-I kimberlites, and other fO_2 results for the cratonic mantle lithosphere, other mantle derived magmas, diamondiferous kimberlites (Lac de Gras, Somerset Island and Dutoitspan kimberlites), kimberlites with low diamond potential (NKF kimberlites), and the Paraná flood basalts. Considering that fO_2 affects the properties and textures of diamonds preserved in the magma, we demonstrated that the high fO_2 of the Rosário do Sul and Alfeu-I kimberlite melts increases the possibility that the diamonds may have been partially or completely dissolved in the way to the surface.

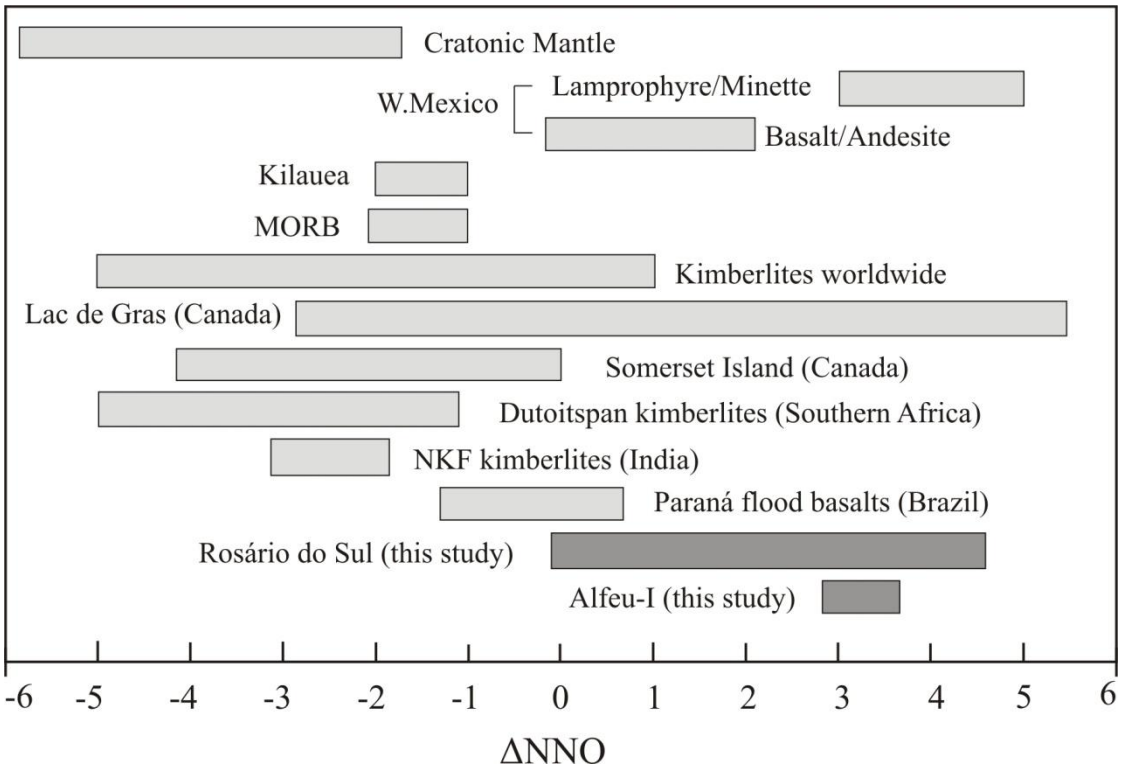

Fig. 8: Oxygen fugacity (ΔNNO) conditions of the Rosário do Sul and Alfeu kimberlites, compared to fO_2 from cratonic mantle lithosphere (Woodland and Koch, 2003; McCammon and Kopylova, 2004); mantle-derived magmas (Carmichael and Ghiorso, 1986; Christie et al., 1986; Carmichael, 1991); Lac de Gras and Somerset Island kimberlites (Canada) (Canil and Bellis, 2007); Dutoitspan kimberlite (South Africa) (Ogilvie-Harris et al., 2009); Narayanpet Kimberlite Field - NKF (India) (Chalapathi Rao et al., 2011); and Paraná flood basalts (Brazil) (Bellieni et al., 1984). Figure modified from Canil and Bellis (2007) and Chalapathi Rao et al. (2011).

6. Conclusions

Rosário do Sul crystallization temperatures registered by olivine-chromite geothermobarometer, are around 1556°C at a pressure of 2 GPa, and 1573°C at 3 GPa. The fO_2 conditions at this temperature are around 3.1 log units more oxidized than the NNO buffer, at a silica activity limited by the crystallization of monticellite (2 GPa and 3 GPa). Calculations from the $CaTiO_3$-perovskite oxygen barometer resulted in less oxidized values of ΔNNO (1.2 at 2 GPa and 0.6 at 3 GPa) than the previous method. The results of both methods indicate that Rosário do Sul kimberlite melt may have suffered some oxidation process, which also increased the Fe^{3+} content in the melt. Alfeu-I kimberlite crystallization temperatures recorded by olivine-chromite geothermobarometer are around 1617°C at 4 GPa, and 1636°C at 5 GPa. The fO_2 calculated from coexisting olivine and chromite at this temperature is ΔNNO 3.0 (4 GPa) and 3.2 (5 GPa). The serpentinization process that occurs in Rosário do Sul olivines, covering olivine macrocrysts rims and olivine microphenocrysts, is due to H_2O-rich fluids from subducted slab materials which also increase the fO_2 of the melt. The origin of these hydrated and carbonated fluids or magmas that caused such a melt oxidation process in Rosário do Sul kimberlite could be related to subducted slab materials from old subduction processes in the kimberlite mantle source. In this geological context, an old oceanic plate would have subducted carbonated and hydrated materials, in addition to basalts, that may have enriched and oxidized the mantle beneath the South American platform, being a potential source for the Paraná flood basalts and alkaline events as Rosário do Sul kimberlite, during the Gondwana breakup. The high fO_2 conditions of the Rosário do Sul and Alfeu-I kimberlite melts also indicates that the diamonds that could have been carried by these kimberlites, undergone partial or complete dissolution in the way to the surface.

Aknowledgments

This research was supported by CNPq (National Counsel of Technological and Scientific Development) from Brazil and the project "Diamonds from Brazil" from the Geological Survey of Brazil (CPRM). We are also very grateful to Andrea Sander, Prof. Márcia E. B. Gomes and Susan Drago for their assistance with Alfeu-I kimberlite data.

References

Ballhaus, C., Berry, R.F. and Green, D.H. (1991) High pressure experimental calibration of the olivine-orthopyroxene-spinel oxygen geobarometer: implications for the oxidation state of the upper mantle. *Contributions to Mineralogy and Petrology*, 107:27-40.

Bellieni, G., Comin-Chiaramonti, P., Marques, L.S., Melfi, A.J., Piccirillo, E.M., Nardy, A.J.R., Roisenberg, A. (1984) High- and low- TiO_2 flood basalts from the Paraná plateau (Brazil): petrology and geochemical aspects bearing on their mantle origin. *Neues Jahrbuch Miner. Abh.* 150(3), 273-306.

Buddington A.F. and Lindsley, D.H. (1964) Iron-Titanium Oxide Minerals and Synthetic Equivalents. *Journal of Petrology* 5(2), 310-357.

Canil, D. and Bellis A.J. (2007) Ferric Iron in $CaTiO_3$ Perovskite as an Oxygen Barometer for Kimberlite Magmas II: Applications. *Journal of Petrology* 48(2): 231–52.

Carmichael, I. S. E. and Ghiorso, M. S. (1986) Oxidation-reduction relations in basic magma: a case for homogeneous equilibria. *Earth and Planetary Science Letters* 78, 200-210.

Carmichael, I. S. E. (1991) The redox states of basic and silicic magmas: a reflection of their source regions? *Contributions to Mineralogy and Petrology* 106, 129-141.

Carniel, L.C., Klemme, S., Conceição, R.V., Rohrbach, A., Berndt, J. The effects of redox conditions on ferric iron in $CaTiO_3$-perovskite from kimberlitic magmas. (*submitted*)

Carniel, L.C., Conceição, R.V., Klemme, S., Gervasoni, F., Cedeño D.G., Berndt, J. Heterogeneity in the South Brazilian Mantle evidenced by the major and trace element compositions of Rosário do Sul kimberlite minerals. (*submitted*)

Chalapathi Rao, N.V., Paton, C. and Lehmann B. (2011) Origin and diamond prospectivity of Mesoproterozoic kimberlites from the Narayanpet field, Eastern Dharwar Craton, southern India: insights from groundmass mineralogy, bulk-chemistry and perovskite oxybarometry. *Geological Journal* 47 (2-3). DOI: 10.1002/gj.1309

Chaves, M.L.S.C., Andrade, K.W., Azzi, A.A., Silveira, F.V. (2014) Minerais indicadores kimberlíticos e prospectividade diamantífera da intrusão Alfeu-01 (Canguçu, RS). *Geociências* 33-4, 535-548.

Christie, D. M., Carmichael, I. S. E. and Langmuir, C. H. (1986) Oxidation states of mid-ocean ridge basalt glasses. *Earth and Planetary Science Letters* 79, 397-411.

Conceição, R.V. (*in prep.*) Mantle heterogeneity on the source of Paraná continental flood basalts: New evidence from 128Ma Rosário do Sul Kimberlitic Province, Southern Brazil.

Droop, G.T.R. (1987) A general equation for estimating Fe^{3+} concentrations in ferromagnesian silicates and oxides from microprobe analyses, using stoichiometric criteria. *Mineralogical Magazine* 51, 431-5.

Edgar, A.D., Arima, M., Baldwin, D.K., Bell, D.R., Shee, S.R., Skinner, M.W., Walker, E.C. (1988) High-pressure-high-temperature melting experiments on a SiO_2-poor aphanitic kimberlite from the Wesselton mine, Kimberley, South Africa. *American Mineralogist* 73, 524-533.

Edgar, A. D. and Charbonneau, H. E. (1993) Melting experiments on a SiO_2-poor, CaO-rich aphanitic kimberlite from 5-10 GPa and their bearing on sources of kimberlite magmas. *American Mineralogist* 78, 132-142.

Ernesto, M., Marques, L.M., Piccirillo, E.M., Molina, E., Ussami, N., Comin-Chiaramonti, P. and Bellieni, G. (2002) Paraná Magmatic Province – Tristan da Cunha plume system: fixed versus mobile plume, petrogenetic considerations and alternative heat sources. *Journal of Vulcanology and Geothermal Researches* 118, 15-36.

Evans, B.W., Hattori, K., Baronnet, A. (2013) Serpentinite: What, Why, Where? *Elements* 9, 99-106.

Fedortchouk, Y. and Canil, D. (2004) Intensive Variables in Kimberlite Magmas, Lac de Gras, Canada and Implications for Diamond Survival. *Journal of Petrology* v.45, n.9, p.1725-1745.

Frost, D.J. and Wood, B.J. (1997) Experimental measurements of the fugacity of CO_2 and graphite/diamond stability from 35 to 77 kbar at 925°C to 1650°C. *Geochimica et Cosmochimica Acta* 61, 1565-1574.

Garland, F., Turner, S., Hawkesworth, C. (1996) Shifts in the source of the Paraná basalts through time. *Lithos* 37, 223-243.

Hawkesworth, C.J., Gallager, K., Kelley, S., Mantovani, M.S.M., Peate, D., Regelous, M., Rogers, N. (1992) Paraná magmatism and the opening of the South Atlantic. In: Storey, B., Alabaster, A., Pankhurst, R. (Eds.), Magmatism and the Causes of Continental Break-up. *Geological Society Special Publication* 68, 221-240. London.

Kennedy, C.S. and Kennedy, G.C. (1976) The Equilibrium Boundary Between Graphite and Diamond. *Journal of Geophysical Research* 81, 14, 2467-2470.

Le Roex, A. P., Bell, D. R. and Davis, P. (2003) Petrogenesis of group I kimberlites from Kimberley, South Africa: evidence from bulk-rock geochemistry. *Journal of Petrology* 44, 2261-2286.

Marques, L.S., Dupré, B., Piccirillo, E.M. (1999) Mantle source compositions of the Paraná Magmatic Province: evidence from trace element and Sr-Nd-Pb isotope geochemistry.

Journal of Geodynamics 28, 439-459.

McCammon, C. and Kopylova, M. G. (2004) A redox profile of the Slave mantle and oxygen fugacity control in the cratonic mantle. *Contributions to Mineralogy and Petrology* 148, 55-68.

Nickel, K.G. and Green, D.H. (1985) Empirical geothermobarometry for garnet peridotites and implications for the nature of the lithosphere, kimberlites and diamonds. *Earth and Planetary Science Letters* 73, 158-170.

Nürnberg, D. and Müller, R.D. (1991) The tectonic evolution of the South Atlantic from late Jurassic to present. *Tectonophysics* 191, 27-53.

Ogilvie-Harris, R.C., Field, M., Sparks, R.S.J., Walter, M.J. (2009) Perovskite from Dutoitspan kimberlite, Kimberley, South Africa: implications for magmatic processes. *Mineralogical Magazine* 73, 915–928.

O'Neill, H. and Wall, V. J. (1987) The olivine–orthopyroxene–spinel oxygen geobarometer, the nickel precipitation curve, and the oxygen fugacity of the Earth's upper mantle. *Journal of Petrology* 28, 1169–1191.

Peate, D.W., Hawkesworth, C.J., Mantovani, M.S.M., Rogers, N.W., Turner, S.P. (1999) Petrogenesis and stratigraphy of the high-Ti/Y Urubici magma type in the Paraná flood basalt province and implications for the nature of 'Dupal'- type mantle in the South Atlantic region. *Journal of Petrology* 40 (3), 451-473.

Piccirillo, E.M., Melfi, A.J. (1988) The Mesozoic Flood Volcanism of the Paraná Basin: Petrogenetic and Geophysical Aspects. *Universidade de São Paulo,* São Paulo, p. 600.

Price, S. E., Russell, J. K. and Kopylova, M. G. (2000) Primitive magma from the Jericho Pipe, NWT, Canada: constraints on primary kimberlite melt chemistry. *Journal of Petrology* 41, 789-808.

Provenzano, C.A.S. (2016) Caracterização petrográfica, química mineral e petrogênese do kimberlito Alfeu I- Canguçu/RS e uma revisão conceitual de magmatismo e rochas kimberlíticas. Dissertação (Mestrado), 215 f. – *Universidade Federal do Rio Grande do Sul*. Porto Alegre.

Rocha-Júnior, E.R.V., Puchtel, I.S., Marques, L.S., Walker, R.J., Machado, F.B., Nardy, A.J.R., Babinski, M., Figueiredo, A.M.G. (2012) Re-Os isotope and highly siderophile element systematics of the Paraná Continental Flood Basalts (Brazil). *Earth and Planetary Science Letters* 337-338, 164-173.

Rocha-Júnior, E.R.V., Marques, L.S., Babinski, M., Nardy, A.J.R., Figueiredo, A.M.G., Machado, F.B. (2013) Sr-Nd-Pb isotopic constraints on the nature of the mantle sources involved in the genesis of the high-Ti tholeiites from northern Paraná Continental Flood Basalts (Brazil). *Journal of South American Earth Sciences* 46, 9-25.

Renne, P.R., Ernesto, M., Pacca, I.G., Coe, R.S., Glen, J., Prev, M., Perrin, M. (1992) The age of Paraná flood volcanism, rifting of Gondwanaland, and the Jurassic - Cretaceous boundary. *Science* 258, 975-979.

Renne, P.R., Glen, J..M., Milner, S.C., Duncan, A.R. (1996) Age of Etendeka flood volcanism and associated intrusions in southwestern Africa. *Geology* 24, 659-662.

Shee, S. R. (1986) The petrogenesis of theWesselton mine kimberlites, Kimberley, South Africa. Ph.D. thesis, *University of Cape Town*.

Stagno, V., Ojwang, D.O., McCammon, C.A., Frost, D.J. (2013) The oxidation state of the mantle and the extraction of carbon from Earth's interior. *Nature*, 493, 84-88.

Turner, S., Regelous, M., Kelley, S., Hawkesworth, C.J., Mantovani, M. (1994) Magmatism and continental break-up in the South Atlantic: high precision 40Ar-39Ar geochronology. *Earth and Planetary Science Letters* 121, 333-348.

Wells, P.R.A. (1977) Pyroxene Thermometry in Simple and Complex Systems. *Contr. Mineral. Petrol.* 62, 129-139.

Wood, B.J., Banno, S. (1973) Garnet-orthopyroxene and orthopyroxene-clinopyroxene relationships in simple and complex systems. *Contrib. Mineral. Petrol.* 42, 109-124.

Woodland, A. B. and Koch, M. (2003) Variation in oxygen fugacity with depth in the upper mantle beneath the Kaapvaal craton, Southern Africa. *Earth and Planetary Science Letters* 214, 295-310.

Zhao, D., Esse, E.J., Zhang, Y. (1999) An oxygen barometer for rutile-ilmenite assemblages: oxidation state of metasomatic agents in the mantle. *Earth and Planetary Science Letters* 166, 127-137.

REFERÊNCIAS BIBLIOGRÁFICAS DA TESE

Adrião, A. B. (2015) Heterogeneidade mantélica na fonte da Província Magmática Paraná: nova evidência de 128 Ma da Província kimberlítica Rosário do Sul, Brasil. Dissertação (Mestrado), 45 f. – *Universidade Federal do Rio Grande do Sul*. Porto Alegre.

Bailey, D. K. (1993) Carbonate magmas. *Journal of the Geological Society*, London 150, 637-651.

Ballhaus, C., Berry, R.F. and Green, D.H. (1991) High pressure experimental calibration of the olivine-orthopyroxene-spinel oxygen geobarometer: implications for the oxidation state of the upper mantle. *Contributions to Mineralogy and Petrology* 107, 27-40.

Ballhaus, C. (1993) Redox States of Lithospheric and Asthenospheric Upper Mantle. *Contributions to Mineralogy and Petrology* 114(3), 331–48.

Bellis, A. and Canil, D. (2007) Ferric Iron in $CaTiO_3$ Perovskite as an Oxygen Barometer for Kimberlitic Magmas I: Experimental Calibration. *Journal of Petrology* 48(2), 219–30.

Bohlen, S.R., Essene, E.J. and Boettcher, A.L. (1980) Reinvestigation and application of olivine-quartz-orthopyroxene barometry. *Earth and Planetary Science Letters* 47, 1-10.

Campbell, A. J., Danielson, L., Righter, K., Seagle, C.T., Wang, Y, Prakapenka, V.B . (2009) High Pressure Effects on the Iron-Iron Oxide and Nickel-Nickel Oxide Oxygen Fugacity Buffers. *Earth and Planetary Science Letters* 286(3-4), 556–64.

Carmichael, I.S.E, and Nicholls, J. (1967) Iron-titanium oxides and oxygen fugacities in volcanic rocks. *Journal of Geophysical Research* 72 (18), 4665-4686.

Carniel, L.C., Klemme, S., Conceição, R.V., Rohrbach, A., Berndt, J. The effects of redox conditions on ferric iron in $CaTiO_3$-perovskite from kimberlitic magmas. (*submitted*)

Chakhmouradian, A. R., and Mitchell, R. H. (2000) Occurrence, Alteration Patterns and Compositional Variation of Perovskite in Kimberlites. *Canadian Mineralogist* 38(4), 975–94.

Chaves, M.L.S.C., Andrade, K.W., Azzi, A.A., Silveira, F.V. (2014) Minerais indicadores kimberlíticos e prospectividade diamantífera da intrusão Alfeu-01 (Canguçu, RS). *Geociências* 33(4), 535-548.

Clark, D.A. (1999) Magnetic Petrology of igneous intrusions: implications for exploration and magnetic interpretation. *Exploration Geophysics* 30, 5-26.

Conceição, R.V. (*in prep.*) Mantle heterogeneity on the source of Paraná continental flood basalts: New evidence from 128Ma Rosário do Sul Kimberlitic Province, Southern Brazil.

Comin-Chiaramonti, P., Gomes, C.B., Castorina, F., Di Censi, P., Antonini, P., Furtado, S., Ruberti, E., Scheibe, L.F. (2002) Geochemistry and geodynamic implications of the Anitápolis and Lages alkaline-carbonatite complexes, Santa Catarina State, Brazil. *Revista Brasileira de Geociências* 32(I), 43-58.

Edler, E., Winter, F., Edwards, R. (1998) The Rosário do Sul Kimberlitic Province, Rio Grande do Sul State, Southern Brazil. *7° International Kimberlite Conference*, Cape Town, South Africa, pp.202-204.

Frost, B. R. (1991) Introduction to Oxygen Fugacity and Its Petrologic Importance. *Reviews in Mineralogy and Geochemistry* 25(1), 1–9.

Frost, D.J. and Wood, B.J. (1997) Experimental measurements of the fugacity of CO_2 and graphite/diamond stability from 35 to 77 kbar at 925°C to 1650°C. *Geochimica et Cosmochimica Acta* 61, 1565-1574.

Fudali, R. F. (1965) Oxygen fugacities of basaltic and andesitic magmas. *Geochimica et Cosmochimica Acta* 29,1063-1075.

Gibson, S.A., Thompson, R.N., Leonardos, O.H., Dickin, A.P., Mitchell, J.G. (1999) The limited extent of plume-lithosphere interactions during continental flood-basalt genesis: geochemical evidence from Cretaceous magmatism in southern Brazil. *Contrib. Mineral. Petrol.* 137, 147-169.

Hasui, Y., Cordani, U.G. (1968) Idades potássio-argônio de rochas eruptivas mesozóicas do Oeste Mineiro e Sul de Goiás. In: *XXII Congresso Brasileiro de Geologia*. Belo Horizonte p. 139-143.

Kaminsky, F.V., Zakharchenko, O.D., Davies, R., Griffin, W.L., Khachatryan-Blinova, G.K., Shiryaev, A.A. (2001) Superdeep diamonds from the Juina area, Mato Grosso State, Brazil. *Contributions to Mineralogy and Petrology* 140 (6), 734-753.

Kaminsky, F.V., Khachatryan, G.K., Andreazza, P., Araujo, D., Griffin, W.L. (2009) Super-deep diamonds from kimberlites in the Juina area, Mato Grosso State, Brazil. *Lithos* 112S, 833-842.

Klemme, S. and O'Neill, H.S. (1997) The reaction $MgCr_2O_4+SiO_2=Cr_2O_3+MgSiO_3$ and the free energy of formation of magnesiochromite ($MgCr_2O_4$). *Contributions to Mineralogy and Petrology* 130, 59-65.

Klemme, S. and O'Neill H.S. (2000) The effect of Cr on the solubility of Al in orthopyroxene: experiments and thermodynamic modeling. *Contributions to Mineralogy and Petrology* 140, 84-98.

Klemme, S. (2010) Experimental constraints on the evolution of iron and phosphorous-rich melts: experiments in the system $CaO-MgO-Fe_2O_3-P_2O_5-SiO_2-H_2O-CO_2$. *Journal of Mineralogical and Petrological Sciences* 105, 1-8.

Kress, V. C., and Carmichael, I.S.E. (1988) Stoichiometry of the Iron Oxidation Reaction in Silicate Melts. *American Mineralogist* 73(11-12), 1267–74.

McCammon, C.A., Frost, D.J., Smyth, J.R., Laustsen, H.M.S., Kawamoto, T., Ross, N.L., van Aken, P.A. (2004) Oxidation state of iron in hydrous mantle phases: implications for subduction and mantle oxygen fugacity. *Physics of the Earth and Planetary Interiors* 143-144, 157-169.

Mitchell, R.H. (1986) Kimberlites: mineralogy, geochemistry and petrology. *Plenum Press*, New York, 442 pp.

Mitchell, R. H., Choi, J. B., Hawthorne, F. C., McCammon, C. A. and Burns, P. C. (1998) Latrappite: a re-investigation. *Canadian Mineralogist* 36, 107-116.

Moreira, M.L., Paris, E.C., Nascimento, G.S., Longo, V.M., Sambrano, J.R., Mastelaro, V.R., Bernardi M.I.B., Andrés, J., Varela J.A., Longo, E. (2009) Structural and optical properties of CaTiO3 perovskite-based materials obtained by microwave-assisted hydrothermal synthesis: An experimental and theoretical insight. *Acta Materialia* 57, 5174–5185.

Muir, I. J., Metson, J. B. and Bancroft, G. M. (1984) ^{57}Fe Mössbauer spectra of perovskite and titanite. *Canadian Mineralogist* 22, 689-694.

Nickel, K.G. and Green, D.H. (1985) Empirical geothermobarometry for garnet peridotites and implications for the nature of the lithosphere, kimberlites and diamonds. *Earth and Planetary Science Letters* 73, 158-170.

Provenzano, C.A.S. (2016) Caracterização petrográfica, química mineral e petrogênese do kimberlito Alfeu I – Canguçu/RS e uma revisão conceitual de Magmatismo e rochas kimberlíticas. Dissertação (Mestrado), 215 f. – *Universidade Federal do Rio Grande do Sul.* Porto Alegre.

Prowatke, S., and Klemme, S. (2006) Trace Element Partitioning between apatite and silicate melts. *Geochimica et Cosmochimica Acta* 70, 4513–27.

Rohrbach, A., and Schmidt, M.W. (2011) Redox Freezing and Melting in the Earth's Deep Mantle Resulting from Carbon-Iron Redox Coupling. *Nature* 472(7342), 209–12.

Wedepohl, K. H. and Muramatsu, Y. (1979) The chemical composition of kimberlites compared with the average composition of three basaltic magma types. In F. R. Boyd and H. O. A. Meyer, Eds., *Kimberlites, Diatremes, and Diamonds: Their Geology, Petrology and Geochemistry*, 300-312.

Wells, P.R.A. (1977) Pyroxene Thermometry in Simple and Complex Systems. *Contr. Mineral. Petrol.* 62, 129-139.

Zhang, C. and Duan, Z. (2009) A Model for C-O-H Fluid in the Earth's Mantle. *Geochimica et Cosmochimica Acta* 73(7), 2089–2102.

Zhao, D., Esse, E.J., Zhang, Y. (1999) An oxygen barometer for rutile-ilmenite assemblages: oxidation state of metasomatic agents in the mantle. *Earth and Planetary Science Letters* 166, 127-137.

ANEXO I

Título da Dissertação/Tese:

" HETEROGENEIDADE MANTÉLICA NA REGIÃO SUL DO BRASIL EVIDENCIADA POR MINERALOQUÍMICA DE KIMBERLITOS "

Área de Concentração: Geoquímica

Autora: **Larissa Colombo Carniel**

Orientador: Prof. Dr. Rommulo Vieira Conceição

Examinador: Prof. Dr. Ricardo Kalikowski Weska

Data: 08/12/2017

Conceito: A (EXCELENTE)

PARECER:

A DOUTORANDA APRESENTOU DOMÍNIO DO TEMA DURANTE A APRESENTAÇÃO E NA TESE ELABORADO.

DESTACO ALGUNS PONTOS QUE SUGIRO CORREÇÃO.

1. SUBSTITUIR PROVÍNCIA POR CAMPO KIMBERLÍTICO, CONFORME MITCHELL (1986)
2. OBSERVAR SE NAS LÂMINAS PETROGRÁFICAS DO PIPE ROSARIO DO SUL REALMENTE EXISTE PELLETAL LAPILLI. SE EXISTIR É DIAGNÓSTICO E NÃO HIPOABISSAL
3. QUANTO A GÊNESE A RELAÇÃO ENTRE KIMBERLITO E BASALTO É UM PRINCÍPIO, SOMENTE ESPACIAL. PRECISAM OBSERVAR A PARTICIPAÇÃO DE FLUIDO NO PITO ENRIQUECIDO.
4. OBSERVAR QUE A fO_2 É IMPORTANTE QUANTO A PRESERVAÇÃO DO DIAMANTE NÃO HÁ IMPLICAÇÃO QUANTO A QUALIDADE.

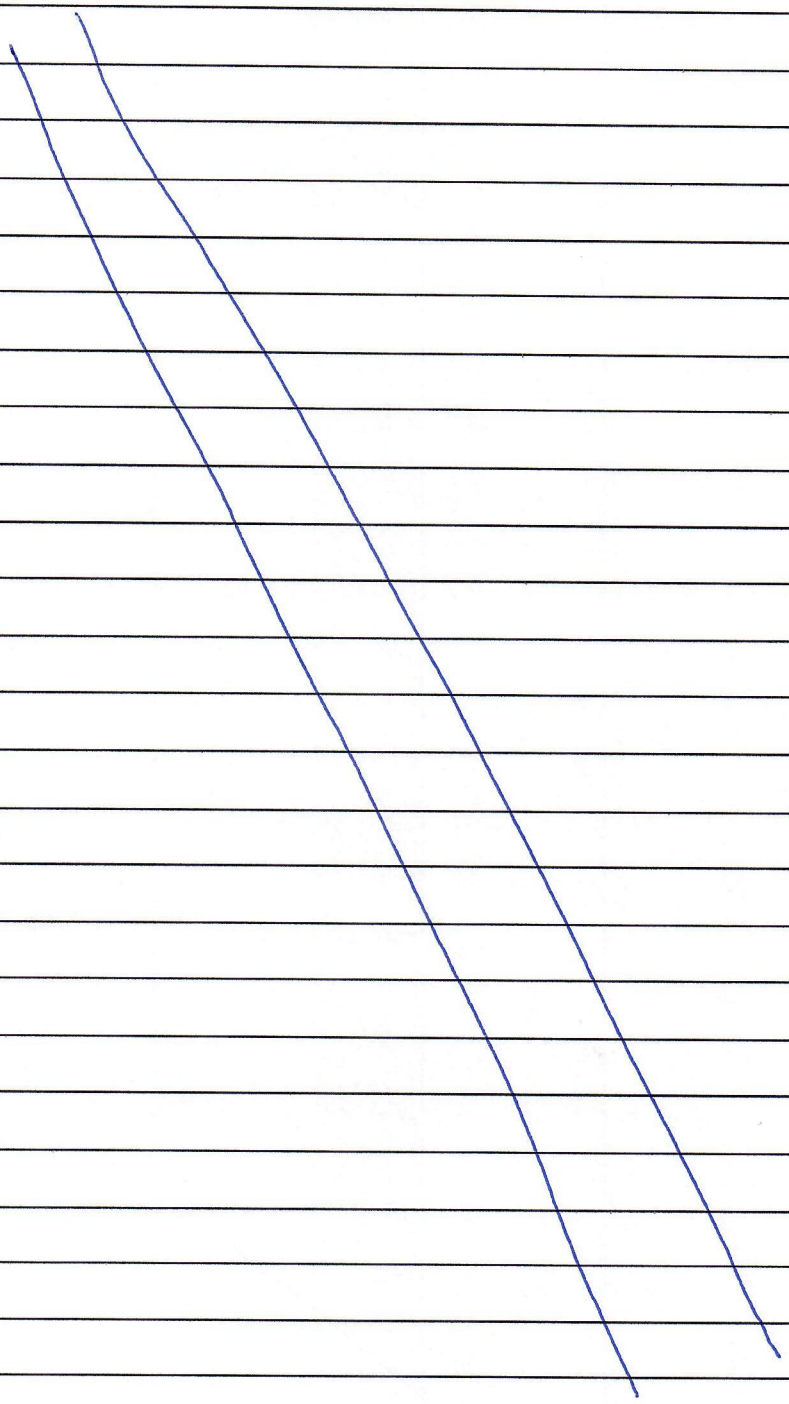

Assinatura: Data: 08/12/2017.

Ciente do Orientador:

Ciente do Aluno:

ANEXO I

Título da Dissertação/Tese:

" HETEROGENEIDADE MANTÉLICA NA REGIÃO SUL DO BRASIL EVIDENCIADA POR MINERALOQUÍMICA DE KIMBERLITOS "

Área de Concentração: Geoquímica

Autora: **Larissa Colombo Carniel**

Orientador: Prof. Dr. Rommulo Vieira Conceição

Examinador: Prof. Dr. Silvio Roberto Farias Vlach

Data: 08 / Dezembro / 2017

Conceito: A

PARECER:

A TESE DE DOUTORADO APRESENTADA É DE EXCELLENTE NÍVEL E REFLETE MUITO BEM A PREPARAÇÃO DA CANDIDATA, QUE SE UTILIZOU DE DIVERSOS METODOS MODERNOS PARA ALCANÇAR SEUS OBJETIVOS.

A TESE CONTEMPLA TRES ARTIGOS SUBMETIDOS A PERIÓDICOS INTERNACIONAIS DE IMPACTO SIGNIFICATIVO. CORRESPONDEM A PESQUISA INÉDITA CONDUZIDA COM ENGAJAMENTO E COMPETÊNCIA.

A APRESENTAÇÃO ORAL DA CANDIDATA FOI MUITO BOA E ELUCIDOU DIVERSOS ASPECTOS ADICIONAIS DO TEXTO.

ESTE RELATOR DESTACOU ALGUNS PONTOS QUE, EMBORA NÃO DIMINUAM EM ABSOLUTA-MENTE NADA O MÉRITO DO TRABALHO SERIAM SUGESTÕES IMPORTANTES P/ MELHORIA.

- ALGUM CUIDADO MAIS ESPECÍFICO NO QUE SE REFERE À QUALIDADE DE DADO ANALÍTICOS (ANALISES DE MICROSONDA) E CHECAGEM DE FÓRMULAS ESTRUTURAIS. TRATAMENTO DESTES DADOS E DAR PREFERÊNCIA A USAR FRAÇÕES MOLARES E/OU CATIÔNICA AO INVÉS DE ÓXIDOS
- REVER E APROFUNDAR AS RELAÇÕES DE FASE ENTRE TITANITA E PEROVSKITA
- REVER O USO DE DADOS MODAIS, USANDO FRAÇÕES EM MASSA

Assinatura: Data: 05/12/2017

Ciente do Orientador:

Ciente do Aluno:

ANEXO I

Título da Dissertação/Tese:

" HETEROGENEIDADE MANTÉLICA NA REGIÃO SUL DO BRASIL EVIDENCIADA POR MINERALOQUÍMICA DE KIMBERLITOS "

Área de Concentração: Geoquímica

Autora: **Larissa Colombo Carniel**

Orientador: Prof. Dr. Rommulo Vieira Conceição

Examinador: Prof. Dr. Pedro Luiz Juchem

Data: 08/12/2017

Conceito: A (excelente)

PARECER:

A tese é de qualidade excepcional e as informações nela contidas foram complementadas pela apresentação oral.

O texto é bem escrito e de fácil leitura e está fundamentado em dados de laboratório consistentes que foram analisados e interpretados com propriedade. Algumas melhorias foram sugeridas e repassadas à candidata, no sentido de aprimorar o entendimento dos textos.

Foi solicitada uma revisão e qualificação do uso do termo "Província Kimberlítica de Rosário do Sul", que pode não ser o mais adequado para se referir aos corpos kimberlíticos desta região.

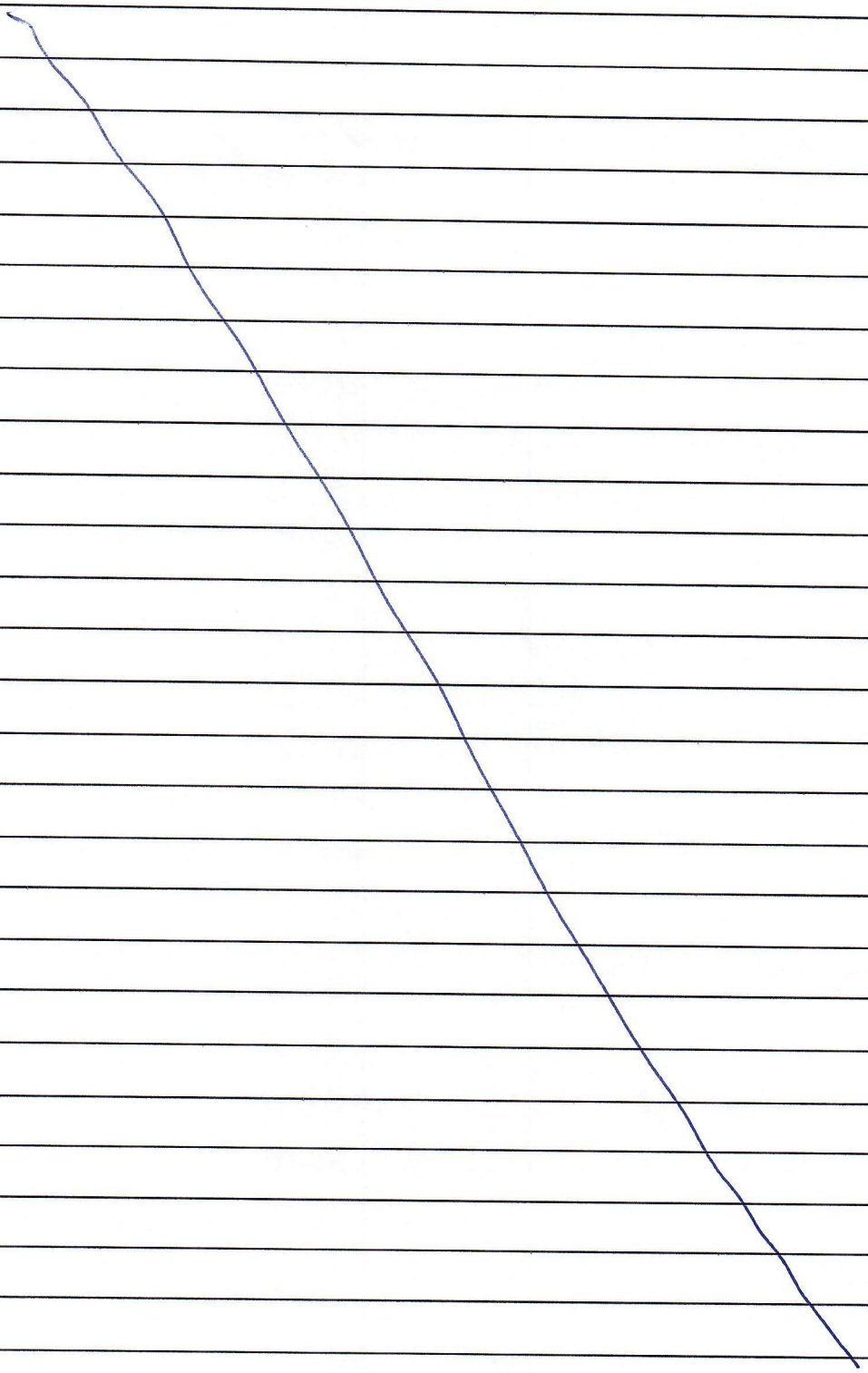

Assinatura: Pedro Luiz Fuchs Data: 06/12/2017

Ciente do Orientador:

Ciente do Aluno: